

SUBHARMONIC MIXERS IN CMOS
MICROWAVE INTEGRATED CIRCUITS

by

BRADLEY RICHARD JACKSON

A thesis submitted to the
Department of Electrical and Computer Engineering
in conformity with the requirements for
the degree of Doctor of Philosophy

Queen's University
Kingston, Ontario, Canada

March 2009

Copyright © Bradley Richard Jackson, 2009

Abstract

This thesis explores the design and applications of subharmonic mixers in CMOS microwave integrated circuits. First, a $2\times$ down-converting subharmonic mixer is demonstrated with a measured conversion gain of 8 dB using a 2.1 GHz RF signal. Extending the concept of the $2\times$ subharmonic mixer, a $4\times$ subharmonic mixer is proposed that operates in the 12 GHz Ku-band. This circuit is the first $4\times$ subharmonic mixer in CMOS, and achieves a 6 dB conversion gain, which is the highest for any $4\times$ subharmonic mixer regardless of circuit topology or fabrication technology. Furthermore, it achieves very high measured isolation between its ports (e.g. $4LO-RF$: 59 dB).

Since both the $2\times$ and the $4\times$ subharmonic mixers require a quadrature oscillator, a new oscillator circuit is presented that could be used with either of the aforementioned mixers. This quadrature oscillator uses active superharmonic coupling to establish the quadrature fundamental relationship. The oscillation frequency is 3.0 GHz and the measured output power is -6 dBm.

A dual-band mixer/oscillator is also demonstrated that can operate as either a fundamental mixer or a subharmonic mixer depending on a control voltage. This circuit operates from 5.0 GHz to 6.0 GHz or from 9.8 GHz to 11.8 GHz by using either the fundamental output or the second harmonic output of the quadrature

oscillator circuit described above and achieves conversion gain over both frequency bands.

A novel frequency tripler circuit is presented based on a subharmonic mixer. This circuit uses the $2\times$ subharmonic mixer discussed above, along with a feedforward fundamental cancellation circuit. The measured fundamental suppression is up to 30 dB and the conversion gain is up to 3 dB. Finally, a frequency divider circuit based on a subharmonic mixer is presented that divides the input signal frequency by a factor of three. This circuit uses a single-balanced version of the $2\times$ subharmonic mixer described above in a regenerative divider topology. The measured input signal bandwidth is 300 MHz (5.2 GHz to 5.5 GHz) with an input power of -7 dBm and the maximum conversion gain is 0 dB.

Acknowledgments

There are many people that I would like to thank for their generous support and encouragement throughout the course of my Ph.D. studies. First, I would like to thank my supervisor, Dr. Carlos Saavedra, for his guidance over the past five years throughout both my Master's and my Ph.D. degrees. He has continually provided me with advice, encouragement, and the opportunities to improve my research and engineering skills.

I would also like to thank several students from the lab for their generous assistance with my research-related problems and for being good partners in our frequent tennis matches. First, and foremost I would like to thank Denis Zheng for his never-ending willingness to give his time over the five years we spent together in the lab. Much assistance and many useful discussions regarding the designs and measurements in this thesis were also provided by Gideon Yong, Stanley Ho, Ahmed El-Gabaly, and John Carr.

The integrated circuits fabricated for this thesis would not be possible without the support and IC grants provided by CMC. I would specifically like to thank Mariusz Jarosz, Patricia Greig, Jim Quinn, and Feng Liu of CMC, for offering technical assistance and equipment that was used for testing the chips in this thesis. Furthermore, many of the measurements performed in this thesis made use of Dr. Brian Frank's

equipment that he generously shared. Thanks also go to several ECE staff members including Greg McLeod for perpetually fixing our Unix server problem du jour, and Debie Fraser & Bernice Ison for always being very friendly and helpful when any administrative issues arose.

My family has been very understanding and supportive over the course of my post-graduate education. In particular, I would like to thank my Mom & Dad, and my Grandfather, as well as the rest of my family: Michelle & Wade, Keagan & Makayla, Sylvia & Bob, Tom, Diane & Gary, Lyn & Dustin, and Jacob & Ava (also Abby for reminding me to relax and not take things too seriously).

Without question, the person that was the most crucial to the completion of this degree was my wife, Elisabeth. From initially encouraging me to start my graduate studies to the completion of this thesis she has been a constant source of motivation and support, and for that I will always be grateful.

Table of Contents

Abstract	i
Acknowledgements	iii
Table of Contents	v
List of Figures	ix
List of Tables	xiv
List of Abbreviations and Symbols	xv
Chapter 1: Introduction	1
1.1 Motivation	1
1.2 Microwave Integrated Circuits in CMOS	3
1.3 Thesis Overview	5
1.4 Contributions	8
Chapter 2: Literature Review	10
2.1 Mixer Background	10
2.1.1 Fundamental Mixers	10
2.1.2 Subharmonic Mixers	12

2.2	Wireless Communication System Architecture	16
2.2.1	Superheterodyne	16
2.2.2	Direct-Conversion	18
2.3	Mixer Circuit Review	21
2.3.1	Fundamental Mixers	21
2.3.2	Subharmonic Mixers	26
2.4	Oscillators Circuit Review	36
2.4.1	Resonators for CMOS Microwave Oscillators	36
2.4.2	Common Oscillator Topologies	38
2.5	Frequency Multiplier Circuit Review	45
2.5.1	Common Frequency Multiplier Topologies	46
2.6	Frequency Divider Circuit Review	51
2.6.1	Common Frequency Divider Topologies	52
Chapter 3: A 2x Subharmonic Mixer in CMOS		57
3.1	Introduction	57
3.2	Concept of the 2x Subharmonic Mixer	58
3.3	Circuit Design	59
3.3.1	Subharmonic Mixer Core	59
3.3.2	RF and LO Input Baluns	66
3.3.3	Output Balun	71
3.3.4	Complete Circuit	72
3.4	Measurement Results	73
3.5	Summary	79

Chapter 4: A CMOS Ku-Band 4x Subharmonic Mixer	81
4.1 Introduction	81
4.2 Concept of the 4x Subharmonic Mixer	82
4.3 Circuit Design	84
4.3.1 Mixer Core	84
4.3.2 Input RF Balun	88
4.3.3 LO Phase Shifters	90
4.3.4 Output Balun	92
4.4 Measurement Results	93
4.5 Summary	101
Chapter 5: Quadrature Oscillator	103
5.1 Introduction	103
5.2 Concept of the Quadrature Oscillator	104
5.3 Circuit Design	105
5.4 Measurement Results	108
5.5 Summary	112
Chapter 6: A Dual-Band Mixer/Oscillator	114
6.1 Introduction	114
6.2 Concept of the Dual-Band Mixer/Oscillator	115
6.3 Circuit Design	116
6.3.1 Voltage-Controlled Quadrature Oscillator	117
6.3.2 Mixer	119
6.4 Measurement Results	123

6.5	Summary	129
Chapter 7: A Frequency Tripler Using a Subharmonic Mixer . . .		131
7.1	Introduction	131
7.2	Concept of the Frequency Tripler	132
7.3	Circuit Design	133
7.3.1	Subharmonic Mixer	133
7.3.2	Fundamental Feedforward Circuit	135
7.3.3	Fundamental Cancellation Circuit	137
7.4	Measurement Results	140
7.5	Summary	148
Chapter 8: A Frequency Divider Using a Subharmonic Mixer . .		149
8.1	Introduction	149
8.2	Concept of the Frequency Divider	150
8.3	Circuit Design	152
8.4	Measurement Results	155
8.5	Summary	159
Chapter 9: Summary and Conclusions		161
9.1	Summary	161
9.2	Review of Contributions	164
9.3	Future Work	166
References		168

List of Figures

2.1	Fundamental mixer block diagram.	11
2.2	Subharmonic mixer block diagram.	13
2.3	Anti-parallel diode pair conceptual circuit.	14
2.4	Block diagram of a superheterodyne receiver.	17
2.5	Block diagram of a direct-conversion receiver.	19
2.6	Potential LO self-mixing paths.	20
2.7	Gilbert-cell mixer.	22
2.8	Resistive FET mixer.	25
2.9	Basic $2\times$ subharmonic mixer circuit used in [25, 28, 31, 35].	27
2.10	Subharmonic mixer circuit proposed in [36].	30
2.11	Passive FET subharmonic mixer.	31
2.12	Subharmonic mixer using an anti-parallel diode-pair.	33
2.13	Common model used for CMOS inductors.	38
2.14	Colpitts oscillator circuit.	39
2.15	Negative resistance generated from cross-coupled FETs.	40
2.16	Cross-coupled FET oscillator.	41
2.17	Complementary cross-coupled FET oscillator.	42
2.18	Quadrature oscillator superharmonic coupling techniques.	44
2.19	Simplified frequency doubler using FET non-linearities.	47

2.20	Simplified circuit of an injection-locked frequency doubler.	48
2.21	Push-push frequency doubler circuit.	49
2.22	Simplified circuit of a regenerative frequency divider.	53
2.23	Simplified circuit of an injection-locked frequency divider.	55
3.1	Block diagram of the proposed $2\times$ subharmonic mixer	58
3.2	Proposed CMOS $2\times$ subharmonic mixer core.	60
3.3	LO frequency doubling in the $2\times$ subharmonic mixer.	60
3.4	LO transistor modeling for the $2\times$ subharmonic mixer	62
3.5	Calculated and simulated conversion gain of the $2\times$ SHM.	65
3.6	Single FET balun circuit.	66
3.7	Differential pair balun circuit.	68
3.8	Common-gate, common-source balun circuit.	68
3.9	Simulated $2\times$ SHM active balun performance.	70
3.10	LO input balun and phase shifters for the $2\times$ SHM.	71
3.11	Output balun and buffer for the $2\times$ SHM.	72
3.12	Photograph of fabricated CMOS $2\times$ subharmonic mixer.	73
3.13	Measured and simulated P_{1dB} for the $2\times$ SHM	75
3.14	Conversion gain at various LO power levels for the $2\times$ SHM.	75
3.15	Measured RF input reflection coefficient for the $2\times$ SHM.	77
3.16	Measured LO input reflection coefficient for the $2\times$ SHM.	77
3.17	Third-order intercept point measurement for the $2\times$ SHM.	78
4.1	The mixer core of the proposed $4\times$ SHM.	83
4.2	Modeling the $4\times$ SHM LO generation circuit	85
4.3	RF active balun circuit for the $4\times$ SHM.	89

4.4	45° phase shifter circuit for the 4× SHM.	91
4.5	90° <i>RC-CR</i> phase shifter used in the 4× SHM.	92
4.6	Output balun circuit for the 4× SHM.	93
4.7	Measured 4× subharmonic mixer output spectrum	94
4.8	Measured P_{1dB} for the 4× SHM	95
4.9	Conversion gain at various LO power levels for the 4× SHM.	96
4.10	Measured IP3 for the 4× SHM	98
4.11	Measured IP2 for the 4× SHM	98
4.12	Measured RF input reflection coefficient for the 4× SHM.	99
4.13	Microphotograph of the proposed 4× SHM.	102
5.1	Quadrature oscillator superharmonic coupling techniques.	104
5.2	Proposed quadrature oscillator core circuit.	106
5.3	Complete quadrature oscillator circuit.	107
5.4	Time-domain measurement setup for the quadrature oscillator.	109
5.5	Measured time-domain quadrature oscillator output.	109
5.6	Measured quadrature oscillator output spectrum.	110
5.7	Measured phase noise of quadrature oscillator.	111
5.8	Photograph of the proposed CMOS quadrature oscillator chip.	112
6.1	Block diagram of the proposed dual-band mixer/oscillator.	115
6.2	Quadrature VCO using superharmonic coupling.	118
6.3	Dual-band mixer/oscillator in subharmonic mode	120
6.4	Circuit schematic of the proposed dual-band mixer/oscillator.	121
6.5	Measured fundamental LO frequency tuning range.	123
6.6	Measured conversion gain for dual-band mixer/oscillator	125

6.7	Measured dual-band mixer/oscillator 1-dB compression point.	125
6.8	Measured IP3 for the dual-band mixer/oscillator	127
6.9	Measured IP2 for the dual-band mixer/oscillator	127
6.10	Microphotograph of the fabricated dual-band mixer/oscillator	129
7.1	Block diagram of the proposed frequency tripler.	132
7.2	Core of the $2\times$ SHM used in the frequency tripler.	134
7.3	Generation of the frequency tripler quadrature LO signals.	135
7.4	Fundamental feedforward circuit used in the frequency tripler.	136
7.5	Tripler active balun, subtractor, and output buffer circuits.	138
7.6	Fundamental suppression calculation for the frequency tripler	139
7.7	Measured frequency tripler output spectrum.	141
7.8	Measured tripler output power levels at various input powers.	142
7.9	Measured tripler output power tuned for optimal performance.	144
7.10	Simulated broadband performance of the tripler using an ideal quadrature input signal with a power of -11 dBm.	145
7.11	Measured input and output phase noise for the frequency tripler.	146
7.12	Microphotograph of the frequency tripler chip.	147
8.1	Traditional Miller regenerative frequency divider.	150
8.2	Block diagram of the proposed divide-by-three frequency divider.	151
8.3	Single-balanced $2\times$ subharmonic mixer circuit.	152
8.4	Tuned differential amplifier circuit.	153
8.5	Simplified schematic of the proposed frequency divider (biasing not shown).	154
8.6	Frequency divider output spectrum	156

8.7	Frequency divider conversion gain at various input frequencies	157
8.8	Frequency divider bandwidth	158
8.9	Frequency divider chip photograph.	159

List of Tables

3.1	2× subharmonic mixer port-to-port isolation simulations.	78
3.2	2× subharmonic mixer circuit performance comparison.	79
4.1	4× subharmonic mixer port-to-port isolation measurements.	100
6.1	Dual-band mixer/oscillator LO feedthrough measurements.	128
7.1	Tripler circuit performance comparison	147

List of Abbreviations and Symbols

Abbreviation	Definition
SHM	Subharmonic Mixer
CMOS	Complimentary Metal-Oxide-Semiconductor
RF	Radio Frequency
LO	Local Oscillator
IF	Intermediate Frequency
ADS	Advanced Design System (software from Agilent)
LPF	Low-Pass Filter
BPF	Band-Pass Filter
ADC	Analog-to-Digital Converter
CPW	Coplanar waveguide
SAW	Surface Acoustic Wave
SoC	System-on-a-Chip
LNA	Low-Noise Amplifier
VCO	Voltage-Controlled Oscillator
RFC	Radio Frequency Choke
IM2	Second-order intermodulation products
IM3	Third-order intermodulation products

IIP2	Input-referred second-order intercept point
OIP2	Output-referred second-order intercept point
IIP3	Input-referred third-order intercept point
OIP3	Output-referred third-order intercept point
DSB	Double Sideband (noise figure)
SSB	Single Sideband (noise figure)
GSG	Ground-Signal-Ground
P_{1dB}	1-dB compression point
FET	Field effect transistor
MOSFET	Metal Oxide Semiconductor Field Effect Transistor
SiGe	Silicon germanium
BiCMOS	A process with both bipolar and CMOS transistors
GaAs	Gallium arsenide
HEMT	High Electron Mobility Transistor
InP	Indium phosphide
RBW	Resolution Bandwidth
VBW	Video Bandwidth
f	Frequency in Hz
ω	Frequency in rad/s
f_T, ω_T	Unity current gain frequency
f_{max}, ω_{max}	Maximum frequency of oscillation
f_{RF}, ω_{RF}	Frequency of the radio frequency signal
f_{LO}, ω_{LO}	Frequency of the local oscillator signal
f_{IF}, ω_{IF}	Frequency of the intermediate frequency signal

Q	Quality factor
W	Transistor gate width
L	Transistor gate length
E_{sat}	Electric field where the electron velocity saturates
g_m	Transconductance
r_g	Series gate resistance
C_{gs}	Parasitic gate-source capacitance
C_{gd}	Parasitic gate-drain capacitance
μ_n	Electron Mobility
C_{ox}	Gate oxide capacitance
I_s	Reverse-bias saturation current
V_t	FET threshold voltage
V_{th}	Diode thermal voltage

Chapter 1

Introduction

1.1 Motivation

Society's demand for wireless communication devices that are faster and more robust with increased functionality has been ongoing for decades and it is not likely that it will subside anytime in the near future. In order to accommodate higher data-rate systems and to avoid the increasingly cluttered frequency spectrum in the low- GHz area, many new systems will need to move to higher frequencies where new challenges in circuit design are encountered. To address this issue, new circuit topologies need to be demonstrated that become increasingly advantageous as the frequency of operation is increased. This is one motivation for the work in this dissertation.

In addition to the relentless desire to increase the performance of wireless communications systems, the desire to reduce costs is universal. The integrated circuit fabrication technology used to realize almost all digital microprocessors is complementary metal-oxide-semiconductor (CMOS) technology, which is very low-cost compared to other fabrication technologies due to economies of scale. It is therefore very desirable

for the RF/microwave circuits in wireless communication devices to use CMOS technology in order to minimize costs. As such, all of the microwave integrated circuits in this thesis use CMOS technology. Furthermore, if both the RF/microwave circuits and the digital circuits use CMOS technology there is the potential for realizing a complete system-on-a-chip (SoC), which can lead to increased functionality, further cost reductions, and significant reductions in device size.

As discussed above, there are many advantages that can be gained if a system-on-a-chip can be realized for a given application. Unfortunately, the most common wireless receiver architecture (superheterodyne) contains components that are often very difficult or impossible to integrate on the same chip as the microwave and digital circuitry. To address this issue, there has been much interest of late in an alternative wireless communication receiver architecture (direct-conversion) that does not require the difficult-to-integrate components. Of course, new challenges are introduced with this alternate architecture, and new circuits need to be investigated to address these issues, which is another motivation for this work.

This dissertation predominantly focuses on an essential circuit used for wireless communications, namely, the mixer, as well as the application of mixers in other frequency conversion circuits. Mixers are fundamental circuit elements that are used in both transmitters and receivers to convert signals in the frequency domain. In general, mixers have three ports: a radio frequency (RF) port, a local oscillator (LO) port, and an intermediate frequency (IF) port. In transmitters, they are used for modulation and up-conversion to ease wireless transmission. Correspondingly, in receivers, mixers are used for demodulation and down-conversion. In most cases, mixers are realized by using the non-linearities in active devices or by using switches.

A specialized type of mixer, a subharmonic mixer (SHM), has unique advantages that can address some of the issues discussed above regarding next-generation wireless communication devices, and as such is the focus of this thesis.

1.2 Microwave Integrated Circuits in CMOS

Over the past 15 years there has been a tremendous amount of interest in the use of CMOS technology for RF and microwave circuits (often referred to as RF CMOS). As mentioned previously, there are significant benefits that can be derived from the use of CMOS for RF circuits including the possibility of achieving the much heralded system-on-a-chip. By combining the RF circuitry with the digital processing circuitry on the same substrate, a significant cost savings can potentially be obtained. Since the predominant technology used for digital circuitry is CMOS there is a natural desire to use CMOS technology for RF circuits as well. In addition to system-on-a-chip aspirations, it is also desirable to use CMOS for RF and microwave applications because it is generally much less expensive than other technologies that have been used in the past (e.g. GaAs). There are, however, significant challenges that are encountered when using CMOS for RF circuits. Prior to the 1990s there was very little work in the area of RF CMOS because the transistor could not attain the required performance at high frequencies. The enormous advances in CMOS technology have in large part been due to the geometrical scaling of the transistor. Two common figures of merit for the high frequency performance of transistors are ω_T and ω_{max} , which are the frequencies at which the current and power gain, respectively, equal unity and are given by [1]:

$$\omega_T = \frac{g_m}{C_{gs} + C_{gd}} \quad (1.1)$$

$$\omega_{max} = \frac{1}{2} \sqrt{\frac{\omega_T}{r_g C_{gd}}} \quad (1.2)$$

where g_m is the transconductance of the transistor, r_g is the series gate resistance, and C_{gs} and C_{gd} are the parasitic gate-source and gate-drain capacitances, respectively. When the transistor is scaled, the parasitic capacitances decrease, which leads to an increase in ω_T and ω_{max} , and improved high frequency performance. For example, it is currently possible to use CMOS technology to realize microwave mixers and low noise amplifiers up to 60 GHz [2], and voltage controlled oscillators up to 192 GHz [3]. Recently, a cutoff frequency of over 400 GHz was achieved using CMOS 45 nm silicon-on-insulator (SOI) technology [4]. With this extremely high cutoff frequency, it is expected that the applications of CMOS technology in the microwave/millimeter-wave will continue to grow for some time into the future. For all of the circuits in this thesis, either CMOS 0.18 μm or CMOS 0.13 μm technology was used. The cutoff frequency, f_T , for CMOS 0.18 μm is approximately 45 GHz and for CMOS 0.13 μm it is approximately 105 GHz [5].

In addition to the high-frequency performance of the CMOS transistor, the other major challenge to using CMOS for RF circuits is in regards to obtaining high quality passive components, or more specifically, inductors. Inductors in RF CMOS circuits are typically realized using a spiral. There are several metal layers available in any modern CMOS technology and the inductors are generally fabricated on the top metal

layer. There are two primary reasons for this: (1) the top metal layer is generally the thickest and thus has the lowest ohmic losses and (2) the relatively low resistivity of the silicon substrate causes serious parasitic effects, which can be reduced by increasing the distance between the inductor and the substrate. At high frequencies there can be significant capacitive coupling to the substrate and image currents produced that can seriously degrade an inductor's performance. Furthermore, since these structures can be relatively large in order to yield the desired value of inductance, the inductor's metal lines are correspondingly quite long and in many cases narrow, which can cause significant ohmic losses. The combination of these parasitic effects results in inductors with relatively low quality factors (Q -factors).

1.3 Thesis Overview

This thesis is organized topically by chapter. After a literature review, each chapter explores a different application of subharmonic mixers in CMOS microwave integrated circuits, with a summary in the final chapter.

A literature review is first presented in Chapter 2 that allows the contributions of this thesis to be placed into a broader context. A brief discussion of the previous work relevant to each of the circuits demonstrated in this thesis is presented.

Chapter 3 explores a $2\times$ subharmonic mixer circuit using CMOS technology. This circuit investigates the level of performance attainable and design issues with SHMs in CMOS in preparation for designing a more advanced $4\times$ subharmonic mixer circuit. Included in this work is a circuit that generates a quadrature LO signal from a single-ended LO input. Furthermore, an RF input active balun is used to generate a differential RF signal from a single-ended input and an output active balun is used to

convert back to a single-ended signal for measurement. A conversion gain equation for the mixer core circuit is derived and measurement results are shown.

Having verified the $2\times$ subharmonic mixer topology in Chapter 3, the concept is extended in Chapter 4 to realize a $4\times$ subharmonic mixer that operates as a Ku-band down-converter. This circuit requires octet-phase LO input signals, and as such, a circuit is included on-chip to generate these signals from a differential LO input. An RF input balun similar to the one used in Chapter 3 is implemented at a much higher frequency (12.1 GHz as opposed to 2.1 GHz). A mathematical analysis of the mixer is presented that explains how this circuit internally multiplies the frequency of the LO signal by a factor of four.

Since the mixers presented in both Chapters 3 and 4 rely on a quadrature local oscillator signal, Chapter 5 presents a compact quadrature oscillator that is suitable for use with either mixer. This quadrature oscillator uses a technique called active superharmonic coupling to enforce the quadrature fundamental relationship. Measurement results are shown for the oscillator including output power spectrum, phase noise, and quadrature accuracy.

Having explored subharmonic mixer circuits as well as an oscillator, Chapter 6 combines these circuits to realize a dual-band oscillator/mixer circuit for C-band and X-band applications. The mixer operates using either the fundamental oscillator output, or the second-harmonic output of the oscillator depending on the state of a set of complementary switches. Therefore, this circuit can operate as either a fundamental mixer, or a subharmonic mixer depending on a single control voltage. In fundamental-mode, the circuit operates with RF input signals in C-band (5.0 GHz to 6.0 GHz), and in subharmonic-mode the circuit operates with RF input signals in

X-band (9.8 GHz to 11.8 GHz). Measurement results are shown for both states of the circuit.

In Chapter 7, a frequency multiplier is presented that uses a subharmonic mixer to realize a frequency multiplication by three. Whereas most frequency multipliers are even-ordered, a subharmonic mixer with the same input signal for the RF and LO ports will produce an output signal that has a component at the fundamental frequency and a component at three times the fundamental frequency. A feedforward circuit is used to cancel the fundamental output of the subharmonic mixer, leaving (ideally) only the tripled frequency component. Measurement results are shown that indicate high-levels of fundamental suppression can be achieved using this technique without a filter.

In Chapter 8, a frequency divider is demonstrated that divides the input signal frequency by a factor of three using a single-balanced version of the $2\times$ subharmonic mixer described in Chapter 3. A regenerative frequency divider topology is used with the $2\times$ subharmonic mixer in CMOS 0.13 μm technology to realize a frequency divider that accepts an input signal from 5.2 GHz to 5.5 GHz and outputs a signal from 1.73 GHz to 1.83 GHz. Measurement results for this frequency divider are shown including the output power spectrum as well as the bandwidth obtainable for different input power levels.

Finally, a summary of the thesis is presented, as well as a review of the contributions made to the field of microwave integrated circuits through this work. The thesis concludes with a discussion of potential directions for future work on subharmonic mixers in microwave integrated circuits.

1.4 Contributions

The major contributions of this thesis are as follows:

- The first $4\times$ subharmonic mixer demonstrated in CMOS technology, and the highest conversion gain for any $4\times$ subharmonic mixer regardless of technique or technology used. A measured conversion gain of 6 dB was achieved along with very high isolation between ports, which demonstrates the potential of high-order subharmonic mixers in CMOS technology. (Chapter 4) [6].
- A unique frequency tripler circuit that uses a subharmonic mixer and fundamental cancellation to achieve conversion gain of 3 dB and fundamental suppression of up to 30 dB without a filter (Chapter 7) [7].
- The first $2\times$ subharmonic mixer demonstrated in CMOS technology with measured results using the proposed topology, and one of the first CMOS subharmonic mixers overall. Active baluns were used for all ports to realize a compact layout, and the measured conversion gain of 8 dB demonstrates the potential for high conversion gain with this topology. (Chapter 3) [8].
- The most compact quadrature oscillator using the superharmonic coupling technique and a phase noise of -116 dBc/Hz at a 1 MHz offset for a 3.0 GHz output frequency, which is the lowest phase noise for a quadrature oscillator using active superharmonic coupling (Chapter 5) [9].
- A novel dual-band mixer/oscillator circuit that uses a single mixer core and a single oscillator circuit for operation in both C-band and X-band. This circuit

achieves a conversion gain for RF input signals from 5.0 GHz to 6.0 GHz and from 9.8 GHz to 11.8 GHz (Chapter 6) [10].

- A novel frequency divider circuit that divides the input signal frequency by a factor of three using a subharmonic mixer in a regenerative topology. This circuit can achieve a conversion gain of up to 0 dB and an input signal bandwidth of up to 430 MHz. Since the majority of frequency dividers are even-order (often divide-by-two or four), the proposed odd-order divider circuit can add flexibility to microwave circuit design (Chapter 8) [11].

Chapter 2

Literature Review

2.1 Mixer Background

This section will provide a brief background on both fundamental mixers and sub-harmonic mixers in order to set the stage for a more detailed literature review of previous mixer circuits.

2.1.1 Fundamental Mixers

By far the most common type of mixer is the fundamental-mode mixer. In this type of mixer, the sum and difference of the two input frequencies are produced at the output, as shown in Figure 2.1. Specifically, in the case of down-conversion, if f_{RF} and f_{LO} are the two mixer input signal frequencies, then the IF output signal will have frequency,

$$f_{IF} = f_{RF} - f_{LO} \quad (2.1)$$

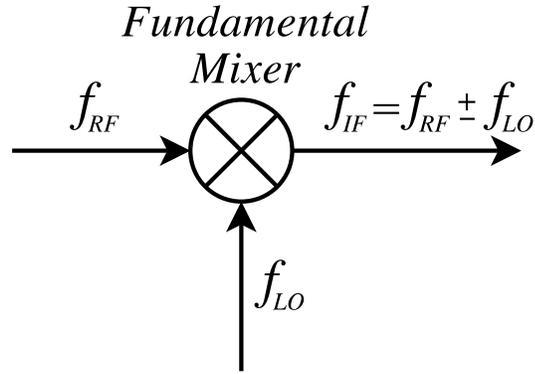


Figure 2.1: Fundamental mixer block diagram.

Alternatively, if the mixer is being used for up-conversion with f_{IF} and f_{LO} inputs, the RF output signal will have frequency,

$$f_{RF} = f_{IF} + f_{LO} \quad (2.2)$$

In order to generate this frequency translation, a nonlinear device is required. A straight-forward mathematical identity can illustrate how a nonlinearity can produce this operation. Consider two signals, $\cos(\omega_1 t)$ and $\cos(\omega_2 t)$, that are multiplied together through a device nonlinearity,

$$\cos(\omega_1 t)\cos(\omega_2 t) = \frac{1}{2}(\cos((\omega_1 - \omega_2)t) + \cos((\omega_1 + \omega_2)t)). \quad (2.3)$$

It is clear that the sum and difference frequencies are produced as desired for a fundamental mixer. Potential nonlinear devices that can be used for mixing include diodes, transistors, and superconducting junctions for sub-millimeter waves. For example, by considering the I - V relationship for a diode it is easy to see how it could be used as a mixer. Conceptually, consider a single diode with an applied voltage that is the sum

of two sinusoids, v_{RF} and v_{LO} , where

$$v_{RF} = A_{RF} \cos(\omega_{RF} t) \quad (2.4)$$

$$v_{LO} = A_{LO} \cos(\omega_{LO} t). \quad (2.5)$$

Thus, the voltage across the diode is:

$$v_d = A_{RF} \cos(\omega_{RF} t) + A_{LO} \cos(\omega_{LO} t). \quad (2.6)$$

The diode current, I_d , is given by:

$$i_d = I_s \left(e^{\frac{v_d}{V_{th}}} - 1 \right) = I_s \left[1 + \frac{v_d}{V_{th}} + \frac{1}{2!} \left(\frac{v_d}{V_{th}} \right)^2 + \frac{1}{3!} \left(\frac{v_d}{V_{th}} \right)^3 + \dots - 1 \right] \quad (2.7)$$

where I_s is the reverse-bias saturation current and V_{th} is the diode thermal voltage. From (2.6) and (2.7) it is clear that a large number of spectral components will be produced. For example, the *squared* term in (2.7) will produce the sum and difference frequencies, $(\omega_{RF} + \omega_{LO})$ and $(\omega_{RF} - \omega_{LO})$, respectively as well as double frequency terms, $2\omega_{RF}$ and $2\omega_{LO}$. The *cubic* term in (2.7) will produce frequency components at $3\omega_{RF}$, $3\omega_{LO}$, $(2\omega_{RF} \pm \omega_{LO})$ and $(2\omega_{LO} \pm \omega_{RF})$. Therefore, a diode can be used to perform both fundamental and subharmonic mixing.

2.1.2 Subharmonic Mixers

In a subharmonic mixer (SHM), the LO frequency is internally multiplied, thus producing mixing components from the RF frequency and an integer multiple of the LO frequency, as shown in Figure 2.2. If f_{RF} is the RF input frequency and f_{LO} is the LO input frequency then the output signals will have frequency,

$$f_{IF} = f_{RF} \pm n f_{LO} \quad (2.8)$$

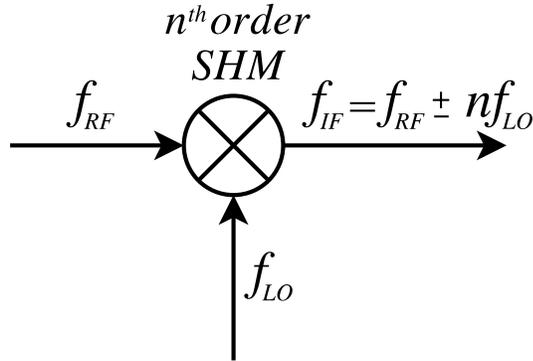


Figure 2.2: Subharmonic mixer block diagram.

where n is the order of the subharmonic mixer. The use of a subharmonic mixer with order $n = 4$, for example, permits the use of an LO with *one-quarter* the frequency that would be required with a fundamental-mode mixer.

In this thesis, when $n = 2$ the circuit will be referred to as a $2\times$ subharmonic mixer and when $n = 4$ the circuit will be called a $4\times$ subharmonic mixer. The reduction in LO frequency can potentially simplify the LO design and can improve the phase noise performance of the oscillator, which can ultimately improve the overall system performance. At high-frequencies in particular, it may be difficult to design an LO with the required output power and phase noise, which makes the subharmonic mixing technique attractive.

As mentioned previously, a single diode could be used to implement a subharmonic mixer. However, as the order of the subharmonic mixer increases, the amplitude rapidly decreases as can be seen from Equation (2.7). Furthermore, since there are many intermodulation products generated by the diode, the system may require a very high-performance filter. Subharmonic mixers used at millimeter-wavelengths are often implemented with diode circuits since it can be difficult to realize LO signals

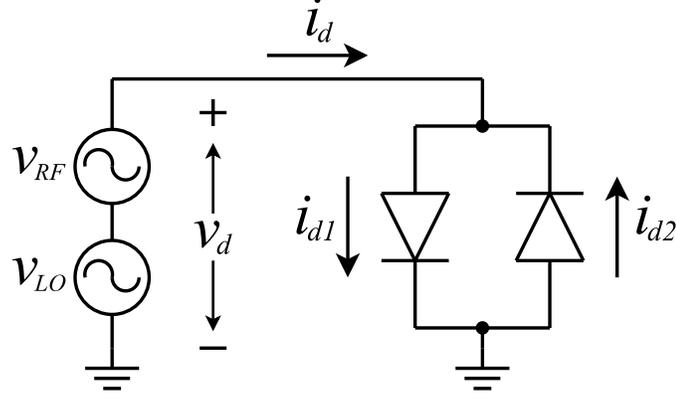


Figure 2.3: Anti-parallel diode pair conceptual circuit.

and transistor-based mixer circuits at such high-frequencies.

The most common type of subharmonic mixer circuit is based on the anti-parallel diode pair (APDP), shown in the conceptual circuit in Figure 2.3 [12]. In this circuit, the sum of the RF and LO signals are applied to the APDP,

$$v_d = v_{RF} + v_{LO} = A_{RF} \cos(\omega_{RF} t) + A_{LO} \cos(\omega_{LO} t) \quad (2.9)$$

and the currents through each of the diodes is given by:

$$i_{d1} = I_s \left(e^{\frac{v_d}{V_{th}}} - 1 \right) \quad (2.10)$$

$$i_{d2} = I_s \left(e^{\frac{-v_d}{V_{th}}} - 1 \right) \quad (2.11)$$

where I_s is the reverse-bias saturation current and V_{th} is the diode thermal voltage.

The total current flowing through the APDP is

$$i_d = i_{d1} - i_{d2} = I_s \left(e^{\frac{v_d}{V_{th}}} - e^{\frac{-v_d}{V_{th}}} \right) \quad (2.12)$$

which, expanding the Taylor-series to the third-power, gives

$$i_d = I_s \left[1 + \left(\frac{v_d}{V_{th}} \right) + \frac{1}{2} \left(\frac{v_d}{V_{th}} \right)^2 + \frac{1}{6} \left(\frac{v_d}{V_{th}} \right)^3 \right]$$

$$-1 - \left(\frac{-v_d}{V_{th}} \right) - \frac{1}{2} \left(\frac{-v_d}{V_{th}} \right)^2 - \frac{1}{6} \left(\frac{-v_d}{V_{th}} \right)^3 \Big], \quad (2.13)$$

which simplifies to

$$i_d = I_s \left[2 \left(\frac{v_d}{V_{th}} \right) + \frac{1}{3} \left(\frac{v_d}{V_{th}} \right)^3 \right]. \quad (2.14)$$

Substituting (2.9) into (2.14) and using basic trigonometric identities yields

$$\begin{aligned} i_d = I_s & \left[\frac{2}{V_{th}} (A_{RF} \cos(\omega_{RF} t) + A_{LO} \cos(\omega_{LO} t)) + \frac{1}{3V_{th}^3} (A_{RF}^3 \cos^3(\omega_{RF} t) \right. \\ & + 3A_{RF}^2 A_{LO} \cos^2(\omega_{RF} t) \cos(\omega_{LO} t) + 3A_{RF} A_{LO}^2 \cos(\omega_{RF} t) \cos^2(\omega_{LO} t) \\ & \left. + A_{LO}^3 \cos^3(\omega_{LO} t)) \right]. \quad (2.15) \end{aligned}$$

Since the amplitude of the RF signal will generally be much smaller than the LO signal amplitude, the approximation can be made that $A_{LO} \gg A_{RF}$, which simplifies the diode current expression to

$$\begin{aligned} i_d = I_s & \left[\frac{2}{V_{th}} (A_{RF} \cos(\omega_{RF} t) + A_{LO} \cos(\omega_{LO} t)) \right. \\ & \left. + \frac{1}{3V_{th}^3} (3A_{RF} A_{LO}^2 \cos(\omega_{RF} t) \cos^2(\omega_{LO} t) + A_{LO}^3 \cos^3(\omega_{LO} t)) \right]. \quad (2.16) \end{aligned}$$

The frequencies contained in the expression for i_d given in (2.16) are: ω_{RF} , ω_{LO} , $2\omega_{LO} + \omega_{RF}$, $2\omega_{LO} - \omega_{RF}$, and $3\omega_{LO}$. The presence of the $2\omega_{LO} + \omega_{RF}$ and $2\omega_{LO} - \omega_{RF}$ signal components clearly verify the potential for using an APDP to implement a subharmonic mixer. The APDP structure conveniently eliminates the even-order intermodulation products, however, the fundamental RF and LO signals feedthrough to the output and therefore this topology generally requires a filter at the output.

While diode-based subharmonic mixer circuits have been the most common type, there are many advantages to using transistor-based subharmonic mixers, such as the potential for conversion gain. This thesis focuses on FET-based subharmonic

mixers, which, while less common than diode-based subharmonic mixers, have been growing in popularity as interest in direct-conversion receivers has increased, and as the high-frequency performance of CMOS transistors has improved.

2.2 Wireless Communication System Architecture

The predominant applications of subharmonic mixers have in the past been in high-frequency systems where it is advantageous or necessary to use a lower LO frequency. Recently, direct-conversion receiver architectures have grown in popularity, which has led to an increased interest in subharmonic mixers because of their inherent ability to reduce LO self-mixing and increase overall receiver performance. In this section, the applications of subharmonic mixers will be discussed in both superheterodyne and direct-conversion architectures to provide context for the work in this thesis.

2.2.1 Superheterodyne

For over 75 years the dominant receiver architecture has been the superheterodyne technique. Patented in the United States by Edwin Armstrong in 1920 [13], the superheterodyne receiver method solved several problems at the time by down-converting the received radio frequency signal to a lower intermediate frequency where filtering and amplification could be more easily implemented.

A block diagram of a simplified superheterodyne receiver is shown in Figure 2.4. The signal received by the antenna is filtered using a bandpass filter (BPF) and then amplified by a low-noise amplifier (LNA). A local oscillator (LO) signal is generated and its frequency is multiplied, if necessary, to the required value. The RF signal is

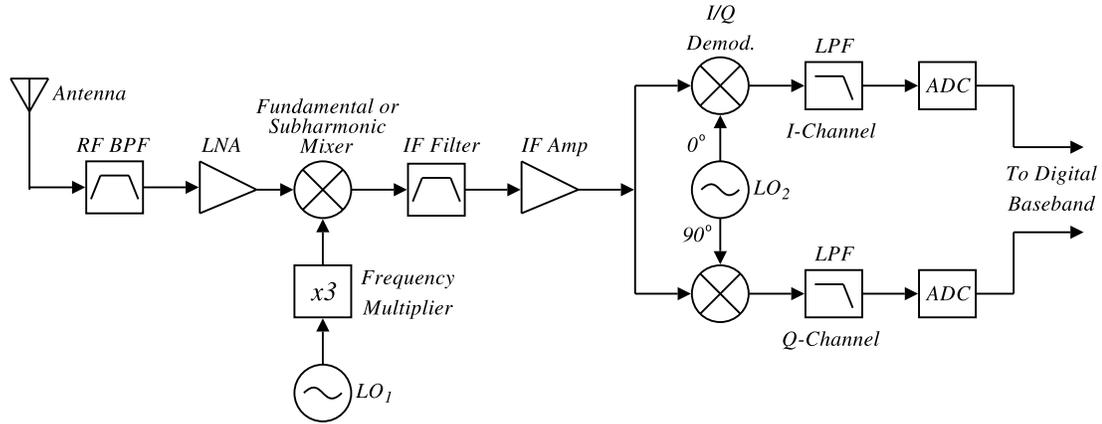


Figure 2.4: Block diagram of a superheterodyne receiver.

down-converted to a lower frequency (IF) for further processing using a mixer. After the signal has been down-converted to IF, it is filtered and amplified. The IF filter is often implemented off-chip using a surface acoustic wave (SAW) filter, which is a significant disadvantage to using the superheterodyne technique and can be avoided by using direct-conversion (discussed in the next section). An I/Q demodulator is then used to convert the signal to baseband. The demodulator uses another LO and two more mixers to convert the signal to baseband where it goes through a low-pass filter (LPF) and is then converted to the digital-domain via the analog-to-digital converters (ADC) where it can be processed further. While only one IF stage is shown in Figure 2.4, in some applications there would be two or more intermediate frequency stages.

The work in this thesis on subharmonic mixers could be implemented in several places in the block diagram of the superheterodyne receiver shown in Figure 2.4. First, any or all of the three mixers shown in Figure 2.4 could be subharmonic mixers. Since subharmonic mixers internally multiply the frequency of the LO, a lower LO frequency

could be used, which has several potential benefits such as ease of design and improved oscillator phase noise. A reduction in oscillator phase noise can ultimately result in a lower receiver noise figure and improved receiver sensitivity. Furthermore, at very high frequencies (e.g. millimeter-wave), it may not be possible to realize an LO at the desired frequency and there may be no choice but to use a subharmonic mixer or a frequency multiplier. A reduction in the DC power consumption of the local oscillator might also be possible since it operates at a much lower frequency when using a subharmonic mixer, which would ultimately result in a longer battery life for portable electronics. Of course, the savings in LO power consumption needs to be compared to any additional DC power required by a subharmonic mixer over a fundamental mixer. A frequency multiplier is shown in Figure 2.4 connected to the output of a local oscillator. In this thesis, a new design for a frequency tripler is proposed that is based on a subharmonic mixer. Also demonstrated in this thesis is a new quadrature oscillator circuit that could be used for the LOs in Figure 2.4. Subharmonic mixers could also be used in the transmitter in a similar way in order to lower the LO frequency.

2.2.2 Direct-Conversion

As discussed in the previous section, superheterodyne receivers convert the RF signal to a lower IF where it is filtered and amplified. While IF amplification is easily achieved on an integrated circuit, realizing a high-performance IF filter on-chip is very difficult. In fact, an external filter (often a SAW filter) is usually required, and therefore it is not possible to design an entire system-on-a-chip (SoC). In a direct-conversion receiver, the RF signal is converted directly to baseband, and as such there

is no image frequency to reject and no off-chip components are required.

A block diagram of a simplified direct-conversion receiver is shown in Figure 2.5. This receiver architecture clearly requires fewer components than the superheterodyne receiver in Figure 2.4. Most importantly, there are no IF filters required, since the RF signal is converted directly to baseband. After the signal is received by the antenna, it is filtered in the bandpass filter and amplified in the LNA. The RF signal is then converted directly to baseband by using mixers and an LO that has a frequency equal to the RF carrier. The down-converted signal is then low-pass filtered and amplified before being converted to the digital domain.

While the elimination of the IF filter is a significant advantage to using direct-conversion, there are challenges that must be overcome in order to use this architecture, one of the most significant of which is LO self-mixing, which can seriously degrade performance through increased noise and intermodulation distortion [14]. Since the RF carrier is converted to DC, any DC offsets that are created by the mixer

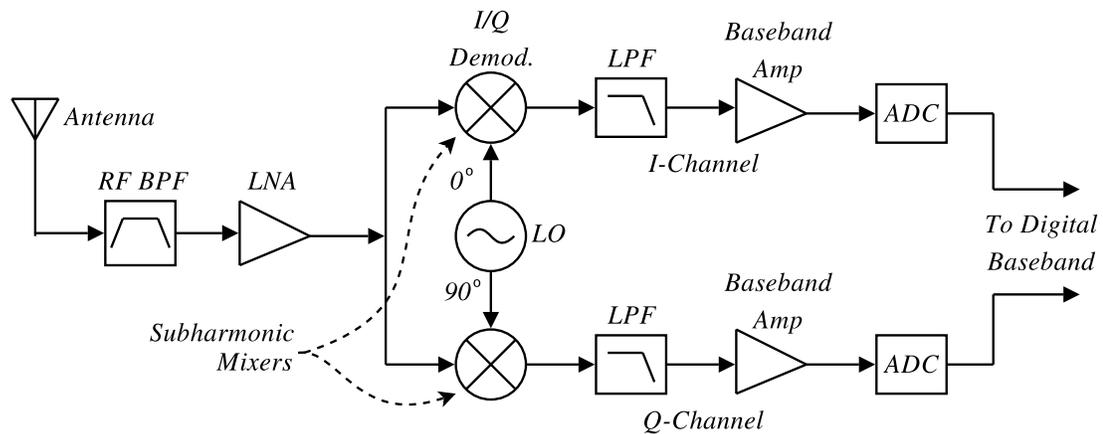


Figure 2.5: Block diagram of a direct-conversion receiver.

itself can interfere with the desired signal since many efficient modulation formats have significant spectral content at or near DC (e.g. GMSK, QPSK, etc.). Given that the LO is generally a strong signal, it can easily couple to various circuits on the chip, which can result in a DC offset from the LO signal mixing with itself. There are several possible paths for LO self-mixing, as shown in Figure 2.6 [15]. Path 1 represents the LO signal that is coupled to the RF port of the mixer, which will then mix with itself and produce a DC offset. Path 2 represents LO coupling to the input of the LNA, which can be particularly problematic since it will then be amplified along with the RF signal before entering the RF port. Path 3 in Figure 2.6 represents the LO signal coupling to the antenna where it is radiated and reflections of this signal by nearby objects are received by the antenna and are shown in Path 4. Path 4 can also represent a strong nearby interfering signal that is received by the antenna and could couple to the LO port and self-mix, also producing a DC offset. Whereas Paths 1 and 2 would generate static DC offsets, the results of paths 3 and

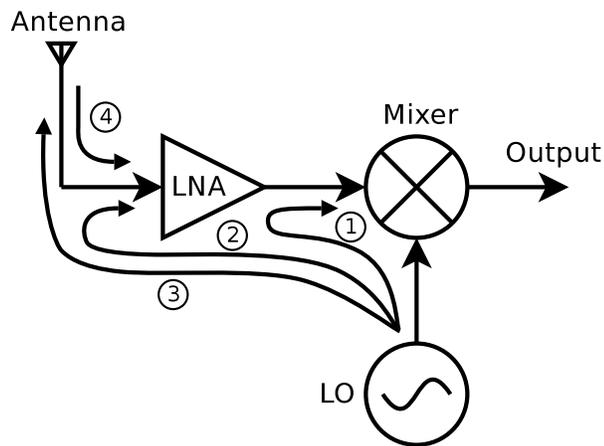


Figure 2.6: Potential LO self-mixing paths.

4 would be dynamic due to the changing operating environment. Complementary metal oxide semiconductor (CMOS) technology, in particular, is very susceptible to LO self-mixing due to the relatively low substrate resistivity that easily allows energy to couple to other sub-circuits on the chip.

To combat the LO self-mixing problem, several techniques have been suggested such as the use of a frequency doubler at the output of the LO [16] and the use of a subharmonic mixer. While fundamental mixers could be used in Figure 2.5, subharmonic mixers are very attractive in direct-conversion receivers since they can reduce LO self-mixing by using an LO frequency that is much lower than the RF. Furthermore, since the frequency of the LO is reduced there can be significant additional benefits regarding performance and ease of design, as discussed previously.

2.3 Mixer Circuit Review

In this section, a literature review of current state-of-the-art mixer circuits will be discussed. Fundamental mixers will first be explored, followed by $2\times$ and $4\times$ subharmonic mixers.

2.3.1 Fundamental Mixers

2.3.1.1 Diode-Based Mixers

The use of diodes in mixer circuits is extensive. Recent research on diode-based mixers generally focuses on very high-frequencies where the use of more complex techniques (e.g. the Gilbert-cell, discussed in the next section) are not possible due to limited high-frequency transistor performance. Since the work in this dissertation is focused

on FET-based mixers, a literature review of diode-based mixers is beyond the scope of this thesis.

2.3.1.2 FET-Based Mixers

A plethora of mixer circuits have been realized using field-effect transistors, the most popular of which is the Gilbert-cell, shown in Figure 2.7 [17]. This mixer can easily be implemented monolithically using either bipolar transistors or field-effect transistors and has several advantages such as excellent isolation between its ports due to its double-balanced structure and can have a reasonably high conversion gain.

The operation of the Gilbert-type mixer is as follows. The differential RF signal is fed into the gates of the bottom two transistors, $M1$ and $M2$, and the differential LO signal is applied to the upper transistors ($M3$ – $M6$). The upper two pairs of transistors

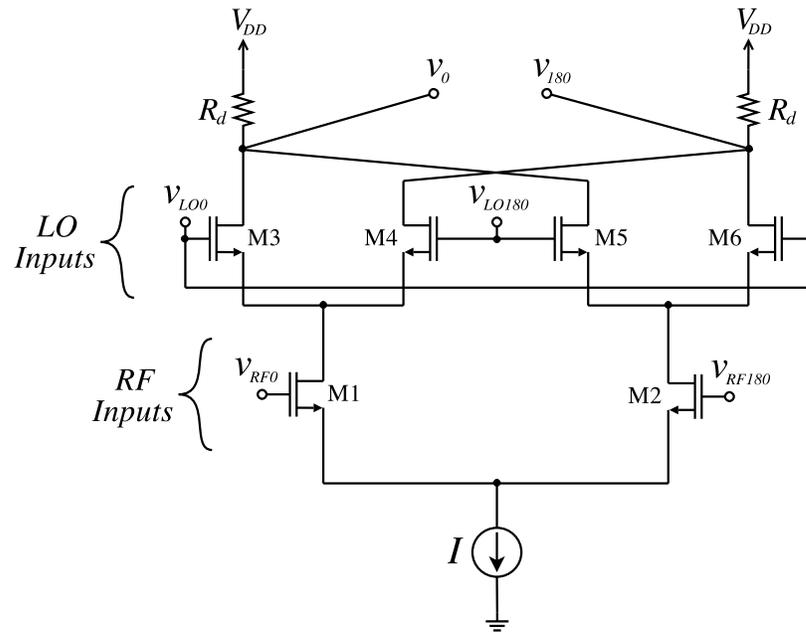


Figure 2.7: Gilbert-cell mixer.

are cross-coupled and act as current switches, changing the polarity of the currents flowing through the drain resistors, R_d . The output signal is taken differentially between v_0 and v_{180} . Degeneration resistors can be inserted in the sources of the bottom (RF) transistors to provide feedback and improve the linearity of the mixer. Inductors are also commonly used for this purpose, and are preferable from a noise standpoint, since, ideally, they do not contribute any noise to the system. Of course, all real inductors have an associated resistance that generates noise, but there can still be a significant reduction in the overall noise figure for the mixer by using this technique. The drawback to using degeneration inductors is the additional IC area that they require. Using on-chip degeneration inductors will use much more area than resistors, and thus will increase the cost of the chip.

Since this mixer circuit has two stacked transistors, and possibly more depending on how the current source is implemented, the use of this circuit topology may not be possible in a low-supply voltage, low-power application. The noise-figure of Gilbert-cell mixers is obviously technology-dependent, but it can be somewhat high since there are at least six active devices contributing noise, as well as possibly two or more resistors. The input reflection coefficient to a Gilbert-cell mixer will be very high due to the high input impedance presented by the gates of the FETs since they are predominantly capacitive. To obtain a reasonably good input impedance match, a matching network is typically required if the mixer is to be used as a discrete component. This matching network can be implemented using on-chip inductors and capacitors, or off-chip with packaged inductors/capacitors or transmission line structures. A matching network on-chip will use a significant area, which will increase the cost of the circuit. Off-chip matching networks generally require taking the signal

off-chip and then back on which adds noise to the system and the losses may result in the need for additional amplification.

A recent example of a CMOS Gilbert-cell is presented in [18]. In this work, CMOS 0.13 μm technology was used to realize a wideband 9 GHz to 50 GHz down-convert mixer. This circuit used the basic Gilbert-cell shown in Figure 2.7 with a couple of additions. First, on-chip transformers were used to convert the single-ended RF and LO signals to differential. At the output, source follower buffers were used to drive the 50 Ω load of either the measurement equipment or the next stage in the receiver. Finally, a current injection technique was used to increase the g_m of the RF transistors, and improve the overall conversion gain. The mixer achieved a measured conversion gain of over 5 dB from 9 GHz to 50 GHz and $RF-IF$ isolations of over 40 dB and $LO-RF$ isolations over 20 dB in this frequency range. The IIP3 of the mixer at 20 GHz was 1.2 dBm and the noise figure (DSB) was 16.4 dB. The power consumption of the circuit was 97 mW and the chip was relatively compact at $0.5 \times 0.5 \text{ mm}^2$.

In [19], another wideband CMOS Gilbert-cell mixer was presented that operated from 0.3 GHz – 25 GHz. LC ladder matching networks were used to achieve such a wideband input impedance match. The conversion gain was approximately 10 dB from 10 GHz to 25 GHz and the return loss was better than -7 dB from 3 GHz to 25 GHz. The $RF-LO$ and $LO-RF$ isolations were better than 25 dB. The power consumption of the mixer core was 71 mW. Due to the inductors that were integrated on-chip, the area of the IC was larger than otherwise would be necessary at $0.8 \times 1.0 \text{ mm}^2$.

While the most common type of FET mixer is the Gilbert-cell topology (or variations thereof), there are many other FET circuits that can be used to realize a

fundamental mixer. For example, one popular technique is the resistive FET mixer, shown in Figure 2.8. Resistive mixers using FETs are passive mixers that use the nonlinearity of the FET resistance to enable mixing. More specifically, since the LO is generally a large signal, the non-linear characteristics of the transistor alter the FET resistance with the LO signal. The FET is generally biased in the resistive, or triode region of operation, and filters are used for the RF and IF ports. Advantages of resistive FET mixers include their relative simplicity (compared to Gilbert-cell mixers, for example) and that they generally do not consume any DC power. However, they can have significant conversion losses which offsets these advantages. An example of a FET resistive mixer from the literature is given in [20]. In this work, 90 nm CMOS silicon-on-insulator (SOI) technology was used to realize a 26.5 GHz to 30 GHz resistive mixer. The circuit in Figure 2.8 was used in [20] with parallel LC filters for both the RF and IF ports as well as an LO gate inductor for matching. The conversion loss for this circuit was between 9 dB and 13 dB from 26.5 GHz to

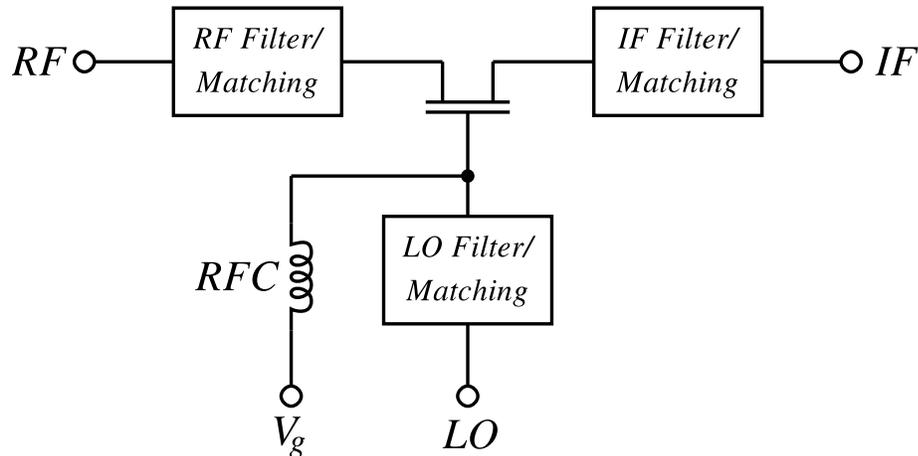


Figure 2.8: Resistive FET mixer.

30 GHz with an LO power of 5 dBm. The IIP3 was 12.7 dB and the single-sideband noise figure was 11.4 dB. The measured isolations were between 22 dB and 33 dB for all ports.

2.3.2 Subharmonic Mixers

As discussed previously, direct-conversion receivers convert the received signal directly to baseband as opposed to first converting to an intermediate frequency. The primary advantage to using direct-conversion is that there is no image frequency produced, and, consequently much simpler and inexpensive filtering can be used. To this end, and to take advantage of the benefits of a lower LO frequency, there have been many $2\times$ subharmonic mixers (SHMs) demonstrated in the literature. There are a large number of $2\times$ SHMs based on the APDP configuration discussed earlier in this chapter, however, there are also many transistor-based $2\times$ SHMs. Since the circuits proposed in this thesis are FET-based SHMs, the $2\times$ SHM literature review section will focus on transistor-based subharmonic mixers. In a following section that examines existing $4\times$ subharmonic mixers there will be a discussion of several APDP SHMs, since these are the dominant type of $4\times$ subharmonic mixers.

2.3.2.1 $2\times$ Subharmonic Mixers

There have been many $2\times$ SHMs proposed (e.g. [21–37]). In most cases (e.g. [22, 23, 31–33, 35, 36]), modifications to the Gilbert-cell mixer (Figure 2.7) were made in order to generate the double frequency LO component to mix with the RF. One common modification to the Gilbert-cell to enable subharmonic mixing is by using an additional level of LO switching transistors and using quadrature LO signals rather

than differential [25, 28, 31, 35]. This circuit, shown in Figure 2.9 with bipolar transistors, has three-levels of transistors with the 0° and 180° LO signals applied to the gates of the *middle* LO-transistor level, and the 90° and 270° LO signals applied to the gates of the *top* LO-transistors. This configuration generates the doubled LO frequency signal, $2f_{LO}$, that mixes with the differential RF signal that is applied to the gates of the *bottom* transistors. Since this technique requires three levels of transistors, it generally requires a higher DC supply voltage than the basic Gilbert-cell and its use may not be possible in low-voltage applications. The topology shown

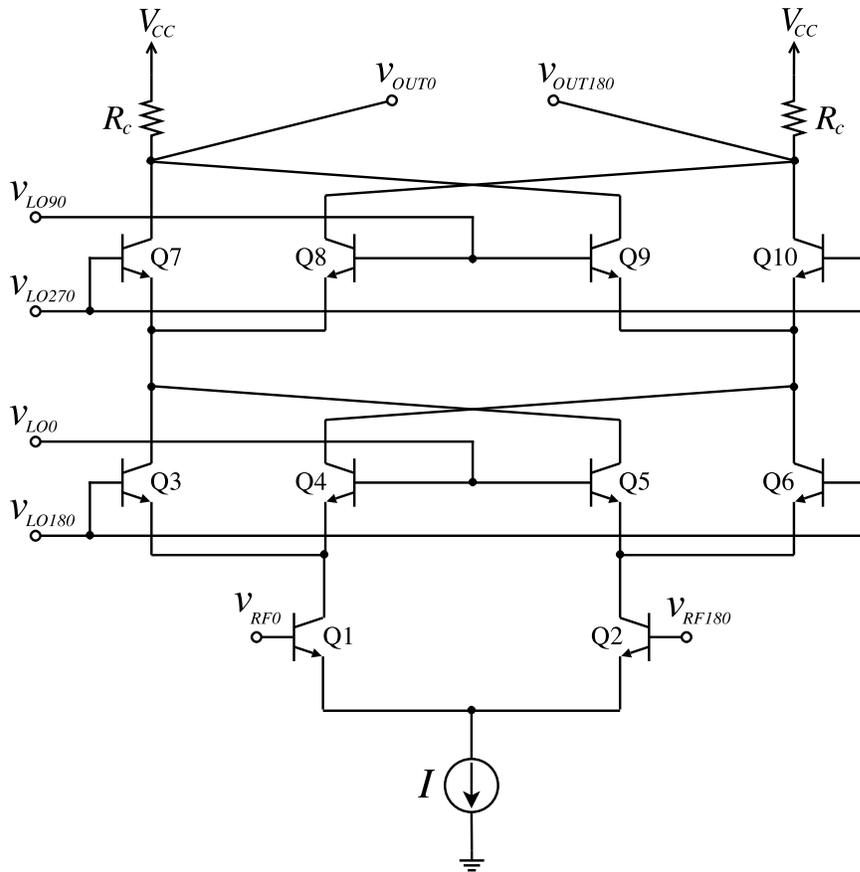


Figure 2.9: Basic $2\times$ subharmonic mixer circuit used in [25, 28, 31, 35].

in Figure 2.9 was introduced by [35], where it was implemented using a Si/SiGe HBT technology and using passive on-chip RC phase shifters to generate quadrature LO signals. This circuit was designed for direct-conversion applications with an RF signal from 1 GHz to 2 GHz and an LO frequency from 500 MHz to 1 GHz. With a DC supply voltage of 2.5 V, the measured conversion gain was 13.5 dB with an LO power of 10 dBm, a double sideband (DSB) noise figure of 10.4 dB, an IIP2 of 29.7 dBm, and an IIP3 of -3.5 dBm.

The circuit shown in Figure 2.9 was also used in [31] with a SiGe BiCMOS process. Polyphase filters were used to generate the required quadrature LO signals in this work and the circuit was designed for RF signals from 5 GHz to 6 GHz and an IF of 50 MHz. The voltage conversion gain of the mixer was measured to be 6 dB, with an IIP2 of 29 dBm. The $2LO-RF$ isolation was measured to be greater than 55 dB and the $LO-RF$ isolation was greater than 50 dB. The power consumption for the mixer was 16.5 mW and the chip area was $2.3 \text{ mm} \times 1.8 \text{ mm}$.

A circuit similar to the one in Figure 2.9 was also used in [28], however, in this work CMOS $0.13 \mu\text{m}$ technology was used and the circuit was adjusted for passive operation. The circuit was designed for 24 GHz direct-conversion applications and used an RF preamp as well as LO and IF buffers. The quadrature LO signals were generated using an off-chip 90° hybrid along with on chip active baluns. The measured overall conversion gain of the circuit was 3.2 dB and the DSB noise figure was 10 dB. The 1-dB compression point was -12.7 dBm and the power consumption including the RF preamp and buffers was 13.6 mW. The measured $2LO-RF$ isolation was 57 dB and the size of the fabricated chip was $0.9 \text{ mm} \times 0.65 \text{ mm}$.

Yet another implementation of the basic subharmonic mixer circuit shown in Figure 2.9 is presented in [25]. In this work, an $RC-CR$ phase shifter network is used to generate the required quadrature LO signals and CMOS 0.18 μm technology was used for RF input signals in the 5 GHz band. The measured maximum conversion gain of this circuit was 9.5 dB and the $LO-RF$ isolation was 48 dB. The IIP3 was -7.5 dBm, the 1-dB compression point was -20 dBm, and the power consumption was 17.5 mW.

A different modification to the Gilbert-cell to enable $2\times$ subharmonic mixing is demonstrated in [36] using a 0.35 μm BiCMOS technology. This circuit, which is shown in Figure 2.10, uses only two levels of transistors similar to the traditional Gilbert-cell, however, it exchanges the position of the LO and RF transistor (i.e. the LO transistors are on the *bottom* and the RF transistors are on the *top*). Similar to the circuit in Figure 2.9, quadrature LO signals are also required for this topology. In [36], the quadrature signals were generated on-chip from a differential LO input using $RC-CR$ networks. The circuit in [36] was designed for an RF signal at 1.9 GHz and an LO signal at 900 MHz (a 100 MHz IF). The measured conversion gain for this circuit was 7.5 dB and the single-sideband (SSB) noise figure was 10 dB. The input 1-dB compression point was -8 dBm and the IIP3 was -3 dBm. The power consumption was 24 mW.

A comparison between the three most common transistor-based $2\times$ subharmonic mixers circuits is presented in [33]: (1) the circuit in Figure 2.9 (three-level), (2) LO transistors on the bottom (Figure 2.10), and (3) LO transistors on the top (not shown, but used in [23]). It was found through this comparison that the circuit topology in Figure 2.9 can operate with the lowest LO power levels, but requires a

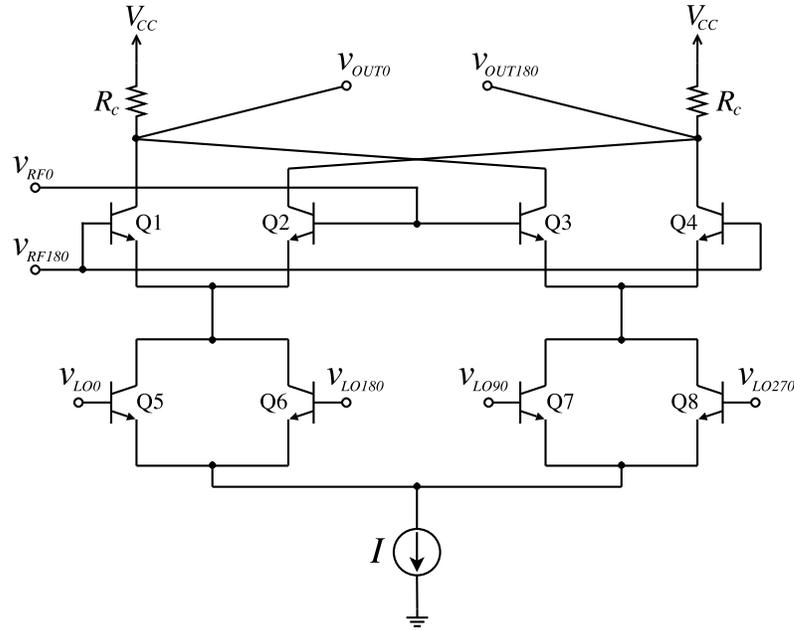


Figure 2.10: Subharmonic mixer circuit proposed in [36].

higher DC voltage supply compared to the other two topologies. Furthermore, the circuit in Figure 2.9 has the lowest maximum operating frequency out of the three topologies. The bottom-LO SHM shown in Figure 2.10 has advantages in terms of power consumption, linearity, $RF-IF$ isolation, and noise figure. The third topology discussed (LO transistors on top, [23]) can achieve a higher conversion gain and higher $2LO-RF$ isolation.

Clearly, from the preceding discussion of $2\times$ subharmonic mixers, the requirement of quadrature LO signals is very common (e.g. [22–25, 28, 32, 36]). Furthermore, in [29–31], octet-phase signals of the LO were used with subharmonic mixers.

There are several circuits that have been used to realize $2\times$ subharmonic mixers using FETs that are not based on the Gilbert-cell. For example, in [37], the RF

signal was applied to the gate of a FET while the LO signal was applied to the bulk connection of the FET (using CMOS 0.18 μm technology). This technique of injecting the LO signal into the bulk of the transistor has the effect of modulating the threshold voltage and exploiting the non-linearity that results to realize a subharmonic mixer. The measured conversion gain in [37] was 10.5 dB with an RF frequency of 2.1 GHz and LO frequency of 1.025 GHz. The input 1-dB compression point was -12 dBm and the IIP3 was -3.5 dBm. The measured noise figure (DSB) was 17.7 dB and the power consumption was 2.5 mW.

As a final example of a $2\times$ subharmonic mixer, a 9 GHz to 31 GHz $2\times$ subharmonic passive mixer was demonstrated in 90 nm CMOS technology in [21]. A simplified schematic of the circuit used in [21] is shown in Figure 2.11. This basic circuit can operate with either the RF signal applied to the gate and the LO applied to the source, or vice-versa (LO-source-pumped or LO-gate-pumped, respectively). The capacitor

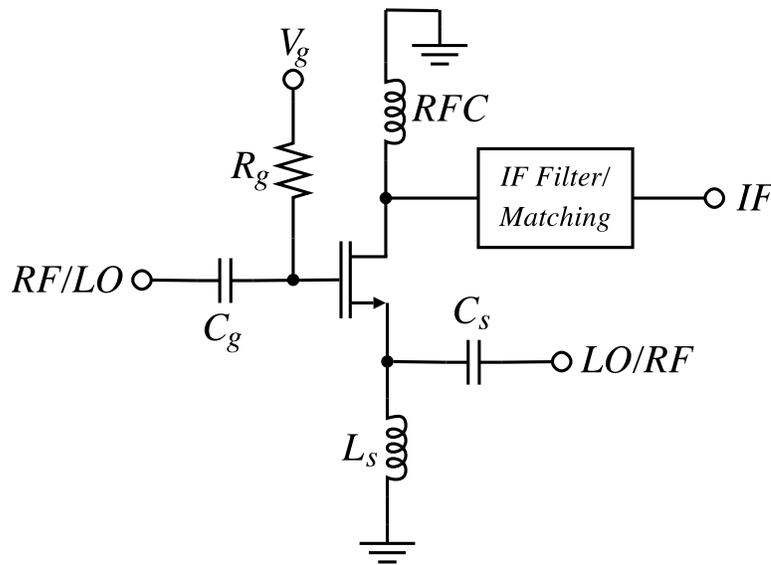


Figure 2.11: Passive FET subharmonic mixer.

C_g is used primarily as a DC-block and L_s and C_s are used as a high-pass filter and for input matching. The FET's gate bias is provided by V_g through a large resistor, R_g . Since it is a passive mixer, there is no DC current through the transistor (both the drain and source are DC-ground). The implementation of the circuit in Figure 2.11 in [21] used a π -network composed of two capacitors and one inductor to implement a low-pass filter at the IF output. This circuit is unique in that it can operate with either a $\frac{1}{2}f_{LO}$ or $\frac{1}{3}f_{LO}$ (i.e. either a $2\times$ or $3\times$ SHM). The conversion loss for the $2\times$ SHM-mode was between 8 dB to 11 dB over the RF frequency range and it was 12 dB to 15 dB for the $3\times$ SHM-mode over the RF frequency range. The IIP3 was 3 dBm for the $\frac{1}{2}$ -LO source pumped mode and 7 dBm for the $\frac{1}{3}$ -LO source-pumped mode. The minimum $2LO-RF$ isolation for the $\frac{1}{2}$ -LO source-pumped mode was 27 dB over the band of operation and the minimum $3LO-RF$ isolation was 45 dB for the $\frac{1}{3}$ -LO source pumped mode. The dimensions of the fabricated chip were $0.9 \text{ mm} \times 1.0 \text{ mm}$ and given its passive operation there was no DC power consumption used by this SHM.

2.3.2.2 $4\times$ Subharmonic Mixers

There have been several $4\times$ SHMs previously demonstrated [38–43]. The vast majority of these circuits used diodes to perform the mixing, which eliminates the possibility of achieving conversion gain. As discussed previously, it is possible to use an anti-parallel diode pair for subharmonic mixing, and this diode configuration conveniently cancels some of the undesired mixing products. In fact, nearly all $4\times$ SHM circuits use an APDP and filters in configurations such as the one shown in Figure 2.12.

For example, in [41], an APDP was used for a direct-upconverter using the

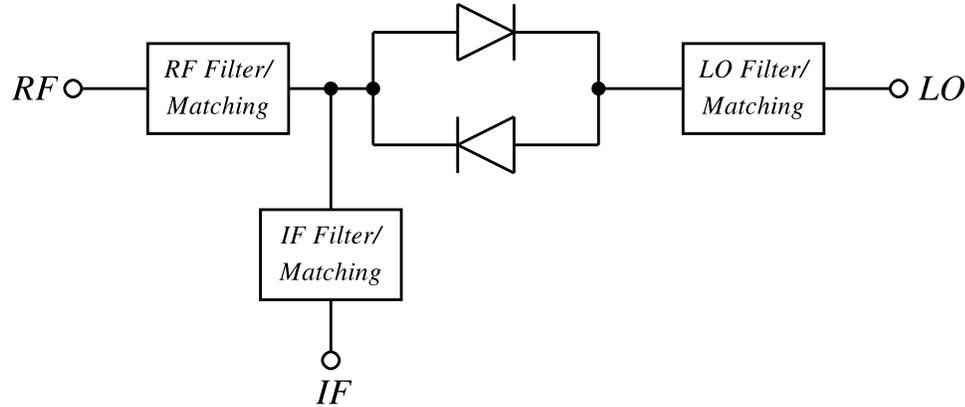


Figure 2.12: Subharmonic mixer using an anti-parallel diode-pair.

basic circuit shown in Figure 2.12. The RF and IF filters were implemented by an RF/baseband duplexer that used coupled-line filters combined with a stepped impedance low-pass filter and rejection stubs. A transmission line matching network was used for the LO signal to minimize the LO input reflection coefficient. In this work, a baseband input signal was used along with a ~ 10 GHz LO signal to produce a ~ 40 GHz RF output signal. The measured isolation between the RF and IF (baseband in this case) ports was greater than 30 dB. The conversion loss of this hybrid microwave circuit was quite high (21 dB to 15 dB, as the LO power is increased from 6 dBm to 11 dBm).

An MMIC implementation of the APDP circuit shown in Figure 2.12 was presented in [39]. In this work, a 94 GHz quadruple subharmonic mixer ($4\times$ SHM) was designed and measured using GaAs MESFET technology. A coupled-line bandpass filter was used for the RF port and stub filters were used at the IF and LO ports. The 94 GHz RF input signal was mixed with a ~ 23.5 GHz LO input signal to down-convert the RF to a 100 kHz IF. The maximum conversion gain for this design was measured

to be -11.4 dB at an LO input power of 10 dBm and the input 1-dB compression point of this SHM was approximately -6 dBm. The fabricated chip dimensions were $0.9 \text{ mm} \times 1.4 \text{ mm}$.

In [40], a $4\times$ SHM was presented again using APDP in a hybrid implementation with two packaged diodes and a 10 mil duroid substrate. The RF signal used in this work was in the upper Ka-band (38.5 GHz to 40 GHz) and the LO frequency was in X-band, which produced a IF output centered at 2.5 GHz. Matching and filtering for all three ports was accomplished primarily with transmission line stub filters. The minimum conversion loss of this circuit was measured to be 9 dB and the return loss for the RF, IF, and LO ports was approximately -20 dB, -20 dB, and -15 dB, respectively.

In the GaAs-based MMIC APDP-based $4\times$ subharmonic mixer presented in [38] a number of anti-parallel diodes were used in addition to transmission line stub filters in order to extract the signal at $(\omega_{RF} - 4\omega_{LO})$. More specifically, this design replaced the single APDP shown in Figure 2.12 with a triple diode implementation (six diodes in total with three in each direction). The purpose of the triple APDP was to reduce the diode series resistance in an attempt to decrease the conversion loss of the mixer. The circuit operates with an LO input frequency range from 12 GHz to 16 GHz and RF input frequency range from 50 GHz to 65 GHz. The minimum conversion loss for the circuit is 11 dB with a 7 dBm LO input signal. The $LO-IF$ isolation was measured to be as low as 17 dB and the $LO-RF$ isolation was measured to be as low as 33 dB in the intended frequencies of operation (other isolation measurements, such as $4LO-RF$ were not given). Linearity measurements were not reported for this work.

As a final example of a $4\times$ SHM based on the APDP circuit shown in Figure 2.12, a V-band MMIC was presented in [42]. This work used GaAs PHEMT technology along with CPW transmission lines. Stub filters were used for the RF and LO signals, while lumped element inductors and capacitors were used for IF matching and low-pass filtering. In addition to the APDP, this design also used FETs for amplification, which enables the possibility of obtaining conversion gain from the overall circuit (the APDP that does the actual mixing of course still has a conversion loss). The LO frequency was 14.5 GHz and the RF signal was 60.4 GHz, producing an IF output at 2.4 GHz. The maximum measured conversion gain was 0.8 dB for an LO input power of 12 dBm. The $LO-RF$ and $LO-IF$ isolations were both higher than 40 dB. The dimensions of the fabricated MMIC were $1.9\text{ mm} \times 2.6\text{ mm}$.

One of the very few instances where a $4\times$ subharmonic mixer has been demonstrated not using diodes is presented in [43]. In this work, GaAs MESFETs were used in a cascode configuration along with several stubs for RF and LO port filtering. The FETs were used to generate and enhance the fourth harmonic of the LO input signal and then mix it with the input RF signal. Lumped inductors and capacitors were used at the IF output for both matching and low-pass filtering. The RF range for this circuit was from 59.4 GHz to 60.9 GHz with an LO input frequency of 14.5 GHz. The measured conversion gain was 2.5 dB to 3.4 dB for an LO input power of 13 dBm. Isolation measurements showed an $LO-RF$ isolation of 46.2 dB and an $LO-IF$ isolation of 53.6 dB. The fabricated chip dimensions were $1.9\text{ mm} \times 1.8\text{ mm}$.

Generally, and as would be expected, $4\times$ SHMs have more loss than $2\times$ SHMs, which in turn generally have more conversion loss than fundamental mixers. In most cases, $4\times$ subharmonic mixers do not exhibit a conversion gain.

2.4 Oscillators Circuit Review

Oscillators are fundamental components in wireless communications systems that can be used for several applications. Communication systems that use phase shift keying modulation frequently require a pair of LO signals that are in quadrature, or 90° out-of-phase. Furthermore, quadrature signals are commonly required in direct-conversion receivers or low-IF systems as well as in digital radio communication systems such as GSM and DECT [44]. Every mixer, whether fundamental, or subharmonic, requires a local oscillator signal, and as such, a literature review of CMOS oscillator circuits will be presented in this section.

2.4.1 Resonators for CMOS Microwave Oscillators

A microwave resonator is the component in a microwave oscillator that determines the frequency of oscillation. There are many ways to implement a resonator. The decision as to which type to use can depend on many factors, such as operational frequency, required performance, cost, and required area. A resonator can be as straight-forward as a series or parallel LC network, and in fact, almost all CMOS oscillators use simple LC resonators. Regardless of what type of resonator is used, most resonators can be modeled as a parallel or series RLC circuit around resonance.

The resonant frequency for parallel and series RLC resonant circuits is given by:

$$\omega_0 = \frac{1}{\sqrt{LC}}. \quad (2.17)$$

The quality factor, or Q -factor, is a characterization of the loss of a resonant structure (higher Q implies lower loss). It is defined as

$$Q = \omega \frac{\text{Average energy stored}}{\text{Energy loss per second}} \quad (2.18)$$

and for a series RLC circuit, it is:

$$Q = \frac{1}{\omega_0 RC}. \quad (2.19)$$

For a parallel RLC circuit, the Q -factor is given by:

$$Q = \omega_0 RC. \quad (2.20)$$

LC resonators are the easiest to implement on-chip at relatively low microwave frequencies, and are the type used for most CMOS oscillators. However, the Q -factor of the resonant circuit can be quite low due primarily to the low quality factor of the inductor, which can lead to poor phase noise performance. In fact, the phase noise of an oscillator is proportional to $1/Q^2$. Therefore, by improving the Q -factor of the inductor (which is usually the limiting element in the Q -factor of an LC resonator) the performance of the oscillator can be vastly improved.

Spiral inductors in standard CMOS technology are often modeled as shown in Figure 2.13 [45]. In this model, L_s is the low-frequency inductance, R_s is the series resistance of the coil, C_s is the capacitance between the different windings of the inductor, C_1 and C_2 are the capacitances in the oxide layer between the coil and the substrate, C_{p1} and C_{p2} are the capacitances between the coil and the ground through the silicon substrate, and R_{p1} and R_{p2} are the eddy current losses in the substrate. This model has proven to be an accurate representation of CMOS inductors and is used extensively. While minor performance improvements can be obtained in CMOS inductors by using patterned ground shields [46], they are generally limited to about $Q < 20$ by the intrinsic properties of the CMOS process (and often have a Q -factor of about 5 in CMOS 0.18 μm technology). It is therefore very difficult to design an oscillator in CMOS technology that has very low phase noise.

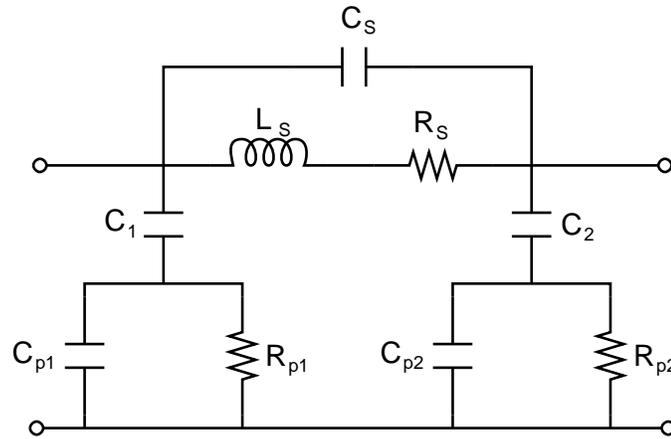


Figure 2.13: Common model used for CMOS inductors.

2.4.2 Common Oscillator Topologies

There are many different oscillator topologies that can be used to implement microwave oscillators in CMOS technology. This section will focus on the state-of-the-art for two of the most common oscillator topologies in CMOS: the Colpitts oscillator and the cross-coupled FET oscillator. Lastly, techniques for generating quadrature output signals are discussed.

2.4.2.1 Colpitts Oscillator

A very common oscillator circuit that can easily be implemented monolithically is the Colpitts oscillator, one configuration of which is shown in Figure 2.14. The detailed analysis of this circuit is covered in many standard microelectronics texts (e.g. [47]) and will not be repeated here. Essentially, the circuit oscillates by providing positive feedback from a capacitive voltage divider to an amplifier. The oscillation frequency

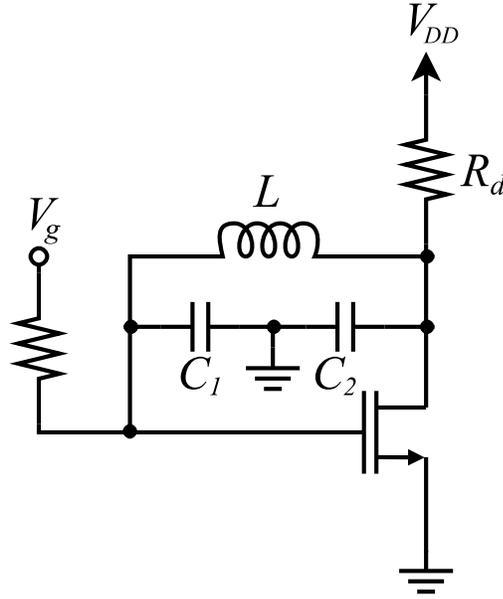


Figure 2.14: Colpitts oscillator circuit.

is given by:

$$\omega_0 = \frac{1}{\sqrt{LC_{eq}}} \quad (2.21)$$

where

$$C_{eq} = \frac{C_1 C_2}{C_1 + C_2}. \quad (2.22)$$

This circuit is more applicable to CMOS integration compared to other variants of this oscillator topology. For example, the Hartley oscillator uses a tapped inductor for feedback rather than a tapped capacitor, and is therefore much less attractive for CMOS implementations. Of course, the performance of this oscillator will be primarily determined by the quality of the resonator, and thus the quality of the inductors and capacitors used.

An example of a CMOS Colpitts oscillator from the literature is demonstrated

in [48]. In this work, a 5 GHz Colpitts oscillator using 0.18 μm technology was presented. A differential form of the standard Colpitts oscillator was used along with varactors in the place of static capacitors. In the differential version of the Colpitts oscillator, two single-ended Colpitts oscillators (Figure 2.14) were coupled to ensure odd-mode oscillation (and suppression of even-mode oscillation). The tuning range of the circuit was from 4.61 GHz to 5.0 GHz and the output power was 4 dBm. The phase noise was measured to be -120.42 dBc/Hz at a 1 MHz offset and the DC power consumption of the oscillator core was 3 mW.

2.4.2.2 Cross-Coupled MOSFETs

The cross-coupled FET oscillator is the most common microwave oscillator topology used in CMOS technology. An LC oscillator can be modeled with the capacitor and inductor in parallel with a resistor to model the losses in the tank as well as a negative resistance that models the active device. One way of generating the negative resistance to compensate for the losses in the LC tank is to use a cross-coupled differential pair as shown in Figure 2.15. The resistance, R_{in} , looking into the cross-

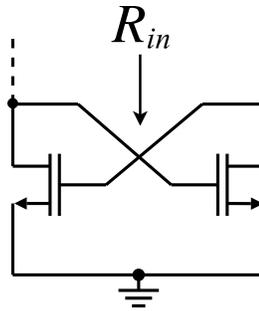


Figure 2.15: Negative resistance generated from cross-coupled FETs.

coupled pair is given by:

$$R_{in} = -\frac{2}{g_m}, \quad (2.23)$$

where g_m is the transconductance of each of the FETs in the cross-coupled pair. Therefore, with an appropriate device size and biasing, the value of negative resistance required to counteract the losses in the tank can be realized. A commonly used LC oscillator circuit using the cross-coupled differential pair is shown in Figure 2.16. In this implementation a relatively low supply voltage is possible since there are only two levels of transistors, but it requires two inductors, which can consume significant chip area.

The oscillator topology shown in Figure 2.16 was used in [49]. In this work, CMOS 0.13 μm technology was used to design a 60 GHz VCO with a 6 GHz tuning range. The capacitor shown in Figure 2.16 was replaced with a varactor to enable the frequency tuning. The signal output power was approximately -10 dBm and the

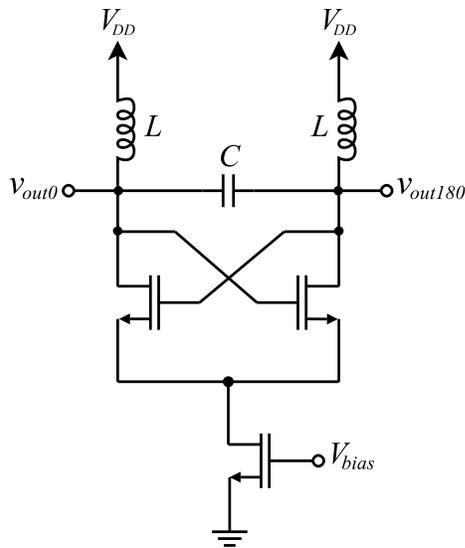


Figure 2.16: Cross-coupled FET oscillator.

phase noise at a 1 MHz offset was -90.7 dBc/Hz.

A slight modification to this topology is shown in Figure 2.17. It has been shown [50] that by including the cross-coupled PMOS transistors at the top of the circuit the phase noise can be reduced considerably. Furthermore, only one inductor is required, which is an advantage over the previous circuit. However, since there are now three levels of transistors, implementations with a very low power supply such as in [51] would not be possible with this configuration. The oscillation frequency for this circuit can be found from the formula for the resonant frequency of an LC tank:

$$f_0 = \frac{1}{2\pi\sqrt{LC_{tot}}}, \quad (2.24)$$

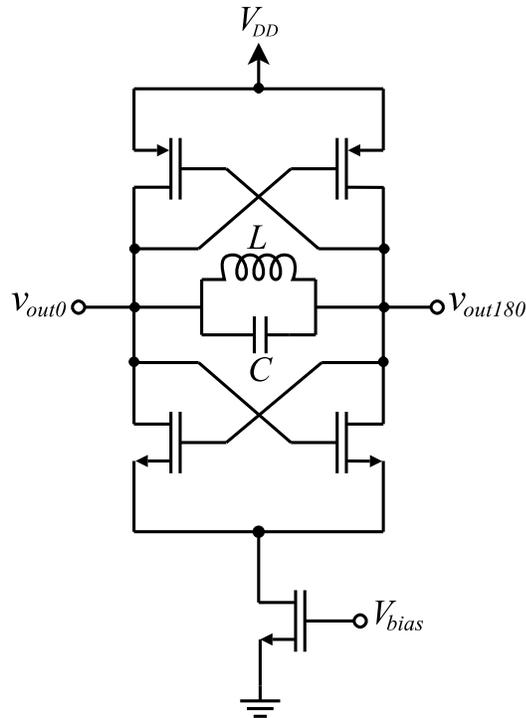


Figure 2.17: Complementary cross-coupled FET oscillator.

where L is the value of the on-chip spiral inductor and C_{tot} is the total capacitance between the drains of the two cross-coupled transistors (including any parasitic capacitance). Of course, by using a varactor instead of the static capacitor in the tank, a voltage controlled oscillator can be realized.

A circuit using the cross-coupled topology shown in Figure 2.17 was described in [52]. Standard CMOS 0.18 μm technology was used in this design to realize a VCO that operates from 9.3 GHz to 10.4 GHz. The phase noise performance was -89 dBc at a 100 kHz offset and the DC power consumption of the VCO core was 5.8 mW. The spiral inductor (0.5 nH) had a Q -factor of 10 while the varactor had a Q -factor of 38.

2.4.2.3 Quadrature Oscillators

The oscillator circuits discussed above produce either a single-ended or a differential output signal. There are several techniques that can be employed to generate quadrature signals. One straight-forward method is to use an RC - CR phase shift network with a standard oscillator to create a 90° phase shift [53]. Since the phase shift is completely dependent on the values of the resistors and capacitors, any deviation in the fabricated values of these components will directly lead to a error in the accuracy of the quadrature signals. Resistors, in particular, have large tolerances in most CMOS processes, and therefore this method can lead to poor accuracy in the quadrature signals that are generated.

Another approach to generate quadrature signals is to use a digital *divide-by-two* frequency divider that follows an oscillator running at twice the fundamental frequency [54]. The use of this technique at high frequencies is inherently limited

since an oscillator operating at double the desired frequency is required.

A third common technique is to force two VCOs to run in quadrature by using coupling transistors working at the fundamental frequency [55]. This technique suffers from a trade-off between quadrature accuracy and phase noise due to the effects of the coupling circuit on the oscillation frequency. To avoid this problem, a quadrature oscillator can be realized using superharmonic coupling. As illustrated in Figure 2.18a, by employing differential coupling at the common-mode nodes where the second harmonic is predominant, quadrature signals are generated at the fundamental frequency. To implement the coupling of the second harmonic with a 180° phase shift, an inverting on-chip transformer has been used [56–58] (Figure 2.18b).

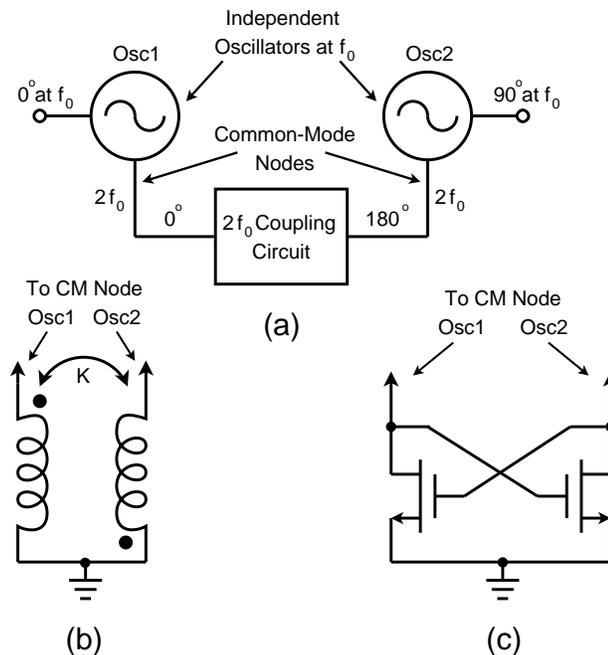


Figure 2.18: Quadrature oscillator superharmonic coupling techniques.

In [57], passive superharmonic coupling was used with an on-chip transformer in $0.35\ \mu\text{m}$ technology to enforce a quadrature relationship between two cross-coupled oscillators (similar to Figure 2.17). This VCO was tunable from 4.57 GHz to 5.21 GHz and achieved a phase noise of $-138\ \text{dBc/Hz}$ at a 1 MHz offset. The output signal power was $-9\ \text{dBm}$, the DC power consumption of the oscillator core was 5.1 mW, and the dimensions of the chip were $1250\ \mu\text{m} \times 1250\ \mu\text{m}$. The disadvantage of the passive superharmonic coupling technique in general is that on-chip transformers consume a significant area on-chip and have a limited Q -factor, particularly in CMOS technology.

A method of replacing the inverting transformer with a cross-coupled differential pair was proposed in [59] (Figure 2.18c), which can significantly reduce the required chip area. In [59], a quadrature voltage controlled oscillator was designed at 6 GHz in SiGe technology using the coupling circuit shown in 2.18c along with two of the oscillator circuits shown in Figure 2.16. The measured output power was $-5.3\ \text{dBm}$ and a 24% tuning range was obtained. The phase noise at a 1 MHz offset was measured to be $-105.8\ \text{dBc/Hz}$.

2.5 Frequency Multiplier Circuit Review

Frequency multiplier circuits are used in a wide range of applications in communication systems. They are fundamental components that are often used to generate a high-quality reference signal, as well as in frequency synthesizers. Using frequency multiplication, oscillators can be designed at lower frequencies and then converted to higher ones, which can simplify the design of the oscillator, possibly improve the phase noise of the resulting signal, and reduce power consumption. The phase noise

of a signal going through a frequency multiplier is degraded by $20\log(n)$, where n is the order of multiplication. However, the resulting phase noise is often an improvement over the performance of an oscillator that is designed to operate directly at the higher frequency. Furthermore, it is also possible that the incorporation of frequency multipliers can reduce the number of voltage controlled oscillators (VCOs) required in multi-band transceivers. Frequency doublers are most often used because they generally offer greater conversion gain (or lower conversion loss) compared to higher-order multipliers. This section will present a literature review of several common frequency multiplier circuits.

2.5.1 Common Frequency Multiplier Topologies

2.5.1.1 Single-FET Frequency Multipliers

Many CMOS frequency multiplier circuits have been demonstrated using various methods. A common technique is to use the nonlinearities of a transistor with a large input signal such as in [60]. A simplified schematic of this type of frequency multiplier circuit is shown in Figure 2.19 as a frequency doubler. With this method, the output has many harmonic spectral components that are generated from the non-linear $I-V$ characteristic of the FET, among which is the desired output frequency signal. As shown in Figure 2.19, input matching at the fundamental frequency is generally used, along with filtering and matching for the desired frequency component at the output. In [60], the basic circuit shown in Figure 2.19 was used to realize a frequency doubler using CMOS 90 nm silicon-on-insulator (SOI) technology. Lumped inductors and capacitors were used for input matching and for output matching/filtering. The DC voltages were applied through the matching/filtering circuits, which elim-

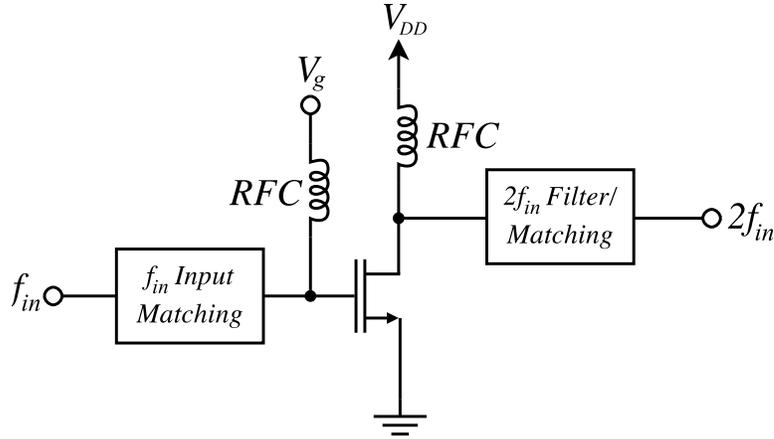


Figure 2.19: Simplified frequency doubler using FET non-linearities.

inated the need for RF chokes. This circuit operated with input signal frequencies between 13.25 GHz and 14.25 GHz to produce an output signal between 26.5 GHz and 28.5 GHz. A maximum conversion gain of 1.5 dB was measured and the input return losses for both ports were approximately 10 dB. The suppression of the fundamental was less than 10 dB at the output, and only 5 dB at the input power level where the conversion gain of 1.5 dB was obtained. The circuit is very compact at $0.37 \text{ mm} \times 0.27 \text{ mm}$ and the DC power consumption was 10 mW.

2.5.1.2 Common-Mode Node Frequency Multipliers

Another frequency multiplier technique is to use the common-mode output nodes of an oscillator. Shown in Figure 2.20 is a simplified circuit demonstrating an injected fundamental signal, f_{in} , which forces the cross-coupled oscillator to lock to this frequency. The doubled frequency, $2f_{in}$ can then be obtained at the common-mode node as shown in the figure. This technique was used in [61] where a regenerative

2.5.1.3 Push-Push Frequency Multipliers

Push-push circuits have also been used for frequency doubling. For example, in [62] a low-power fully differential frequency doubler is presented (shown in Figure 2.21). Essentially, this technique uses switches to connect the output to the 0° input signal in one half of the input signal period, and the 180° input signal during the other half of the input signal period. The resulting waveform at the output resembles an absolute value waveform, which clearly contains a strong second harmonic component. In [62], CMOS $0.25\ \mu\text{m}$ technology was used with a 450 MHz input signal (900 MHz output). The measured conversion loss was 4 dB and the circuit showed strong suppression of the fundamental (over 50 dB in simulations). Given this circuit's complementary structure, it consumes very little DC power. The exact amount of DC power consumed

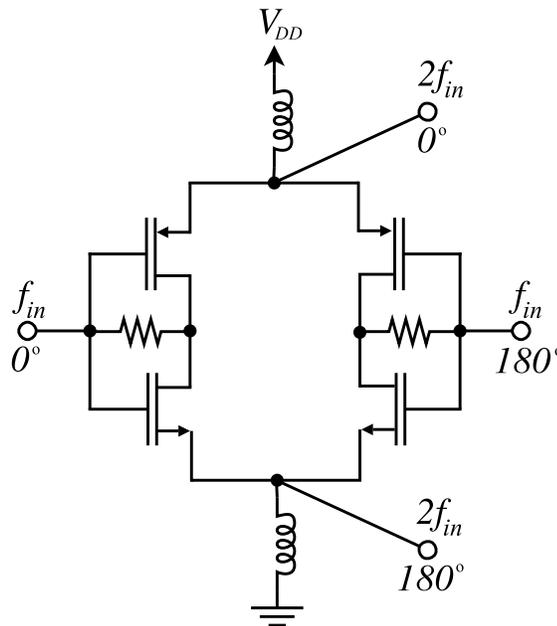


Figure 2.21: Push-push frequency doubler circuit.

by this doubler was not reported (the doubler was combined with a mixer and only the overall DC power consumption was given).

2.5.1.4 Odd-Order Frequency Multipliers

In order to realize odd-order frequency multipliers, such as a frequency tripler, custom-built devices such as heterostructure and quantum barrier varactor diodes [63–65] with strongly non-linear I – V curves are regularly used. To circumvent the use of non-standard semiconductor devices, triplers can be realized by overdriving a transistor with the sinusoidal input signal to generate a clipped waveform rich in odd-order harmonics [66–70]. This method, however, usually requires strong filtering at the output to remove the fundamental and other unwanted frequencies. Often, the filtering has to be accomplished off-chip to improve signal rejection. Balanced frequency tripler circuits based on extracting the third harmonic generated by FET non-linearities are presented in [71, 72] with on-chip filtering and cancellation of unwanted harmonics, but the required chip area can be very large (e.g. 5.0 mm² in [71] and 2.32 mm² in [72]).

Injection-locking can also be used to implement a frequency tripler [73, 74], although, the resonator used in the oscillator can consume large chip area and can limit the bandwidth of the circuit. Recent advances in integrated circuit tripler design [75] have used waveform shaping techniques in order to generate the triple frequency and to relax the output filter requirements. In [75], rather than clip a sinusoidal signal and then extract the third-harmonic, “deep-cuts” were made at the peaks of the sinusoidal input, which results in an enhanced third-harmonic output. In order to generate these cuts in the waveform, an inverter was used along with a non-linear

combiner circuit. Since this technique generates a strong third harmonic and naturally suppresses the fundamental, a simple low- Q high-pass filter can be used on-chip to further attenuate the fundamental to a level that would be acceptable for most applications. CMOS 0.18 μm technology was used in [75] and the circuit was designed for an input frequency range from 1.7 GHz to 2.25 GHz (output frequencies from 5.1 GHz to 6.75 GHz). The minimum measured conversion loss using this technique was 5.6 dB and the fundamental suppression at the output was more than 11 dB. The circuit was very compact at $420 \mu\text{m} \times 320 \mu\text{m}$ including pads, and the DC power consumption was 27 mW.

2.5.1.5 Digital Frequency Multipliers

There are many digital frequency multiplier techniques that have been demonstrated. For example, an all-digital clock multiplier is proposed in [76] for low-frequency clock references that can achieve $2\times$, $3\times$, or $4\times$ frequency multiplications. In general, digital frequency multiplier techniques have lower operational frequency limits than their analog counterparts and often have higher power consumptions. Given the microwave focus of this thesis, digital frequency multiplier techniques will not be discussed in detail.

2.6 Frequency Divider Circuit Review

Frequency dividers can be used in many applications, but are most often used in the feedback path of phase-locked loops (PLLs) in order to achieve frequency multiplication. In the vast majority of frequency dividers presented in the literature an even-order division ratio is used. In fact, most frequency dividers divide the frequency

of an input signal by a factor of two or four and there are very few odd-order frequency dividers that have been demonstrated. In this section a literature review will be presented of common circuit techniques that can be used to realize a frequency divider.

2.6.1 Common Frequency Divider Topologies

2.6.1.1 Digital Frequency Dividers

Many frequency dividers used in PLLs and in other applications use digital flip-flop based dividers. These digital frequency dividers have several advantages, such as wide-band operation and the potential for high division ratios (e.g. [77]). However, digital dividers often have very large power consumptions and in fact can consume a very large percentage of the overall DC power used by frequency synthesizers used in modern wireless systems [78]. Furthermore, the maximum operational frequency of digital frequency dividers is generally lower than in narrow-band analog frequency dividers. Given the narrow-band nature of most wireless signals it is possible to use analog techniques to achieve higher operational frequencies and also reduced power consumption. Given these advantages of analog dividers, as well as this thesis' focus on analog circuits, digital frequency divider techniques will not be discussed in detail.

2.6.1.2 Regenerative Frequency Dividers

A well-known analog frequency divider topology is the regenerative topology, shown in Figure 2.22 and first introduced by Miller in 1939 [79]. As shown in the figure, in its simplest form the regenerative divider consists of a mixer and a low-pass filter. If the input signal to this circuit has a frequency f_{in} then there are two steady-state

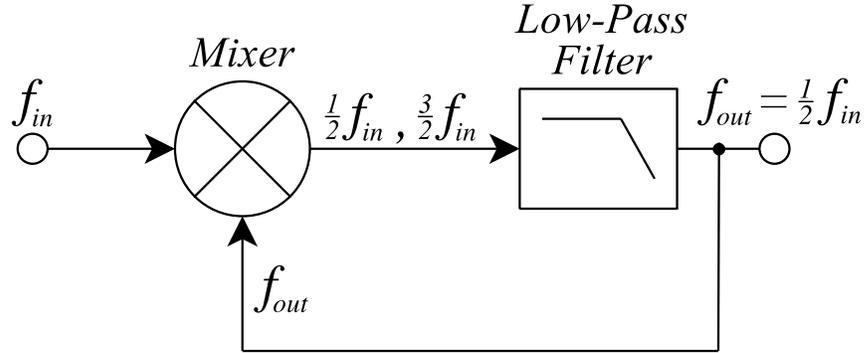


Figure 2.22: Simplified circuit of a regenerative frequency divider.

outputs of the mixer, $\frac{1}{2}f_{in}$ and $\frac{3}{2}f_{in}$. The low-pass filter attenuates the $\frac{3}{2}f_{in}$ signal, thus leaving the $\frac{1}{2}f_{in}$ for the output and for feedback. In practical implementations of the regenerative frequency divider technique an amplifier may also be required after the filter in order to achieve the required gain around the feedback loop that will enable the circuit to operate. Practical implementations of this technique are presented in [80] and [81]. In [80], a 40 GHz frequency divider was designed in CMOS 0.18 μm technology that consisted of two Miller divider stages that divided the input 40 GHz signal to 10 GHz at the output. The mixers used in this work were modified Gilbert-cells that used inductive loads to achieve higher frequency operation as well as the filtering required for the regenerative topology. This circuit obtained an input bandwidth of approximately 2.5 GHz and required a minimum input power of 3 dBm to operate. The conversion loss for this circuit was quite high at around 19 dB and the power consumption was 77.5 mW.

The regenerative frequency dividers demonstrated in [81] used GaAs technology to realize both a 28 GHz and a 14 GHz version of their frequency divider design. In this work, a single-FET mixer was used along with a tuned amplifier and coupler for

the feedback path consisting of lumped inductors and capacitors. Conversion gain was obtained for both the 28 GHz and 14 GHz versions of this frequency divider design with DC power consumptions of approximately 100 mW. Both versions also reject the fundamental signal by at least 15 dB and have bandwidths of 11% and 5.7% for the 14 GHz and 28 GHz versions, respectively.

2.6.1.3 Injection-Locked Frequency Dividers

As discussed in the previous sections, it is possible to lock an oscillator to an injected signal. In the frequency multiplier implementation described previously, an input signal was injected to lock the fundamental oscillation frequency with the external signal's frequency and then the doubled frequency component was taken as the output at a common-mode node (see Figure 2.20). A similar technique can be used to realize a frequency divider [82–85]. For example, a simplified cross-coupled injection-locked frequency divider is shown in Figure 2.23. In this circuit, the input signal is injected to a common-mode node, which locks the frequency of the oscillator second harmonic to this external signal frequency. The result of this configuration is an output signal frequency that has been divided by a factor of two relative to the injected signal.

An injection-locked frequency divider very similar to the circuit shown in Figure 2.23 is presented in [82] using CMOS technology and a division ratio of two. In this work, an input signal at around 3 GHz was injected to the gate of the bottom transistor shown in Figure 2.23, which locked the fundamental oscillator output to half the frequency of the input signal. With no input signal, the free-running oscillation frequency was 1.6 GHz, and with an input signal a locking range of 370 MHz was measured with a DC power consumption of only 1.2 mW.

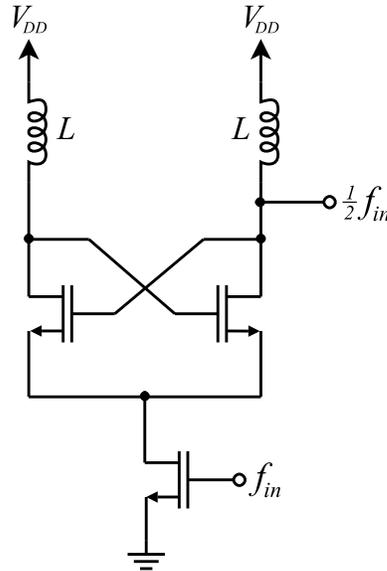


Figure 2.23: Simplified circuit of an injection-locked frequency divider.

Another harmonic injection-locked frequency divider was demonstrated in [83] using $0.18 \mu\text{m}$ SiGe BiCMOS technology at 60 GHz (bipolar transistors were used in this work exclusively). This circuit divided the input signal frequency by a factor of four by mixing it with the third-harmonic of the output signal (generated by an inverter). This frequency divider operated with input frequencies from 59.77 GHz to 60.12 GHz, which is a locking bandwidth of 350 MHz. The circuit required an input power of at least 0 dBm and had an output power of -16.6 ± 0.5 dBm over the locking range. The power consumption of this circuit was 50.4 mW and the chip dimensions were $0.8 \text{ mm} \times 0.7 \text{ mm}$.

One of the relatively few odd-order frequency dividers is presented in [84]. This injection-locked divide-by-three circuit uses a modified version of the circuit shown in Figure 2.23. Specifically, a differential input was applied to the gates of two

transistors, as opposed to the single-ended input applied to the gate of the single transistor at the bottom of Figure 2.23 and the sources of the cross-coupled transistors are no longer connected. This circuit was implemented in CMOS 0.18 μm technology at an input frequency of 18 GHz. As with most injection-locked frequency dividers, the locking range increases as the input power increases. In this circuit, the locking range was 300 MHz for an input power of -14 dBm and 1 GHz for an input power of 0 dBm. The suppression of the undesired harmonics at the output were -23 dB for the second harmonic and -21 dB for the third harmonic relative to the fundamental output power level. The power consumption for the core of this divider circuit was 4.6 mW (45 mW including buffers) and the chip dimensions were $0.9 \text{ mm} \times 0.9 \text{ mm}$.

Chapter 3

A 2x Subharmonic Mixer in CMOS

3.1 Introduction

In this chapter, the design and measurement of a CMOS $2\times$ subharmonic mixer that uses active baluns at the input and at the output is presented. This circuit, which was published in [8], could be used in either a superheterodyne system to reduce the required LO frequency by half, or in a direct-conversion receiver in order to reduce LO self-mixing. As discussed in Chapter 2, the vast majority of subharmonic mixers are realized with diodes, and as such cannot achieve a conversion gain. The goal of this work was to realize a subharmonic mixer in a standard CMOS technology that can achieve a conversion gain and is compatible with a system that uses single-ended signals. This work is one of the first subharmonic mixers demonstrated with measurement results in a standard CMOS fabrication technology, and is the first using the proposed topology. This circuit provides the foundation for a more advanced higher-order and higher-frequency SHM explored in Chapter 4.

3.2 Concept of the 2x Subharmonic Mixer

In order to realize an active subharmonic mixer, modifications to the Gilbert-cell have been shown in [36] and [86] to use four LO signals with relative phase shifts of 0° , 90° , 180° , and 270° to effectively provide switching at twice the rate of the traditional Gilbert-cell. A block diagram of the subharmonic mixer using this technique is shown in Figure 3.1 with differential RF inputs and differential IF outputs. Often, the use of single-ended, or unbalanced, signals is necessary, in particular when interfacing with off-chip components in multi-chip modules. Since the Gilbert-cell relies on differential signals, baluns must be used to perform this conversion if single-ended signals are used. Active baluns have several advantages over passive baluns. For example, active baluns generally consume significantly less area than passive baluns and can also potentially achieve gain. In fact, passive baluns are often implemented off chip, thus potentially increasing noise and cost, as well as eliminating the possibility of realizing a system-on-a-chip. CMOS subharmonic mixers are presented in [87–89], however,

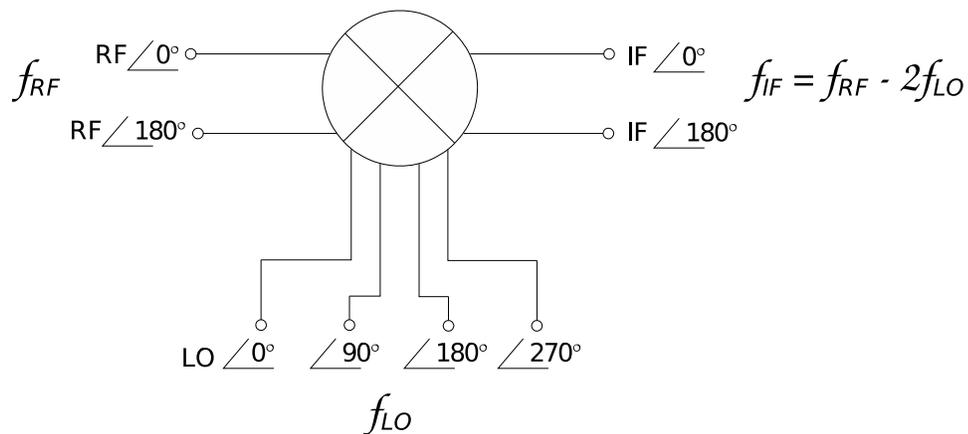


Figure 3.1: Block diagram of a $2\times$ subharmonic mixer used as a down-converter.

only simulation results are shown, and conversion between balanced and unbalanced signals is not discussed.

3.3 Circuit Design

3.3.1 Subharmonic Mixer Core

The core of the subharmonic mixer is shown in Figure 3.2, which is based on the Gilbert-cell topology. Gilbert-cell mixers, in general, have high isolation between ports due to their double-balanced structure. Corresponding to the block diagram in Figure 3.1, the circuit requires RF inputs with relative phase shifts of 0° , and 180° , and LO inputs of 0° , 90° , 180° , and 270° . With this topology, first proposed in [36], the currents i_1 and i_2 are effectively switched at twice the LO frequency, which is the mechanism that results in subharmonic mixing.

For insight into how the LO frequency is doubled, consider the circuit in Figure 3.3. Since the LO input is generally a large signal, the MOSFETs will turn on and off corresponding to the amplitude of the voltages at their gates. As the 0° LO signal rises well above the threshold value, transistor $M5$ turns fully on, causing i_1 to increase and flow predominately through $M5$, since the gate voltage at $M6$ is 180° out of phase and therefore near its minimum. When the amplitude of the 0° LO signal begins to drop and the 180° LO amplitude begins to rise, neither transistor is fully on and, as a result, the current i_1 decreases. As the 180° LO signal nears its maximum and the 0° LO nears its minimum, $M6$ is turned fully on and $M5$ is turned off, meaning that the current i_1 increases and flows through $M6$. By the end of the cycle, neither the 0° nor the 180° LO signals are at a maximum and the current i_1

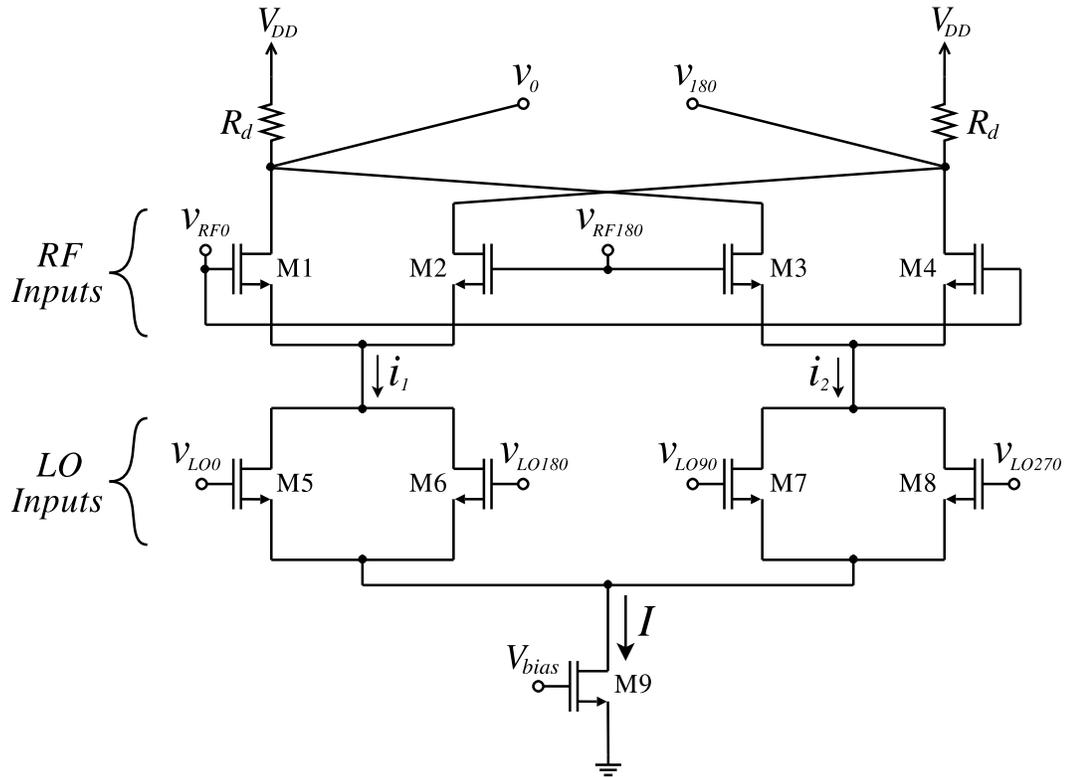


Figure 3.2: Proposed CMOS 2× subharmonic mixer core.

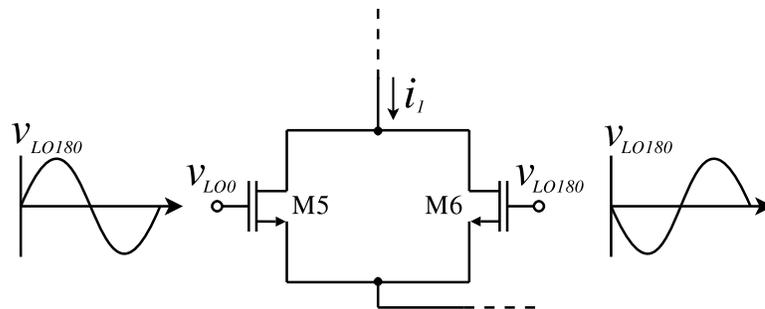


Figure 3.3: LO frequency doubling in the 2× subharmonic mixer.

decreases again. Therefore, during one period of the LO signal, i_1 has two cycles of increasing and decreasing current, thus indicating a doubling of the LO frequency. The same operation occurs for the other LO transistor pair (90° and 270°) and the resulting current, i_2 , is 180° out of phase with i_1 . Therefore, mixing will occur at the RF frequency and twice the input LO frequency. A larger LO input power will be required to achieve the same conversion gain as a fundamental Gilbert-cell mixer, but this circuit has the significant advantage of using half the LO frequency as well as reducing LO self-mixing in direct-conversion receivers (as discussed in Chapter 2).

The LO inputs to the subharmonic mixer are given by:

$$\begin{aligned} v_{LO0} &= A_{LO} \cos(\omega_{LO} t) \\ v_{LO90} &= A_{LO} \cos(\omega_{LO} t - \pi/2) \\ v_{LO180} &= A_{LO} \cos(\omega_{LO} t - \pi) \\ v_{LO270} &= A_{LO} \cos(\omega_{LO} t - 3\pi/2) \end{aligned}$$

and the RF inputs to the mixer core are differential,

$$v_{RF0} = A_{RF} \cos(\omega_{RF} t) \quad v_{RF180} = A_{RF} \cos(\omega_{RF} t - \pi).$$

Since this is a $2\times$ SHM, the up- and down-converted components of the mixer output will be at $f_{RF} + 2f_{LO}$ and $f_{RF} - 2f_{LO}$, respectively.

To gain deeper insight into the operation of the SHM, an analytic expression for the conversion gain of the mixer can be derived. Here, the long-channel transistor models are used for simplicity in order to obtain useful closed-form equations. In the half-SHM circuit shown in Figure 3.4, the LO switching pair transistors $M5$ – $M6$ are modeled as one transistor, $M56$. Assuming that the fundamental currents generated by the differential gate voltage signals on $M5$ and $M6$ perfectly cancel each other,

voltage, and V_t is the threshold voltage. If the currents through $M5$ and $M6$ are i_a and i_b , respectively, the total current from the switching pair with a differential input is

$$i_1 = i_a + i_b = \mu_n C_{ox} \frac{W_1}{L} (V_{GS(LO)} - V_t)^2 + \frac{1}{2} \mu_n C_{ox} \frac{W_1}{L} (v_{LO0}^2 + v_{LO180}^2), \quad (3.2)$$

where $V_{GS(LO)}$ is the DC voltage between the gates and sources of the LO transistors ($M5$ – $M8$). Since $v_{LO0}^2 = v_{LO180}^2$ for a sinusoidal LO signal,

$$i_1 = \mu_n C_{ox} \frac{W_1}{L} (V_{GS(LO)} - V_t)^2 + \mu_n C_{ox} \frac{W_1}{L} v_{LO0}^2. \quad (3.3)$$

This current can then be set equal to the current generated by the $M56$ model transistor (ignoring the nonlinear component),

$$i_1 = \frac{1}{2} \mu_n C_{ox} \frac{W_2}{L} (V_{GS(LO)} - V_t)^2 + \mu_n C_{ox} \frac{W_2}{L} (V_{GS(LO)} - V_t) v_{LOEQ0}. \quad (3.4)$$

Clearly, in order to have equal DC currents, the width of transistor $M56$ must be twice that of $M5$ and $M6$, $W_2 = 2W_1$. The equivalent applied gate signal voltages to the LO switching pair model transistors, $M56$ and $M78$, are:

$$v_{LOEQ0} = \frac{A_{LO}^2}{2(V_{GS(LO)} - V_t)} \cos^2(\omega_{LO} t) \approx \frac{A_{LO}^2}{4(V_{GS(LO)} - V_t)} \cos(2\omega_{LO} t), \quad (3.5)$$

$$v_{LOEQ180} = \frac{A_{LO}^2}{2(V_{GS(LO)} - V_t)} \cos^2(\omega_{LO} t + \pi) \approx \frac{A_{LO}^2}{4(V_{GS(LO)} - V_t)} \cos(2\omega_{LO} t + \pi), \quad (3.6)$$

The approximation made in the equations (3.5) and (3.6) was to ignore the DC component of the \cos^2 term, the effect of which will be discussed below. With this simplification the circuit can be analyzed as a standard Gilbert-cell topology, with the addition of the injection resistors. The output voltage of the mixer, $v_{OUT} = v_0 - v_{180}$, as defined in Figure 3.2, is given by:

$$v_{OUT} = \frac{-R_d v_{idRF}}{V_{GS(RF)} - V_t} (i_1 - i_2) = \frac{-R_d I}{(V_{GS(RF)} - V_t)(V_{GS(LO)} - V_t)} v_{idRF} v_{idLOEQ} \quad (3.7)$$

where $v_{idRF} = v_{RF0} - v_{RF180}$, $v_{idLOEQ} = v_{LOEQ0} - v_{LOEQ180}$, and $V_{GS(RF)}$ is the DC voltage between the gates and sources of the RF transistors ($M1$ – $M4$).

The conversion gain formula for this subharmonic mixer for the up- and down-converted components ($f_{RF} + 2f_{LO}$ and $f_{RF} - 2f_{LO}$) is given by:

$$CG_{dB} = 20 \log \left(\frac{R_d I A_{LO}^2}{4(V_{GS(RF)} - V_t)(V_{GS(LO)} - V_t)^2} \right), \quad (3.8)$$

where I is the bias current set by the gate voltage of transistor $M9$, A_{LO} is the amplitude of the quadrature signal at the gates of the LO transistors $M5$ – $M8$, and all transistors are operating in the saturation region. The values for $V_{GS(RF)}$ and $V_{GS(LO)}$ can be found from a straight-forward DC circuit analysis. From this equation it is clear that the conversion gain will increase with increasing bias current, I .

The formula for the conversion gain in (3.8) does not include the effects of any parasitics, and thus will over-estimate the actual conversion gain. However, the simplification in Equations (3.5) and (3.6) where the DC component of the \cos^2 term was not included mitigates the over-estimation in (3.8) somewhat since there is an additional DC component in the currents that are generated by $M5$ – $M8$ (or $M56$ and $M78$). The SHM was independently simulated and compared to the conversion gain given by (3.8) using a CMOS 0.18 μm process. Shown in Figure 3.5 are the analytic (using Equation (3.8)) and the simulated conversion gains at various LO voltage amplitudes, A_{LO} , for an input RF frequency of 2.1 GHz and input LO frequency of 1.0 GHz, which produces down-converted and up-converted components at 100 MHz and 4.1 GHz, respectively. The calculated and simulated values are within 3 dB of each other up to LO voltage amplitudes of 0.1 V. At higher amplitudes, the transistors become saturated, which explains the increasing difference between the two. In this work, the operational range for the subharmonic mixer has $A_{LO} < 0.15$ V,

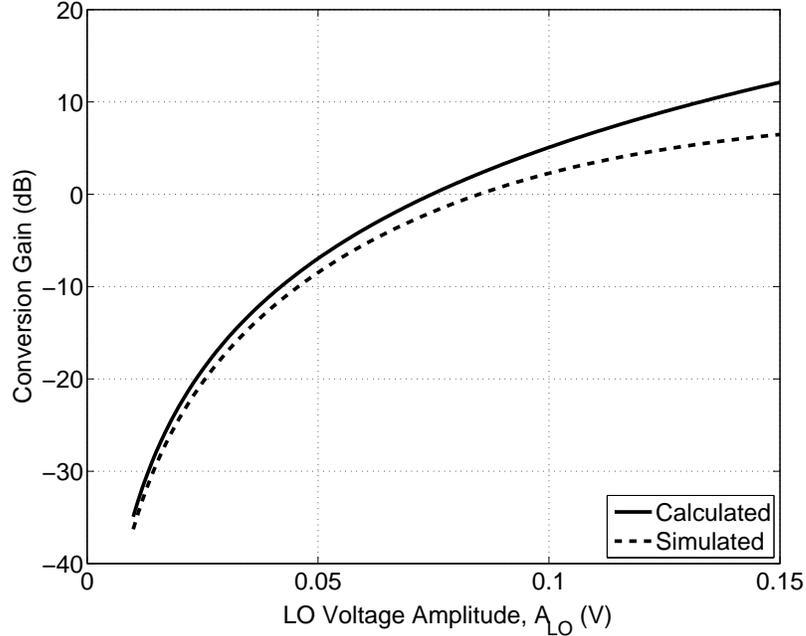


Figure 3.5: Calculated and simulated conversion gain of the subharmonic mixer at various LO voltage amplitudes, A_{LO} .

so the equation given in (3.8) can provide a useful first-order approximation for the conversion gain of the subharmonic mixer.

To improve the linearity of the mixer, source degeneration was used for transistors $M1-M4$. This technique can improve the 1-dB compression point of the circuit, but has the penalty of reducing the conversion gain. Resistive degeneration was used in this work rather than inductive because it requires significantly less chip area and because it does not have a frequency dependence. As a result, a more compact layout of the circuit can be obtained compared to implementations with inductive degeneration. However, with resistive degeneration the noise figure of the mixer will be increased somewhat.

3.3.2 RF and LO Input Baluns

In some cases it is necessary to convert an unbalanced (single-ended) signal to a balanced (differential) signal and vice-versa. In this work, RF and LO active baluns were included on-chip to ease the test and measurement of the subharmonic mixer. As mentioned previously, passive on-chip baluns for RF and microwave frequencies can consume a large area specifically at lower frequencies and are often realized off-chip, which adds to assembly costs and may degrade the conversion gain/loss. It is possible to use transmission line baluns on-chip, but since their size is proportional to wavelength they are not economically feasible except possibly at millimeter-wave frequencies. Several techniques exist to perform the balun operation using active components. The simplest active balun is a FET with resistors in the drain and the source as shown in Figure 3.6 [90]. By properly choosing the value of these resistors, the amplitude of the two outputs can be made equal. Specifically, there

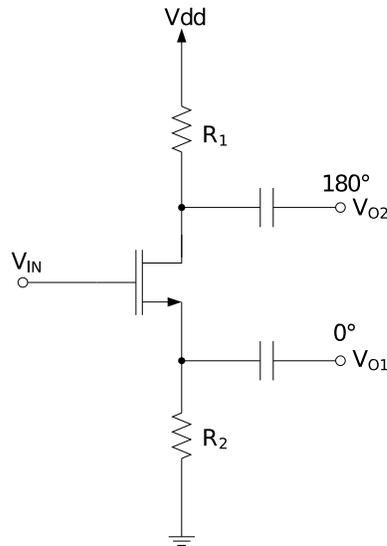


Figure 3.6: Single FET balun circuit.

is approximately unity gain at v_{O1} (i.e. $v_{O1}/v_{IN} \approx 1$) since it is a follower circuit. Therefore, to have equivalent output amplitude at v_{O2} , a design equation can be easily obtained for the resistors R_1 and R_2 to a first-order approximation with:

$$\frac{v_{O2}}{v_{IN}} = \frac{-R_1}{R_2 + 1/g_m} = -1 \quad (3.9)$$

and

$$R_1 = R_2 + \frac{1}{g_m} \quad (3.10)$$

The negative sign in (3.9) indicates that the output at the drain has (ideally) a 180° phase-shift relative to the input, whereas v_{O1} has the same phase as the input. Of course, this basic structure has limitations at high frequencies due to the parasitic elements associated with the transistor. In particular, the gate-drain parasitic capacitance, C_{gd} , seriously degrades the performance at high frequencies since the input signal can feed through this capacitance directly to the output. Two techniques that have improved performance are the differential pair and the cascaded common-gate/common-source (CG-CS) [91], shown in Figure 3.7 and 3.8, respectively.

The differential pair circuit ultimately has a similar frequency limitation as the circuit in Figure 3.6 by considering the parasitics in the half-equivalent circuit. Several other active balun circuits have been proposed (e.g. [92, 93]), however the CG-CS pair of Figure 3.8 was chosen in this work, which has an advantage over the differential pair in that active input matching is possible, although its performance is more sensitive to process variations. It is desirable to have a low input reflection coefficient so that the input power will be absorbed by the circuit, and not reflected.

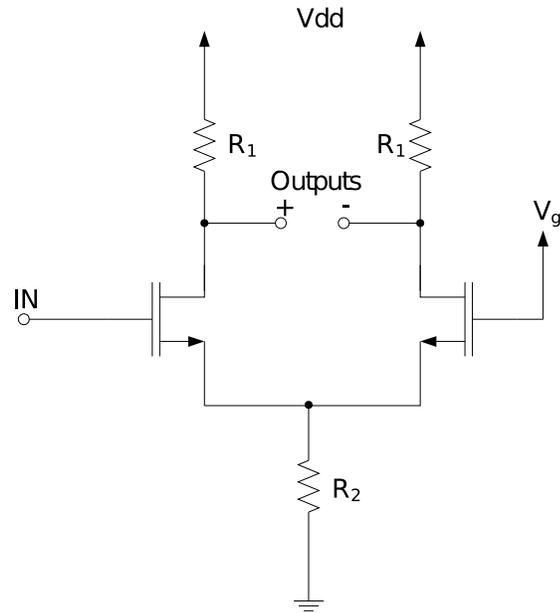


Figure 3.7: Differential pair balun circuit.

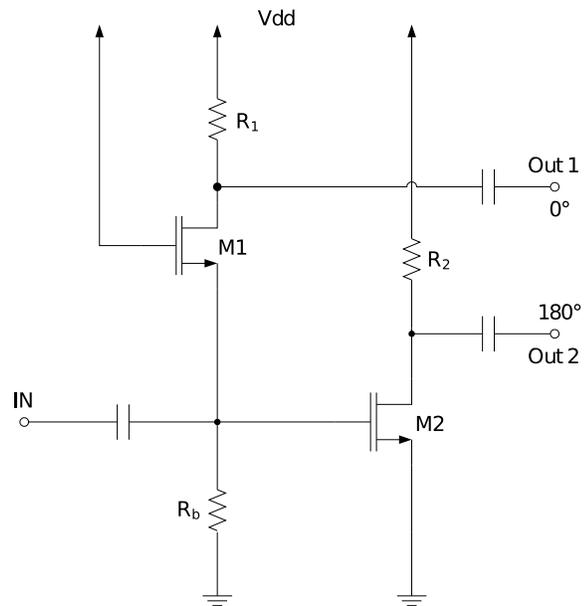


Figure 3.8: Common-gate, common-source balun circuit.

Since the input impedance to the gate of a FET is typically very high due to its large capacitive component, the input reflection coefficient to a common source device, or a differential pair, is generally poor. In contrast, the input impedance to a common-gate device is approximately $1/g_m$. Therefore, an appropriate selection of device size and biasing can yield a $50\ \Omega$ input impedance, as desired. Since the input impedance of the common-gate device is in parallel with the very high input impedance of the common-source transistor, the resulting input impedance is approximately that of the common-gate transistor. This is a significant advantage over other topologies that do not have an acceptable input reflection coefficient. In these instances, a matching network must be implemented using passive devices such as transmission lines, or inductors and capacitors. In this case, the area needed will be much larger and the input matching response will generally not be as broadband as with a common-gate device, although the reflection coefficient could possibly be lower. The resistor, R_b , is large enough that it has a very small impact on the input reflection coefficient. The gate of transistor $M1$ is biased at V_{dd} (1.8 V) and the gate of $M2$ is biased at voltage set by the drop across R_b (which is determined by the current through $M1$).

The balun used for the input RF port was simulated independently in the Spectre simulator using a Cadence extracted layout that included parasitic capacitances and source-follower buffers at the outputs. The amplitude and phase balance are shown in Figure 3.9. The difference in amplitude of the two outputs less than 0.1 dB over the range from 1.0 GHz to 3.0 GHz and the phase difference is less than about 3° .

For this circuit to operate as a subharmonic mixer there must be four LO signals with relative phase shifts of 0° , 90° , 180° , and 270° . The LO input active balun generates the 0° and 180° signals, therefore an additional technique must be used to

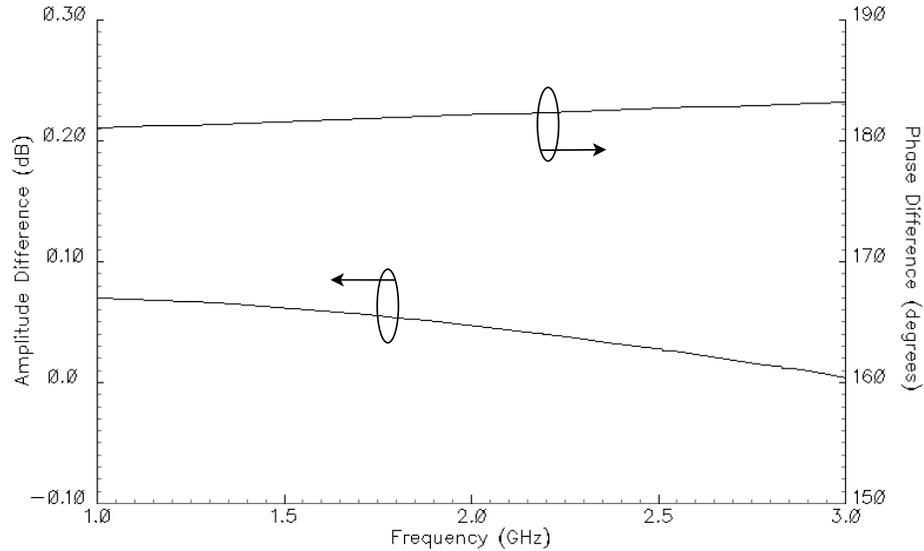
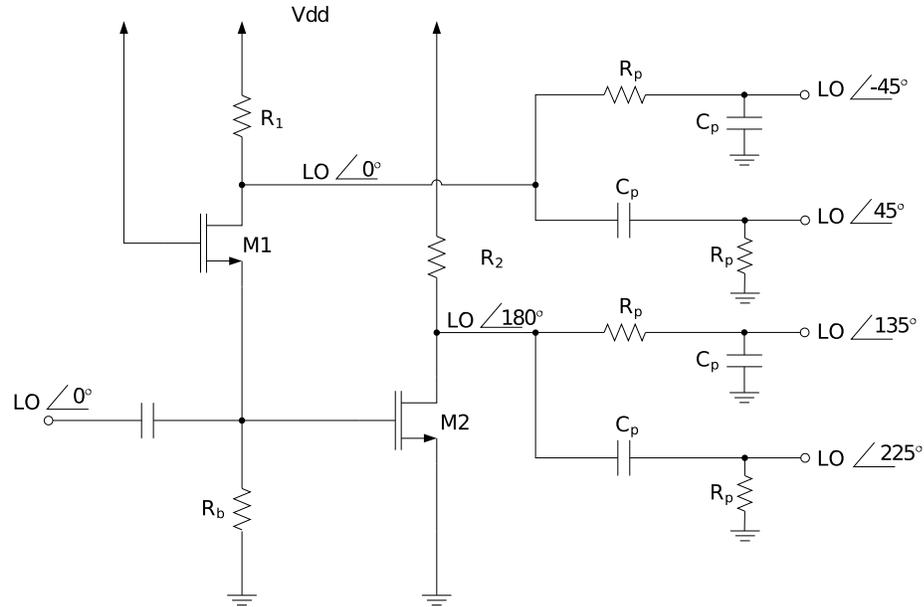


Figure 3.9: Simulated amplitude and phase balance of the $2\times$ SHM's active balun.

generate the quadrature signals. A straight-forward technique to create the 90° phase shifts is with resistor-capacitor polyphase filters. $RC-CR$ quadrature generators are a narrow-band solution with an accuracy that is dependent on the process tolerances. The networks were designed to create a phase shift of 45° at 1.0 GHz by using a resistance value of $R_p = 320 \Omega$ and a capacitor, $C_p = 0.5$ pF. The complete LO input circuit with balun and phase shifters is shown in Figure 3.10 with relative phase shifts indicated at the output for clarity. Using a reference 0° phase of an LO input signal, the phase shift at the outputs in Figure 3.10 would be -45° , 45° , 135° , 225° from top output to bottom relative to the input phase.

Figure 3.10: LO input balun and phase shifters for the 2 \times SHM.

3.3.3 Output Balun

At the output of the subharmonic mixer the signal is differential. To convert to a single-ended signal at this point is very convenient using an active balun since in this case the frequency of the signal is relatively low at 100 MHz. In fact, given the low-frequency of the signal, an active balun is even more attractive than a passive balun due to the much smaller size of the circuit. A differential-pair with a single-ended output connected to a source follower accomplishes the desired goal. This output balun circuit with buffer is shown in Figure 3.11. The differential pair was designed so it would perform as a balun with unity gain. Therefore, the single-ended output voltage signal from the differential pair has the same amplitude as the balanced voltage signal at the output of the mixer. Of course, high harmonic

frequency components will be attenuated somewhat through the balun due to the reduced performance of the differential pair at high-frequencies, thus providing a minor amount of filtering.

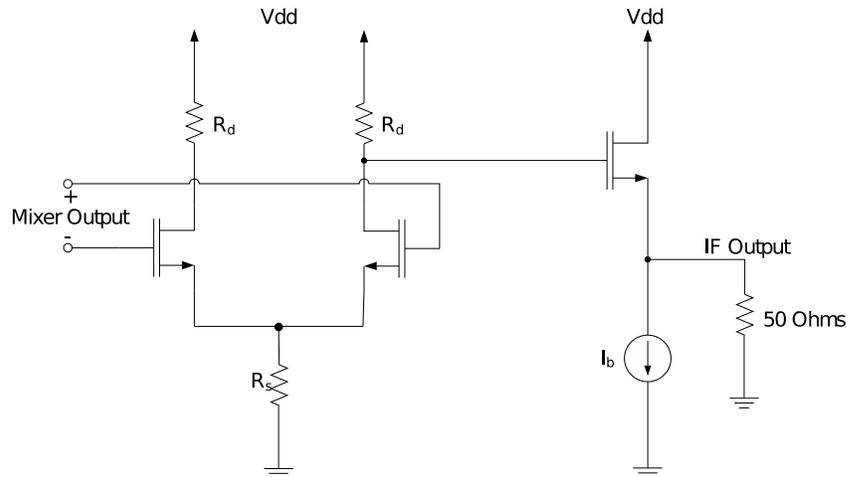


Figure 3.11: Output balun and buffer for the 2 \times SHM.

3.3.4 Complete Circuit

The layout for the complete circuit required an area of approximately $600 \mu\text{m} \times 700 \mu\text{m}$ (0.42 mm^2) including bonding pads and approximately $400 \mu\text{m} \times 500 \mu\text{m}$ (0.2 mm^2) for the circuit excluding bonding pads. The layout is relatively compact, which can be attributed to the fact that there are no inductors in the design. Commonly, inductors are required as part of an input matching network to improve input reflection coefficient. In this case, since the active baluns were designed to have good input matching, inductors, or an off-chip matching network can be avoided. As mentioned above, degeneration resistors were used rather than inductors to improve the

linearity, but require significantly less space on the integrated circuit. A photograph of the fabricated chip is shown in Figure 3.12.

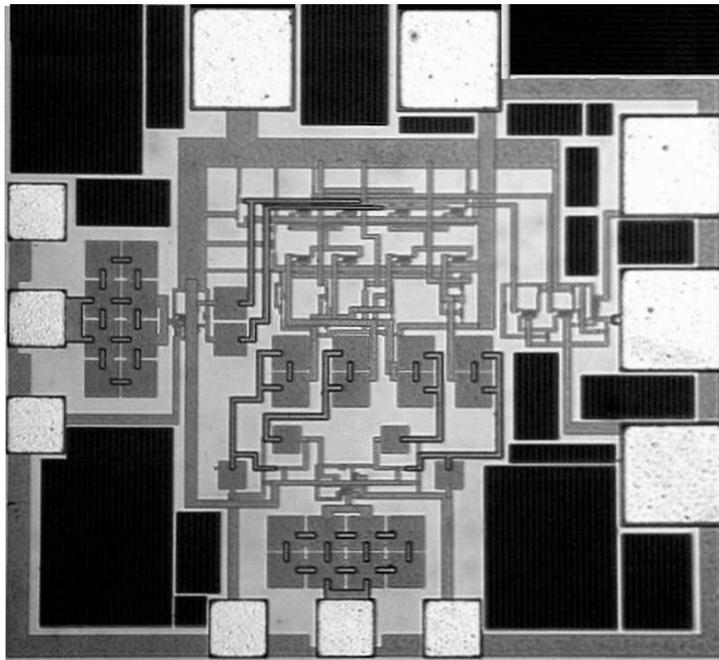


Figure 3.12: Photograph of fabricated CMOS 2 \times subharmonic mixer.

3.4 Measurement Results

To measure the subharmonic mixer, coplanar waveguide probes were used to contact the on-chip pads and a Rohde and Schwarz FS300 spectrum analyzer was used to measure the power spectrum of the output signal. The spectrum analyzer was set to a frequency span of 50 MHz to 150 MHz with a resolution bandwidth (RBW) and a video bandwidth (VBW) both equal to 1 MHz, and continuous sweeping with a sweep time of 25 ms. Averaging was not used for any measurements and no internal

attenuation was used in the spectrum analyzer. The power supply voltage for the circuit, V_{dd} , was set to 1.8 V. To measure the conversion gain of the mixer, the LO was set to a frequency of 1.0 GHz and a power of -10 dBm. A 2.1 GHz RF input was used and its power was swept from approximately -30 dBm to -5 dBm. The output power at 100 MHz ($2.1 \text{ GHz} - 2 \times 1.0 \text{ GHz}$) was observed and the measured and simulated results are shown in Figure 3.13. From this figure, the conversion gain is approximately 8 dB and the 1-dB compression point occurs at an input RF power of approximately -14 dBm. The measurements match the simulation results closely, although the mixer saturates at a lower input power than predicted by simulations.

To find the optimal LO power that provides the maximum conversion gain, the RF input power was held constant while the LO power was swept from -20 dBm to 0 dBm. Figure 3.14 shows that the gain increases relatively linearly with increasing LO power until around -10 dBm at which point the conversion gain is approximately 8 dB. By viewing the spectrum data on the spectrum analyzer over a span of 10 MHz to 3 GHz it was found that an LO power of -10 dBm provides the maximum conversion gain while suppressing all undesired harmonics by at least 25 dB.

A full two-port calibration was performed using a calibration substrate (SUSS MicroTec CSR-3 GSG100-250) and an Agilent 8510C Network Analyzer with a 50-GHz Agilent 8517B S-parameter Test Set was used to measure the input reflection coefficients of both the RF and the LO ports. For both calibration and measurements, a frequency range from 500 MHz to 3 GHz was used with the power of the network analyzer set to -30 dBm to ensure that the mixer is not saturated. The network analyzer was set for 0 dB attenuation for the ports and no averaging or smoothing for the resulting data.

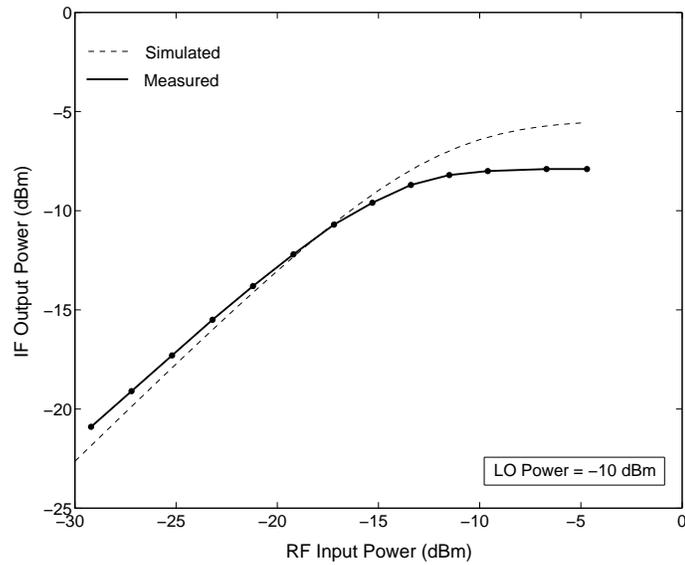


Figure 3.13: Measured and simulated 1-dB compression point.

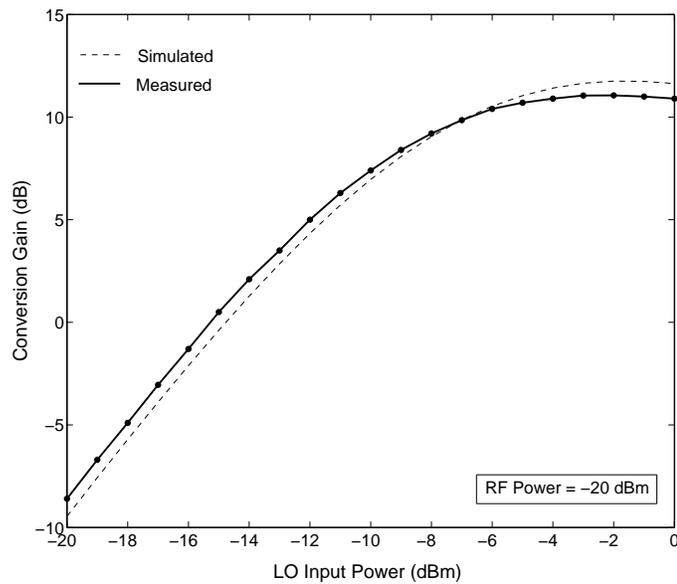


Figure 3.14: Measured and simulated conversion gain at various LO power levels.

The S_{11} for the RF input is shown in Figure 3.15. It is clear that the active input balun provides good matching with an input reflection coefficient less than -10 dB at 2.1 GHz. Similarly, the LO input reflection coefficient, shown in Figure 3.16, is approximately -11 dB at the LO frequency of 1.0 GHz. The slight difference between the RF and the LO input matching is due to minor differences in the active balun circuits that allows a lower input reflection coefficient at the operational frequency of the LO at the expense of higher power consumption. The third-order intercept point (IP3) was measured by using a two-tone RF input signal with frequencies of 2.1 GHz and 2.11 GHz. This produced third-order intermodulation products at 90 MHz and 120 MHz. The results shown in Figure 3.17 indicate an IIP3 of -8.5 dBm and an OIP3 of -0.5 dBm. The IP2 was simulated using the same two-tone RF input signals at the IP3 measurement (2.1 GHz and 2.11 GHz), which produces an IM2 component at 10 MHz. Simulations show an IIP2 of 14 dBm including the output balun circuit, and an IIP2 of over 30 dBm using an ideal output balun (i.e. the IIP2 of the mixer alone is over 30 dBm).

The port-to-port isolation was simulated using ADS in order to determine the isolation between the mixer ports without the effects of the input or output baluns. The results, tabulated in 3.1, show very high-levels of isolation such as 68 dB for the $2LO-RF$ feedthrough. Clearly, this will be very beneficial in direct-conversion applications since the high $2LO-RF$ isolation will result in low LO self-mixing.

The noise figure of the mixer was measured using an Agilent 346C noise source along with the Noise Figure Measurement Personality of the Agilent E4446A PSA Series spectrum analyzer. A calibration was first performed, and the resolution bandwidth was set to 1 MHz. The measured double sideband (DSB) noise figure is 20 dB.

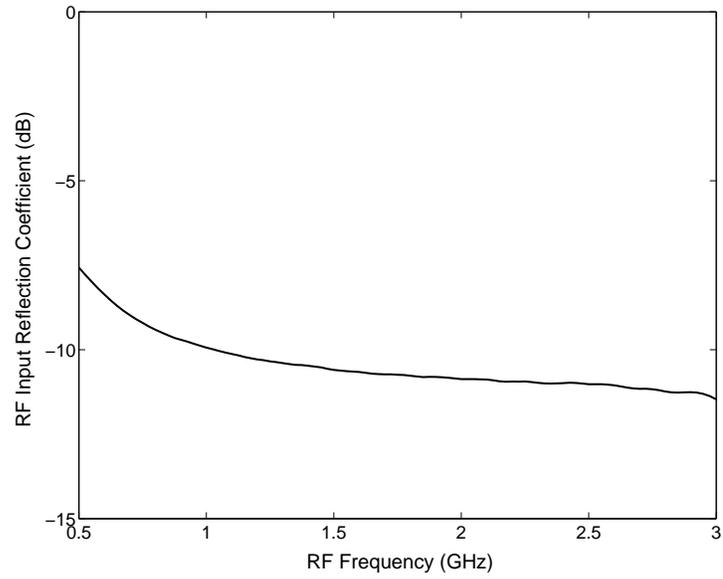


Figure 3.15: Measured RF input reflection coefficient for the 2 \times SHM.

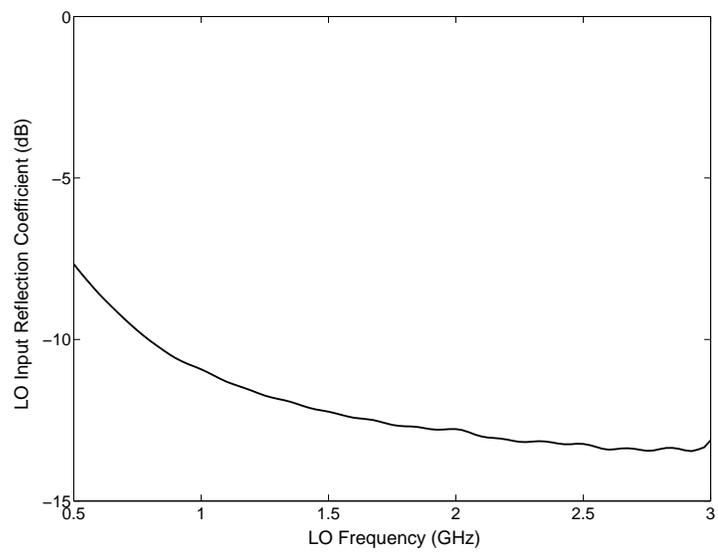
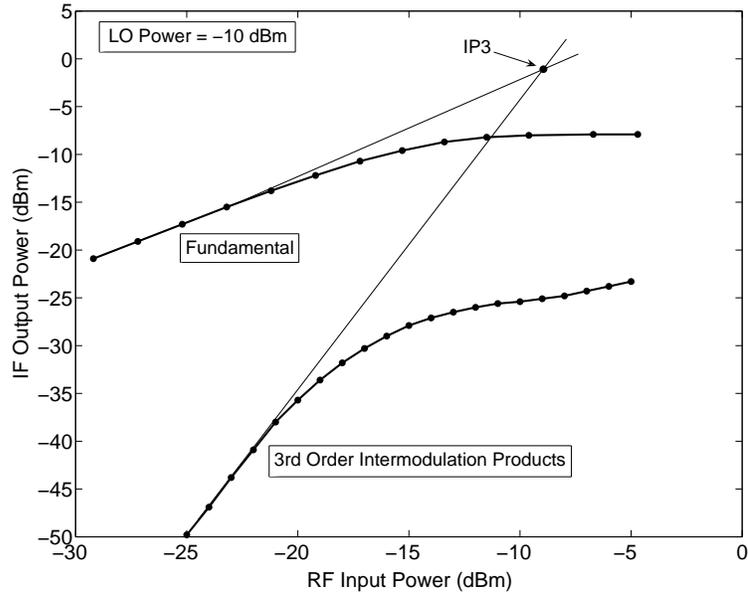


Figure 3.16: Measured LO input reflection coefficient for the 2 \times SHM.

Figure 3.17: Third-order intercept point measurement for the $2\times$ SHM.

<i>Ports</i>	<i>Isolation</i>
RF–LO	62 dB
LO–RF	58 dB
2LO–RF	68 dB
RF–IF	35 dB
LO–IF	37 dB
2LO–IF	49 dB

Table 3.1: $2\times$ subharmonic mixer port-to-port isolation simulations.

Technology	f_{RF}/f_{LO} (GHz)	Gain (dB)	P-1dB (dBm)	IIP3 (dBm)	DC Power (mW)	Ref.
BiCMOS 0.35 μm	1.9/0.9	7.5	-8	-3	24	[36]
SiGe BiCMOS 0.18 μm	5.6/2.8	8.0	-13.5	0	4.67	[87]*
CMOS 0.25 μm	5.6/2.8	8.0	-12	-6.5	5.25	[89]*
CMOS 0.18 μm	2.1/1.0	8.0	-14	-8.5	36 $^{\Delta}$	This Work [8]

* *Simulation results only*

Δ *Includes balun circuits*

Table 3.2: 2 \times subharmonic mixer circuit performance comparison.

The noise figure could be reduced by modifying the input baluns to eliminate the bias resistor R_b , or by using another balun topology. The power consumption for the circuit, including input and output baluns, the mixer core, as well as the output buffer, is 36 mW (the power consumption of the mixer core alone is approximately 1 mW). A comparison of this work with other subharmonic mixers of this type ([36, 87, 89]), is presented in Table 3.2. Note that in these references that they do not use on-chip baluns, and in the case of [87] and [89] only simulation results are shown.

3.5 Summary

In this chapter, a CMOS 0.18 μm 2 \times subharmonic mixer was demonstrated that uses active input and output baluns to generate differential signals from single-ended, and vice-versa. This configuration could be used as part of a direct-conversion receiver where single-ended inputs and outputs are required or in a superheterodyne receiver

where a lower LO frequency is desired. By using a $2\times$ subharmonic mixer, the LO frequency is designed to have half the frequency that would be required with a fundamental mixer. Consequently, the design of the LO can possibly be simplified and improved performance can result due to the reduced oscillation frequency. The RF input frequency was 2.1 GHz and the LO frequency was 1.0 GHz, which results in an output IF of 100 MHz. Active baluns at the RF and LO input ports were designed to have active input matching and the measured results show input reflection coefficients of less than -10 dB at the LO and RF operational frequencies. The 1-dB compression point was found to occur at -14 dBm RF input power and the conversion gain was approximately 8 dB. If a quadrature oscillator is used for the LO, such as the one described in Chapter 5 of this dissertation, it could eliminate the need for the passive RC - CR phase-shifters and the LO balun, and potentially improve performance through increased phase accuracy.

Chapter 4

A CMOS Ku-Band 4x Subharmonic Mixer

4.1 Introduction

In this chapter, a novel 4× subharmonic mixer is presented using CMOS technology that is a significant extension of the 2× SHM described in the previous chapter [6]. An RF frequency in the Ku-band (12 GHz) was used to demonstrate this circuit, which is a very commonly used band for satellite communications. To the best of the author’s knowledge, this is the first 4× subharmonic mixer demonstrated in CMOS technology. Furthermore, it obtains a conversion gain of 6 dB, which is the highest conversion gain for any 4× SHM to date.

Although it is possible to realize an LO that operates directly at Ku-band in CMOS technology, the resulting fundamental mixer would likely have increased self-mixing and therefore degrade the performance of a direct-conversion receiver compared to a subharmonic mixer. Similarly, while it would be possible to use a separate LO

frequency multiplier along with a fundamental or a $2\times$ SHM, the resulting power consumption and required chip area could potentially increase and the port-to-port isolation could suffer, resulting in an increase in self-mixing. The proposed circuit could easily be moved to higher frequencies (mm-wave) where subharmonic mixing may be a necessity, and in this regard it can be viewed as a lower frequency demonstration circuit.

4.2 Concept of the 4x Subharmonic Mixer

The core of the $4\times$ SHM is based on the Gilbert-cell topology [17]. As shown in Figure 4.1, the proposed SHM has the RF and LO ports exchanged compared to a traditional Gilbert-cell. Furthermore, the two transistors typically at the bottom of the Gilbert-cell have been replaced by two sets of four transistors that will generate the fourth harmonic of the LO signal, thus allowing the mixer to operate as a $4\times$ SHM. The inputs to these transistors are octet-phase LO signals, with 0° , 90° , 180° , and 270° applied to the gates of one set of four FETs and 45° , 135° , 225° , 315° applied to the gates of the other set of FETs. In other $2\times$ SHM circuits (e.g. [8, 32, 36]) a similar topology is used, but with two pairs of LO transistors instead of four, and they use only quadrature LO signals.

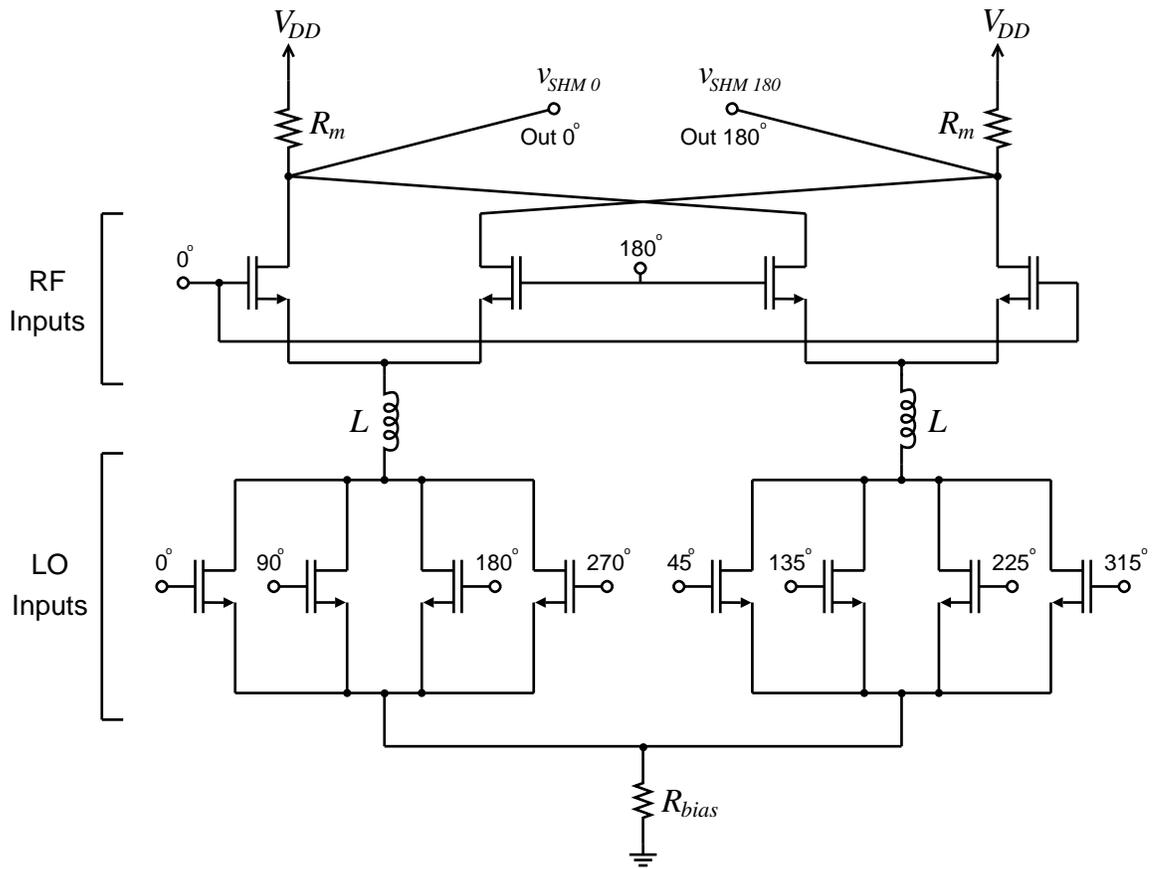


Figure 4.1: The mixer core of the proposed 4x SHM.

4.3 Circuit Design

4.3.1 Mixer Core

To examine the operation of the mixer, consider one set of four transistors, as shown in Figure 4.2a, with LO signals applied to the gates with relative phase shifts of 0° , 90° , 180° , 270° , as shown in Figure 4.2b. The four quadrature LO signals applied to the gates generate a $4f_{LO}$ signal, as opposed to differential gate signals which only generate a $2f_{LO}$ signal as in [8, 32, 36]. The quadrature signals applied to the gates of the other set of four transistors are shifted by 45° . This topology generates a $4f_{LO}$ signal that is 180° out of phase with the other $4f_{LO}$ signal. Therefore, this mixer topology is double-balanced, which allows this topology to achieve high-levels of isolation between the ports. If the LO signals have a DC bias at the transistor threshold voltage, V_t , the signals are given by:

$$\begin{aligned} v_{LO0} &= A_{LO}\cos(\omega_{LO}t) + V_t \\ v_{LO90} &= A_{LO}\cos(\omega_{LO}t - \pi/2) + V_t \\ v_{LO180} &= A_{LO}\cos(\omega_{LO}t - \pi) + V_t \\ v_{LO270} &= A_{LO}\cos(\omega_{LO}t - 3\pi/2) + V_t \end{aligned}$$

where A_{LO} is the amplitude of the LO signal. If it is assumed that the transistors are completely cutoff when the gate voltage is below the threshold voltage (i.e. ignoring sub-threshold current), the LO_0 and LO_{180} pair of transistors can be modeled by one transistor with LO gate voltage of,

$$v_{0,180} = |A_{LO}\cos(\omega_{LO}t)| + V_t \quad (4.1)$$

since only one of the two transistors is on during each half-cycle. Clearly, this waveform contains the double frequency, or second harmonic. Similarly, the LO_{90} and

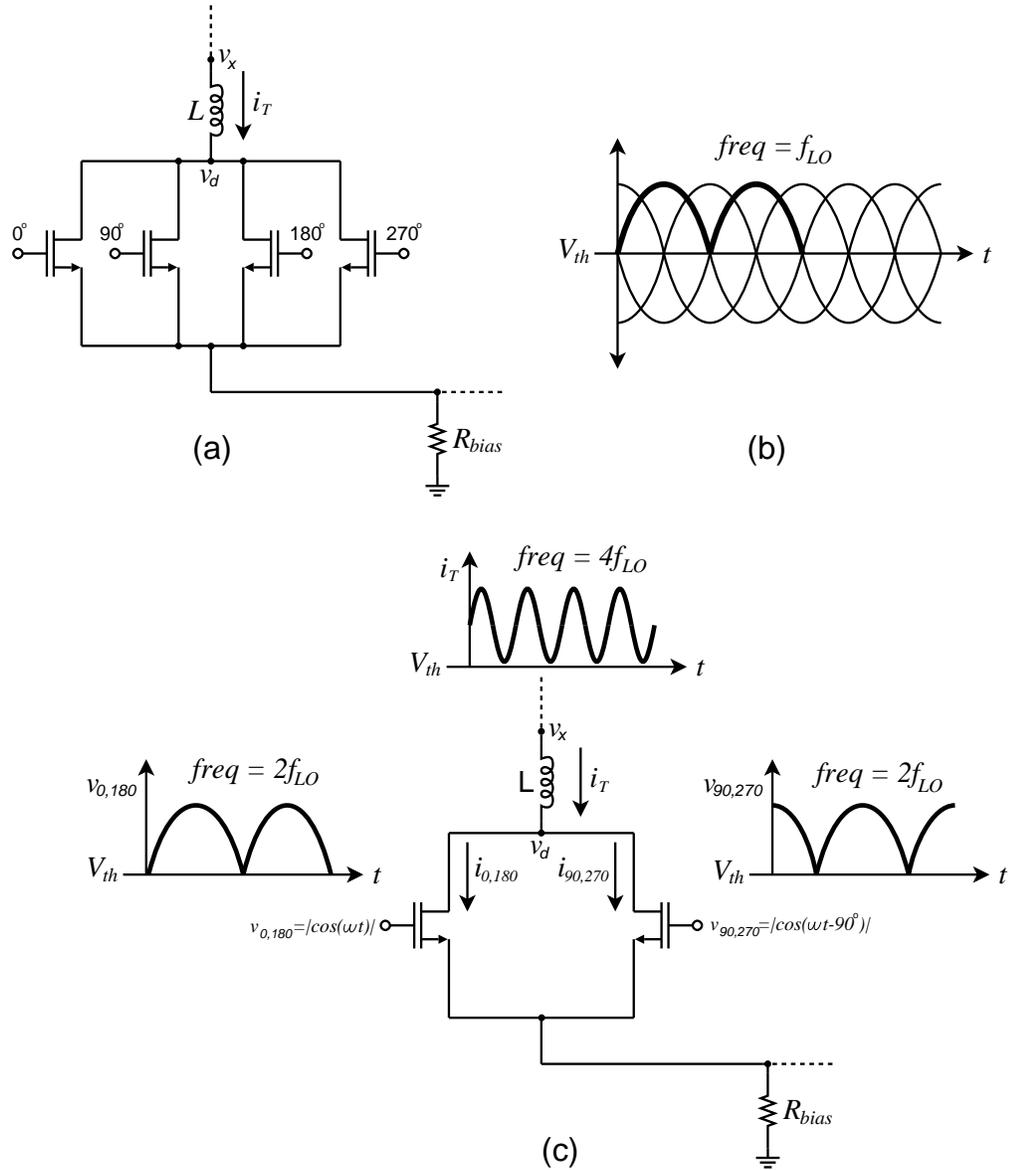


Figure 4.2: (a) One of the two $4 \times$ LO generation circuits, (b) Quadrature LO time-domain signals, and (c) Modeling the $4 \times$ LO circuit.

LO_{270} transistors can be replaced by one transistor with LO gate voltage of,

$$v_{90,270} = |A_{LO} \cos(\omega_{LO}t - \pi/2)| + V_t \quad (4.2)$$

This model is shown in Figure 4.2c. Using the short-channel model, the currents generated by the LO voltages are given by:

$$i_{0,180} = \frac{WC_{ox}V_{sat}(v_{0,180} - V_t)}{1 + LE_{sat}/(v_{0,180} - V_t)} \quad (4.3)$$

$$i_{90,270} = \frac{WC_{ox}V_{sat}(v_{90,270} - V_t)}{1 + LE_{sat}/(v_{90,270} - V_t)} \quad (4.4)$$

To simplify the analysis and to clearly see the generation of the fourth harmonic, the approximation can be made that $(v_{gs} - V_t)/L$ is large compared to E_{sat} such that the denominator $1 + LE_{sat}/(V_{gs} - V_t) \approx 1$. A numerical analysis shows that when the amplitude of the gate signal, A_{LO} , is large, the results of the simplified equations based on this approximation are very close to the results obtained using (4.3) and (4.4). Since the LO signal amplitude will generally be large, it follows that this assumption is reasonable for this circuit. The benefit of using the simplified drain current formula is that more insight can be obtained from the resulting equations. With this approximation, the drain currents are given by:

$$i_{0,180} \approx \frac{1}{2}\mu_n C_{ox} W E_{sat} |A_{LO} \cos(\omega_{LO}t)| \quad (4.5)$$

$$i_{90,270} \approx \frac{1}{2}\mu_n C_{ox} W E_{sat} |A_{LO} \cos(\omega_{LO}t - \pi/2)| \quad (4.6)$$

The total current, i_T , is simply given by $i_T = i_{0,180} + i_{90,270}$, therefore,

$$i_T \approx \frac{1}{2}\mu_n C_{ox} W E_{sat} A_{LO} (|\cos(\omega_{LO}t)| + |\sin(\omega_{LO}t)|) \quad (4.7)$$

Since,

$$|\cos(\omega t)| + |\sin(\omega t)| = \sqrt{|\sin(2\omega t)| + 1} \quad (4.8)$$

the following Taylor series expansion can be applied,

$$\sqrt{x + 1} = \sum_{n=0}^{\infty} \frac{(-1)^n (2n)!}{(1 - 2n)(n!)^2 4^n} x^n \quad |x| \leq 1 \quad (4.9)$$

Therefore, i_T expanded to three terms is given by,

$$i_T \approx \frac{1}{2} \mu_n C_{ox} W E_{sat} A_{LO} \left(\frac{15}{16} + \frac{1}{2} |\sin(2\omega_{LO} t)| + \frac{1}{16} \cos(4\omega_{LO} t) \right). \quad (4.10)$$

The two terms $|\sin(2\omega_{LO} t)|$ and $\cos(4\omega_{LO} t)$ both clearly show the fourth harmonic. The total output current signal, i_T , is dominated by the $|\sin(2\omega_{LO} t)|$ term since its frequency component at $4f_{LO}$ is over three times stronger than the $\frac{1}{16} \cos(4\omega_{LO} t)$ component. The crucial result is that the frequency of the output current is at four times the input LO frequency, or, $4f_{LO}$, as desired. A similar analysis can be performed on the other set of four transistors to show the generation of the fourth harmonic and the anti-phase relationship with (4.10). Since the mixer core maintains a differential structure, the common-mode rejection will be high and similar to that of the traditional Gilbert-cell. Of course, a disadvantage to this topology is that a higher LO input power will be required compared to a fundamental mixer since there is conversion loss in the $4 \times$ LO frequency multiplication circuit.

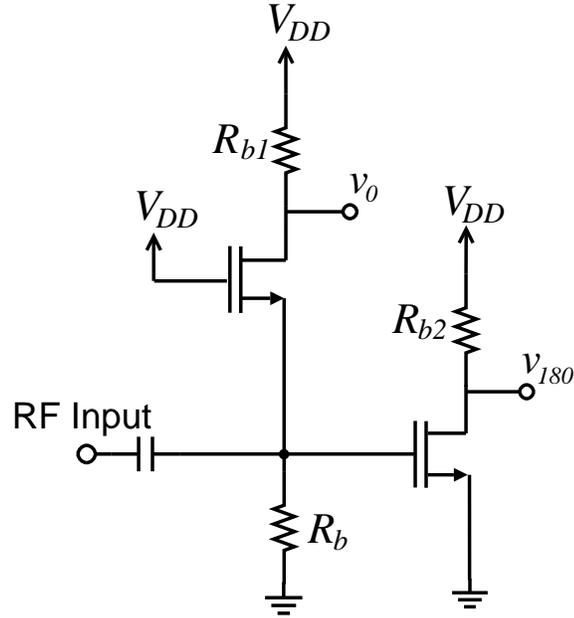
The purpose of the inductors in the mixer core (Figures 4.1 and 4.2a) are to increase the LO voltage swing at the source terminal of the RF transistors as discussed in [26], which ultimately provides higher conversion gain for the mixer at lower LO powers than would be required without the enhancement inductors. The voltage at node v_x shown in Figure 4.2a is given by,

$$v_x = v_d + (R_{ind} + j\omega_{LO}L)i_T \quad (4.11)$$

where v_d is the common drain node of the LO transistors as shown in Figure 4.2a, and R_{ind} and L are the series resistance and the inductance of the on-chip spiral inductor, respectively. Since the desired LO frequency is *four times* the LO input frequency, this inductor provides a large impedance, which increases the voltage swing at v_x and improves the resulting conversion gain. It also provides filtering for any parasitic f_{LO} and $2f_{LO}$ signals that are present since the impedance of the inductor is lower for these signals. It is also possible to trade conversion gain for linearity by using degeneration resistors or inductors in the sources of the RF transistors. In this implementation of the 4× SHM the goal was maximum conversion gain, and therefore degeneration was not used.

4.3.2 Input RF Balun

In some cases, single-ended signals are used as opposed to balanced signals. In order to convert the single-ended RF signal to a balanced signal, an active balun was used in this work primarily for ease of testing. The use of an active balun as opposed to a passive balun enables this circuit to be conveniently implemented on chip since the required size is vastly reduced. The topology of the active balun used is shown in Figure 4.3. The circuit uses a common-source path to produce a 180° phase shift and a common-gate path to produce the 0° signal with equal amplitudes [91]. An advantage to this technique is the ability to achieve a reasonably good input impedance match to 50 Ω since the input to this balun is approximately that of the common-gate circuit, $Z_{in} \approx 1/g_m$ (the resistor R_b is large). Therefore, with appropriate selection of device

Figure 4.3: RF active balun circuit for the $4\times$ SHM.

size and biasing, the input of the balun can produce wideband matching. While this topology may be somewhat more sensitive to fabrication process variations than a differential pair configuration, the elimination of matching inductors that would likely be required with a differential pair balun saves significant chip area.

Simulation results of the active balun at an input frequency around 12 GHz show that the phase error is approximately 6° and the amplitude imbalance is approximately 0.5 dB. The voltage loss through the balun at 12 GHz when the load is the input to the SHM is -3 dB. Obviously, if a balanced RF signal was already available then the RF balun would not be necessary and the resulting conversion gain would be increased. Since the RF signal is not perfectly balanced, the $RF-IF$ isolation may be degraded somewhat. However, since the RF frequency is in the Ku-band and the

IF frequency is quite low, this should not pose a significant problem since it could easily be removed by a simple filter.

4.3.3 LO Phase Shifters

In order to realize the $4\times$ SHM discussed in the previous section, octet-phase LO signals are required. Octet-phase LO signals were also required in the SHMs presented in [29–31, 35], however, all of these circuits were only $2\times$ SHMs. RC – CR polyphase filters were used to generate the required phase shifts in [15]. This technique, although the simplest, can generate phase and amplitude errors due to fabrication tolerances in the resistors. Similarly, the 45° phase shifter in [35] was also a passive network consisting of resistors and capacitors. The technique used to generate the octet signals in this work is similar to the technique used in [29]. This method essentially uses an active summer to add a 0° and a 90° signal to realize a 45° signal,

$$A\cos(\omega t) + A\cos(\omega t + \pi/2) = \sqrt{2}A\cos(\omega t + \pi/4). \quad (4.12)$$

This 45° phase shift is relative to a similar in-phase (0°) adder circuit that adds two signals with the same phase. The purpose of the in-phase adder is to equalize parasitics in the two paths so that a more accurate 45° phase relationship can be obtained. The circuit schematics of the 45° phase shifter and the in-phase adder are shown in Figure 4.4. By the proper scaling of resistors, R_{45} and R_0 , the amplitudes of the 45° phase shifter and the in-phase adders can be made equal and can potentially achieve conversion gain (in this implementation there was a small conversion loss). Since there is a total of eight in-phase and 45° phase shifter circuits, there may be a significant increase in DC power consumption. Passive 45° phase shifter circuits could be used for low-power applications.

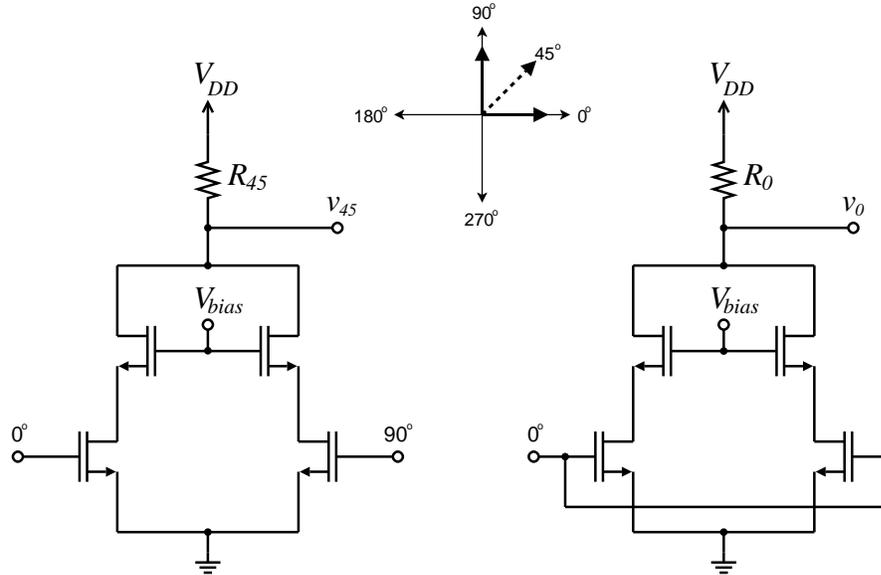


Figure 4.4: 45° phase shifter circuit. 0° and 90° signals are added producing a signal at v_{45} that is 45° out of phase with the output of the in-phase adder, v_0 .

Clearly, to use the aforementioned technique, quadrature LO signals must be available. In many cases, this is not a problem since a quadrature oscillator can simply be used. To verify the proposed $4\times$ SHM in this work, a differential LO input signal was used along with a passive $RC-CR$ 90° phase shifter, as shown in Figure 4.5. Simulation results on the complete octet-phase generator circuit show a phase error of approximately 1° and a amplitude imbalance of less than 1 dB using this technique. The main concern with using this technique is that the tolerance in the various components in the fabrication process can lead to larger phase and amplitude errors than are shown in simulations (particularly in the $RC-CR$ 90° phase shifters) and the resulting mixer performance will be degraded. A detailed analysis of the effects of potential phase and amplitude errors using this technique were presented in [29]. It was found that by following the polyphase filter with the active 45° phase

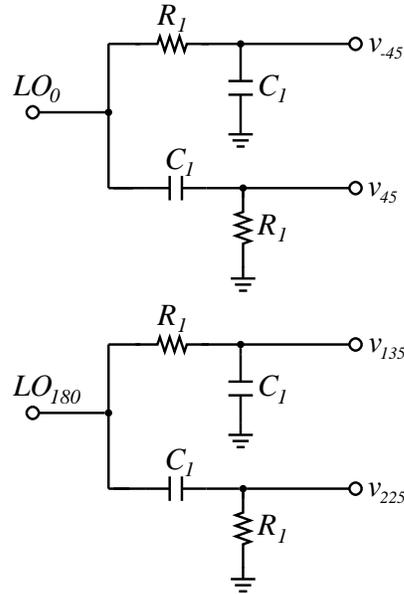
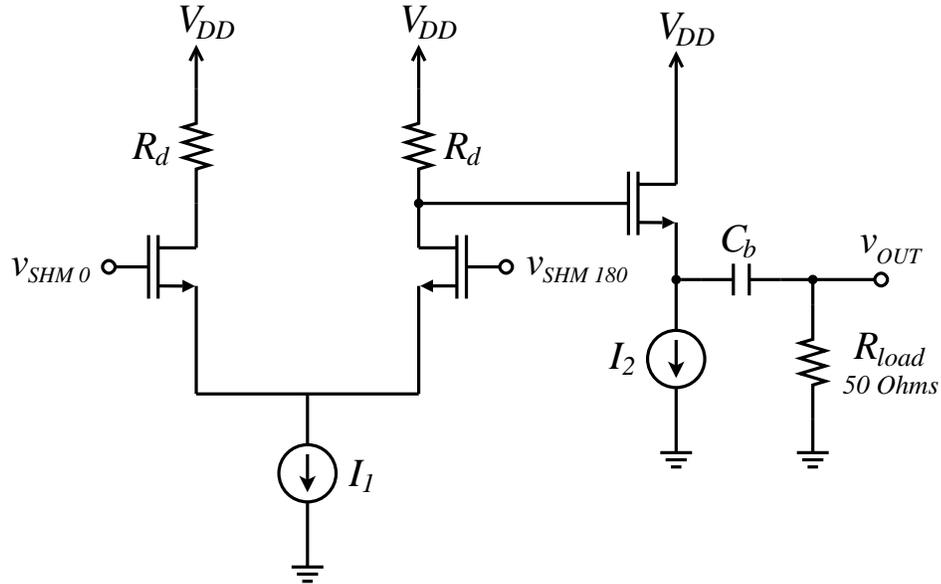


Figure 4.5: $90^\circ RC-CR$ phase shifter used in the $4\times$ SHM.

shifting circuit shown in Figure 4.4 the resulting octet-phase outputs are actually desensitized to phase errors in the polyphase filters. Furthermore, it was determined that even with significant process variations of the resistance in the $RC-CR$ 90° phase shifters the resulting accuracy of the octet-phase signal was still within acceptable limits [29].

4.3.4 Output Balun

In order to convert the differential amplifier output back to single-ended for measurement, another active balun was used. Since the IF output will be at a relatively low frequency (100 MHz, in this case), it makes the use of an active balun very attractive compared to passive techniques, given the large wavelength of the signal. Furthermore, since the frequency is low, it makes the design of this balun very

Figure 4.6: Output balun circuit for the $4\times$ SHM.

straight-forward. The output balun is shown in Figure 4.6 which includes a differential pair with a single-ended output that is connected to a source-follower buffer. The output balun was designed such that the differential voltage amplitude at the mixer output equals the buffer output, $v_{SHM0} - v_{SHM180} = v_{OUT}$. Therefore, there was no gain in this stage that would contribute to the conversion gain of the mixer.

4.4 Measurement Results

To characterize the $4\times$ CMOS SHM, coplanar waveguide (CPW) probes were used for on-chip probing. An Agilent E4446A PSA Series spectrum analyzer was used to observe the output spectrum of the mixer. The DC supply voltage was set to 2.75 V, the RF input signal was -20 dBm at 12.1 GHz, and the LO signal was 10 dBm at

3.0 GHz. Therefore, the desired IF output signal was at 100 MHz ($f_{RF} - 4f_{LO}$). The mixer output spectrum was measured with the state of the spectrum analyzer as follows: a frequency span from 1 MHz to 15 GHz, RBW and VBW equal to 3 MHz, 10 dB internal attenuation, average of 10 sweeps, 601 points, and 30 ms sweep time. The output spectrum is shown in Figure 4.7. The conversion gain is approximately 5.8 dB and all other spectral components are below -45 dBm (more than 30 dB below the IF).

To measure the 1-dB compression point, the gain at various LO input power levels, the IP3, and the IP2, the settings on the spectrum analyzer were adjusted to the following: a frequency span from 1 MHz to 150 MHz, RBW and VBW equal to 1.5 MHz, 10 dB internal attenuation, 10-point averaging, 601 points, and 1 ms sweep time. In order to determine the 1-dB compression point of the mixer, the input

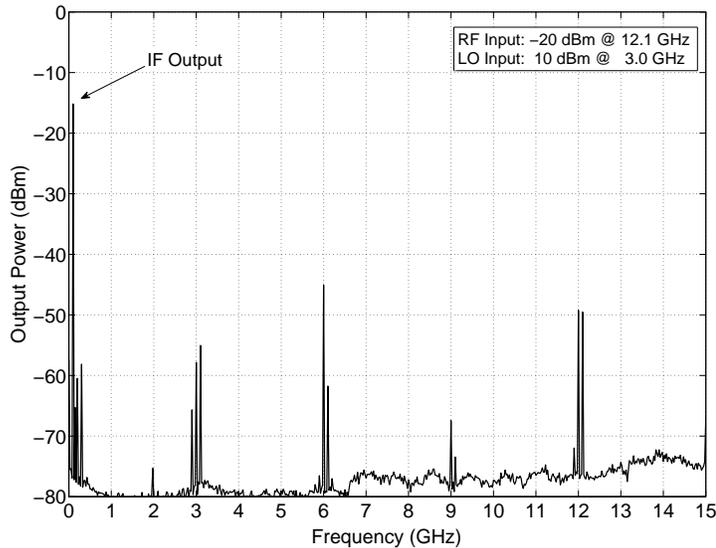


Figure 4.7: Measured mixer output spectrum with -20 dBm RF power and 10 dBm LO power.

power was swept and the IF output power was measured. The measurement and simulation results are shown in Figure 4.8. The measured input 1-dB compression point is -12 dBm. The simulation results are very similar to the measured results, however, the measurements show an earlier saturation than in simulation. The 1-dB compression point would be improved somewhat if a differential RF input signal was fed directly to the mixer without going through the balun circuit. Nevertheless, an input P_{1dB} of -12 dBm is very similar to the subharmonic mixers reported in [24, 25, 28, 29, 37, 41, 42].

A plot of the conversion gain at various LO input power levels is shown in Figure 4.9. From this figure, conversion gain is achieved when the LO power is above 8.4 dBm with a maximum conversion gain of approximately 6.5 dB occurring at 11 dBm LO input power. An optimal conversion gain was determined to occur for an LO input

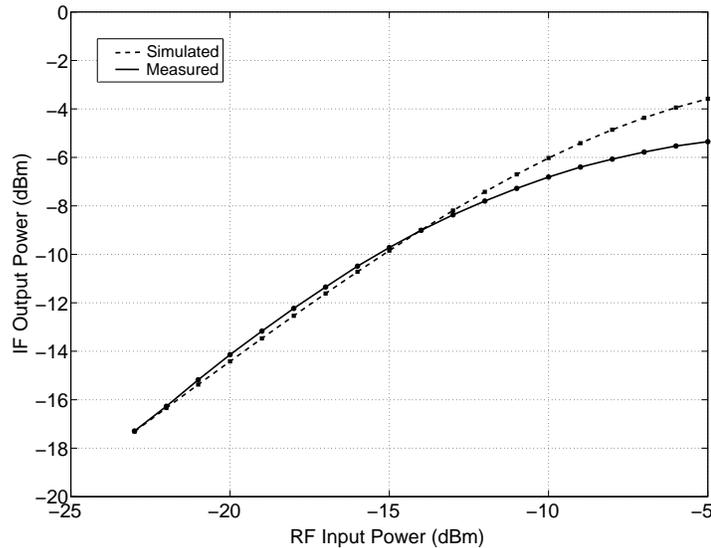


Figure 4.8: 1-dB compression point measurement (LO power = 10 dBm).

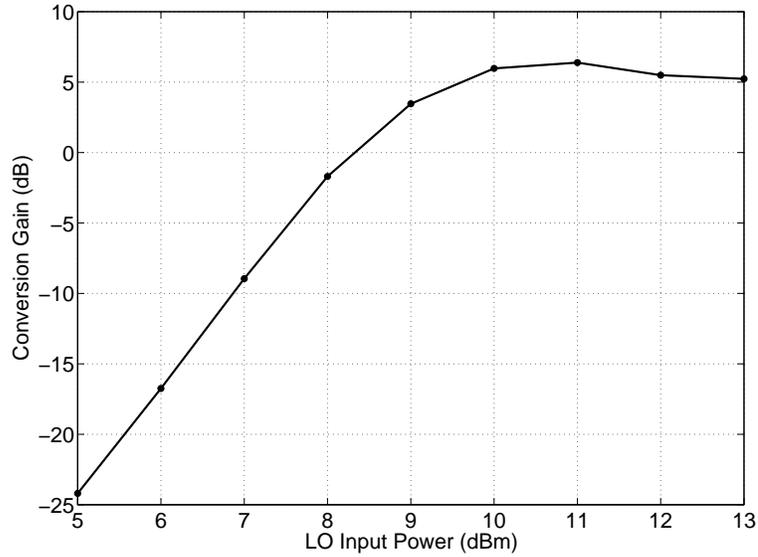


Figure 4.9: Conversion gain at various LO power levels for the $4\times$ SHM.

power of 10 dBm while still having very strong suppression of undesired spectral components (more than 30 dB below the IF). Note that these conversion gain values were obtained while having a 3 dB loss through the RF balun, and therefore higher conversion gains would be possible if a differential RF signal is already available. A conversion gain of approximately 6 dB is the highest that could be found in the literature for a $4\times$ SHM, e.g. [38–43] (most of which exhibit a conversion loss).

The possibility of a lower RF interfering signal mixing with a subharmonic of the LO was also considered. For example, a 6.1 GHz RF interfering signal could mix with the $2\times$ LO component at 6 GHz, which would interfere with the desired IF signal. From the Taylor series expansion of the LO signal in Equation (4.10), there is, ideally, no component at $2f_{LO}$, so the conversion gain from a 6.1 GHz RF to a 100 MHz IF should be very low (ideally zero). Simulations show that this conversion gain is 40 dB

below that of the desired mixing products, and therefore this is not a serious concern (in addition there would likely be an RF filter that would attenuate out of band RF signals anyway).

The third-order intercept point and the second-order intercept point were measured to determine the linearity of the mixer. To measure the IP3, a two-tone RF signal was applied at 12.10 GHz and 12.11 GHz (LO power was 10 dBm at 3.0 GHz). This produced third-order distortion signals at 90 MHz and 120 MHz. The results are shown in Figure 4.10. The IIP3 is approximately -2 dBm and the OIP3 is approximately 4 dBm. Simulations were also performed to determine the maximum IIP3 that could be obtained if source degeneration resistors were used in the sources of the RF transistors to improve linearity. It was found that an IIP3 of over 10 dBm could be achieved while maintaining a conversion gain of 0 dB.

To determine the IP2, the same two RF tones were applied (12.10 GHz and 12.11 GHz), but the spectral component at 10 MHz was observed as the RF input power increased. The plot of this measurement is shown in Figure 4.11. The IIP2 was determined to be approximately 17 dBm. It was found through simulations that the output active balun seriously degrades the IP2. Simulations with an ideal IF output balun show that the IP2 is increased by 14 dB, and therefore, the IIP2 of the mixer itself is greater than 30 dBm.

The input reflection coefficient to the RF port was also measured using an Agilent 8510C Network Analyzer with a 50 GHz Agilent 8517B S-parameter Test Set. Calibration of the network analyzer was performed using a calibration substrate (SUSS MicroTec CSR-3 GSG100-250). The network analyzer was calibrated from 1 GHz to 15 GHz with 401 points and the port power levels were both set to -30 dBm. No

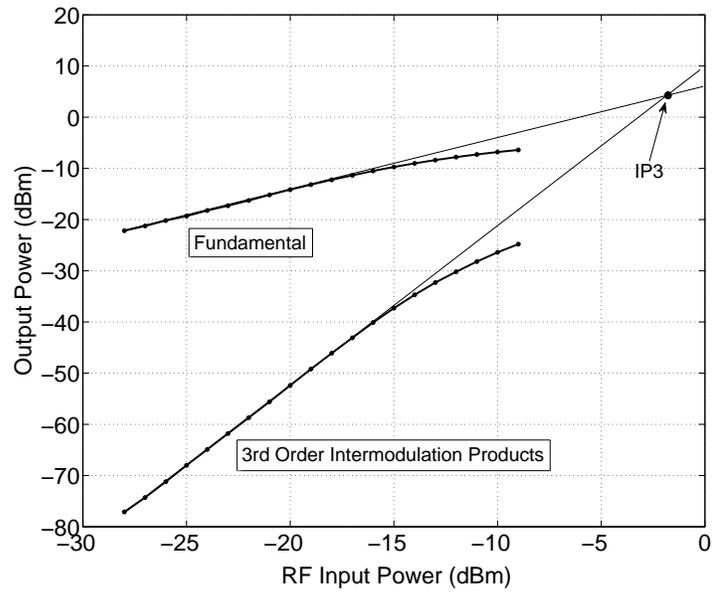


Figure 4.10: Third-order intercept point measurement (LO power = 10 dBm).

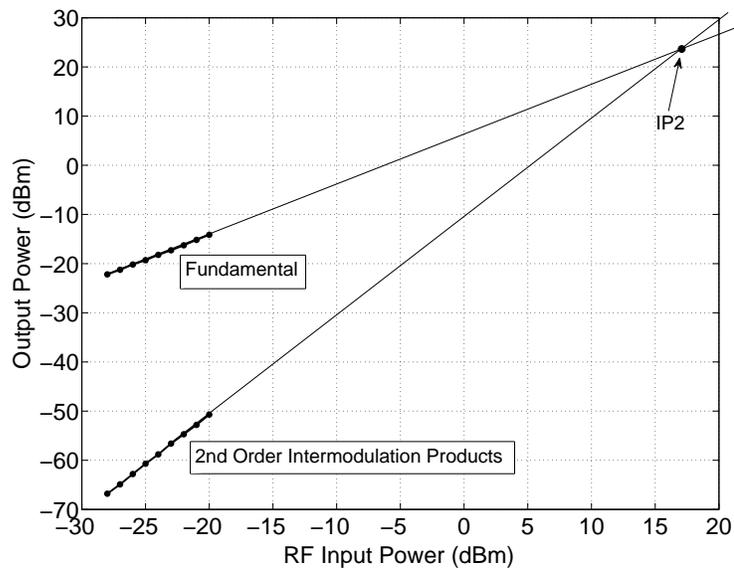


Figure 4.11: Second-order intercept point measurement (LO power = 10 dBm).

internal network analyzer attenuation was used and no averaging or smoothing was performed on the measured data.

The measured S_{11} is shown in Figure 4.12. Due to the common-gate device in the RF balun there is relatively wideband input matching. The input reflection coefficient is better than -10 dB between 10 GHz and 15 GHz.

To evaluate the susceptibility of the proposed SHM topology to DC offsets, the procedure discussed in [15] was used. Specifically, the DC level at the output was measured with three different setups: 1) Under DC bias only (RF and LO signals not applied), 2) DC bias and LO signal applied (no RF signal), and 3) DC bias with the LO signal and RF input. While performing the measurement in Step 1) both the RF and LO ports were terminated in 50Ω loads and in Step 2) the RF port was terminated in a 50Ω load. The difference between the measured DC output

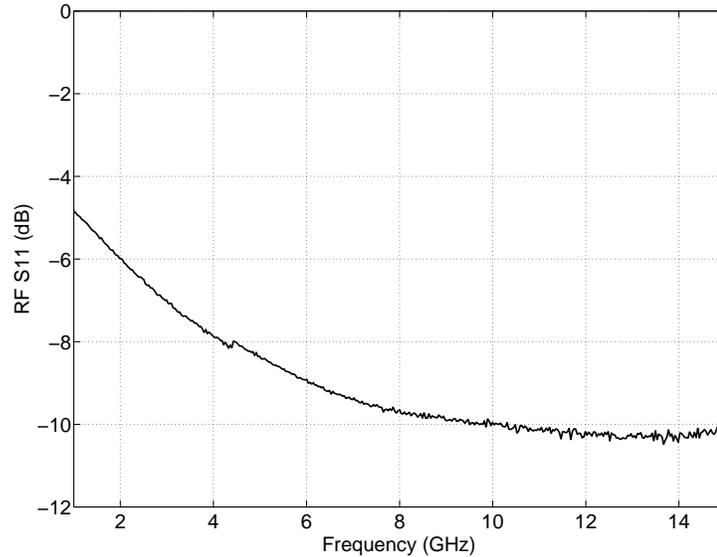


Figure 4.12: Measured RF input reflection coefficient for the $4\times$ SHM.

<i>Ports</i>	<i>Isolation</i>
RF–LO	43 dB
LO–RF	71 dB
2LO–RF	52 dB
4LO–RF	59 dB
RF–IF	30 dB
LO–IF	68 dB
2LO–IF	55 dB
4LO–IF	59 dB

Table 4.1: 4× subharmonic mixer port-to-port isolation measurements.

values in Steps 1) and 2) indicate the amount of LO self-mixing. In the case of the proposed 4× SHM, this value was measured to be 4.2 mV at an LO power of 10 dBm. The measurement in Step 3) includes the effects of the DC offsets produced by second-order nonlinearities. The measured DC offset for this case was 1.2 mV.

The isolation between the ports of the mixer was measured and the results are compiled in Table 4.1. Very high isolations between the ports were measured, with all isolations being greater than 43 dB with the exception of the *RF–IF* isolation (30 dB), which is predominately due to the amplitude and phase imbalance from the RF balun. The *LO–RF* and the *4LO–RF* suppressions, in particular are very high at 71 dB and 59 dB, respectively. These isolation measurements are very competitive and in most cases improvements over previous SHMs (e.g. [21, 25, 27, 29, 33, 38, 42, 43]).

The noise figure for the entire circuit was measured using the Noise Figure Measurement Personality of the Agilent E4446A PSA Series spectrum analyzer along with an Agilent 346C noise source. A noise figure calibration was first performed by

connecting the noise source directly to the spectrum analyzer input. The resolution bandwidth of the spectrum analyzer was 1 MHz for the noise figure measurement. The double sideband (DSB) noise figure was measured to be 15 dB (SSB NF \approx 18 dB), which includes the noise generated in the input RF balun. To determine the noise of the mixer alone, simulations were performed with an ideal input RF balun and the results show that the noise figure decreased by approximately 3 dB. Therefore, if a differential RF is already available, the DSB noise figure would be approximately 12 dB, which is similar to, or an improvement upon, the subharmonic mixers described in [24, 26–28, 33, 34, 37]. Flicker noise measurements were not performed due to an output DC-blocking capacitor. It is expected that the flicker noise will be increased somewhat compared to the traditional Gilbert-cell due to the additional LO switching noise, as discussed in [94].

The DC power consumption for the mixer core was approximately 5 mW and for the entire chip including the RF balun, LO octet-phase generation, mixer core, output balun, and buffer, the power consumption was measured to be 113 mW. The simulated power consumption for the octet-phase generation circuit and the mixer core alone is approximately 50 mW. The chip dimensions were $850 \mu\text{m} \times 850 \mu\text{m}$ including pads. A photograph of the fabricated chip is shown in Figure 4.13.

4.5 Summary

A new $4\times$ subharmonic mixer has been presented using CMOS $0.18 \mu\text{m}$ technology that accepts a 12.1 GHz RF input signal and a 3.0 GHz LO signal and produces a 100 MHz IF output ($f_{RF} - 4f_{LO}$). The circuit requires octet-phase LO signals, which are generated in this work through a polyphase filter and an active 45° phase shifting

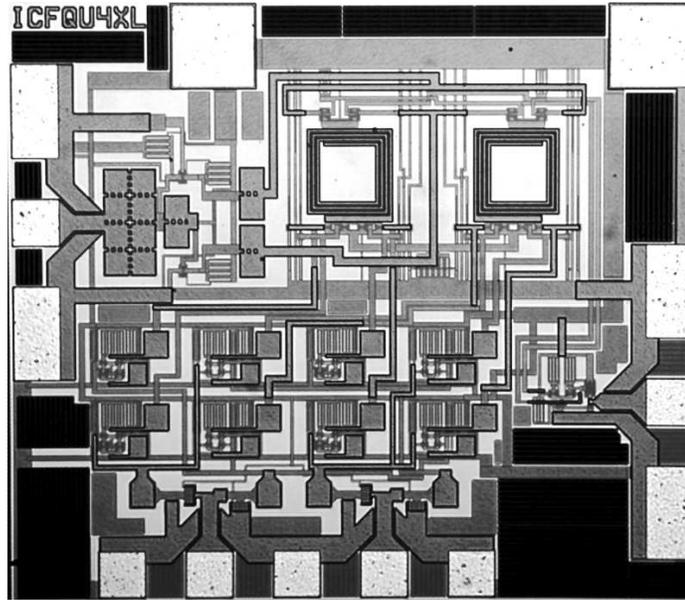


Figure 4.13: Microphotograph of the proposed $4\times$ SHM.

circuit. An active balun was used for the RF port to convert the single-ended 12.1 GHz signal to a differential signal and another active balun is used at the output to convert the differential output signal back to single-ended for measurement. A conversion gain of approximately 6 dB and a 1-dB compression point of -12 dBm was obtained. Very high isolations between the ports were measured with $LO-RF$ isolation of 71 dB and $4LO-RF$ isolation of 59 dB. The measured IIP3 and IIP2 were -2 dBm and 17 dBm, respectively. The circuit dimensions are $850\ \mu\text{m} \times 850\ \mu\text{m}$. To the best of the author's knowledge, this is the first $4\times$ subharmonic mixer demonstrated in CMOS technology and it achieves the highest conversion gain for any $4\times$ SHM to date. This circuit could be used to reduce the LO self-mixing in a direct conversion receiver, or in any mixer application where the reduction of the local oscillator frequency by a factor of four is beneficial.

Chapter 5

Quadrature Oscillator

5.1 Introduction

In this Chapter a quadrature oscillator is presented that uses superharmonic coupling [9]. This quadrature oscillator is suitable for use with both the $2\times$ subharmonic mixer discussed in Chapter 3, as well as the $4\times$ subharmonic mixer discussed in Chapter 4.

The presence of harmonics in CMOS oscillator circuits is unavoidable. These harmonics are generally unwanted signals that appear with the desired fundamental signal. In differential oscillators there exist common-mode nodes (like the two source nodes in a cross-coupled oscillator) where higher-order harmonics are present and the fundamental is essentially absent. These second-order harmonics present at the common-mode nodes of two oscillators can be used to enforce a quadrature relationship between the fundamental outputs through a technique called superharmonic coupling.

5.2 Concept of the Quadrature Oscillator

The superharmonic coupling technique enforces a 180° relationship between the even-ordered harmonics of two oscillator circuits, which produces a quadrature relationship at the fundamental outputs, as shown in Figure 5.1a. While both passive and active superharmonic coupling circuits are possible, this work uses an active circuit in order to significantly reduce the required chip area. The performance of a quadrature oscillator using the superharmonic coupling topology will be determined by the performance of the two individual differential oscillators as well as the coupling network that enforces the anti-phase relationship between the second-order harmonics at the common-mode nodes.

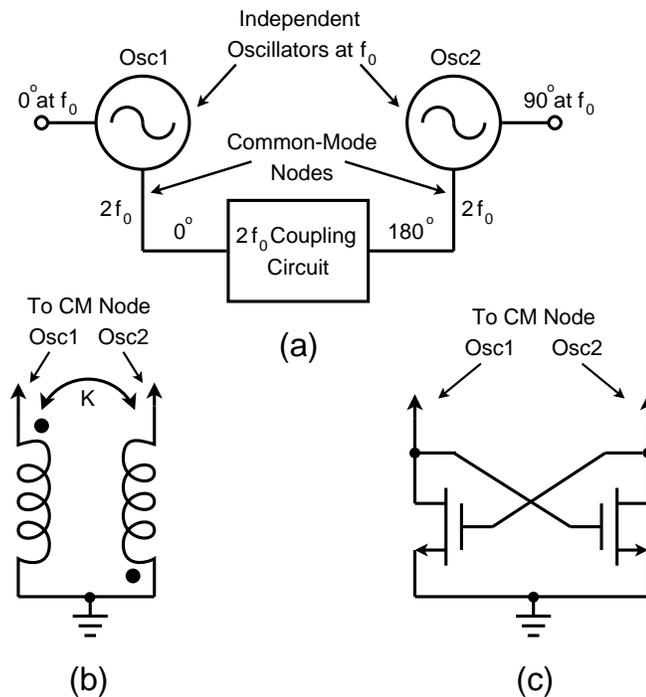


Figure 5.1: Quadrature oscillator superharmonic coupling techniques.

5.3 Circuit Design

A very common way of implementing a CMOS differential LC oscillator is to use a cross-coupled pair to generate the negative resistance required to overcome the losses in the tank. The resistance looking into the cross-coupled pair is given by $-2/g_m$ where g_m is the transconductance of each of the FETs in the cross-coupled pair. Therefore, with an appropriate device size and biasing, the negative resistance required to counteract the losses in the tank can be realized.

The core quadrature oscillator circuit investigated in this work is shown in Figure 5.2. It consists of two cross-coupled oscillators connected through a cross-coupled pair. It has been shown that by including cross-coupled PMOS transistors above the cross-coupled NMOS transistors the phase noise of the oscillator can be improved significantly due to the higher transconductance and faster switching speed of the complementary structure [50]. The oscillation frequency for each oscillator can be found from the familiar formula for the resonant frequency of an LC tank, where L is the value of the on-chip spiral inductor and C is the total capacitance at the tank nodes. The inductors used in this circuit were $150 \mu\text{m} \times 150 \mu\text{m}$ with 4.25 turns. An electromagnetic simulation of this inductor geometry predicted an inductance of 2 nH and a Q -factor of approximately 4 at 3.0 GHz. The total capacitance including the lumped capacitor as well as the parasitic capacitance was 1.4 pF to provide oscillation at 3.0 GHz.

The network used to enforce the 180° phase difference in the second-order harmonics is a critical part of the quadrature oscillator. It is this anti-phase relationship that creates the quadrature phase relationship at the fundamental frequency. Convenient common-mode nodes for coupling the second harmonic are the common-source

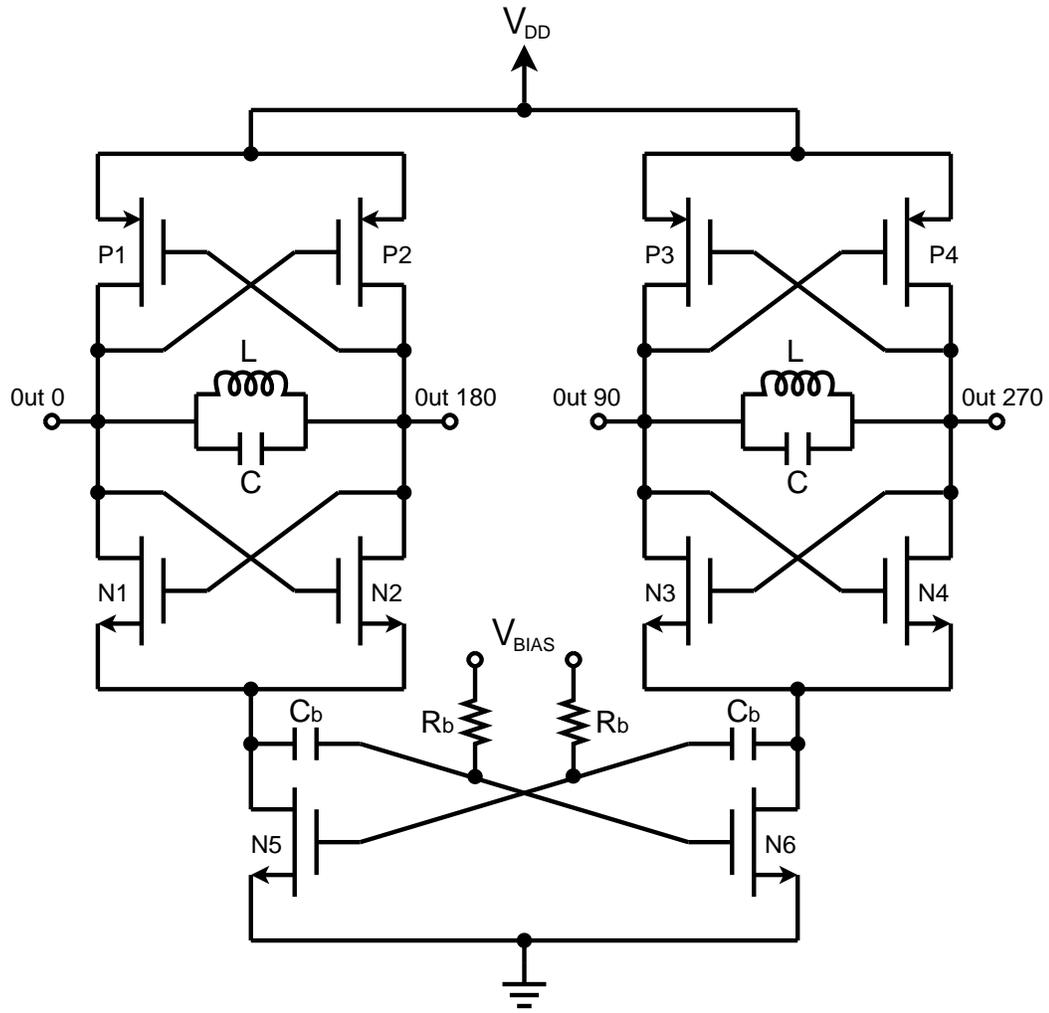


Figure 5.2: Proposed quadrature oscillator core circuit.

nodes in each of the cross-coupled differential pairs, shown as $CM1$ and $CM2$ in the complete oscillator circuit schematic shown in Figure 5.3. DC blocking capacitors were used so that transistors $N5$ – $N6$ could be biased for optimal coupling. Since any practical use of an oscillator involves connecting its output to other circuitry, buffers must be used to ensure that loading does not disrupt the oscillations. Source-follower buffers were used for each of the four outputs so that the oscillator can be measured using equipment with $50\ \Omega$ input impedances. The current sources shown in the buffer circuits in Figure 5.3 were implemented with the common current-mirror configuration. Transistors $N8$ and $N10$ were used to ensure that there is equal loading of the oscillator circuit. The 180° and 270° outputs were terminated on-chip with $50\ \Omega$ loads and the 0° and 90° were connected to CPW pads for on-chip probing.

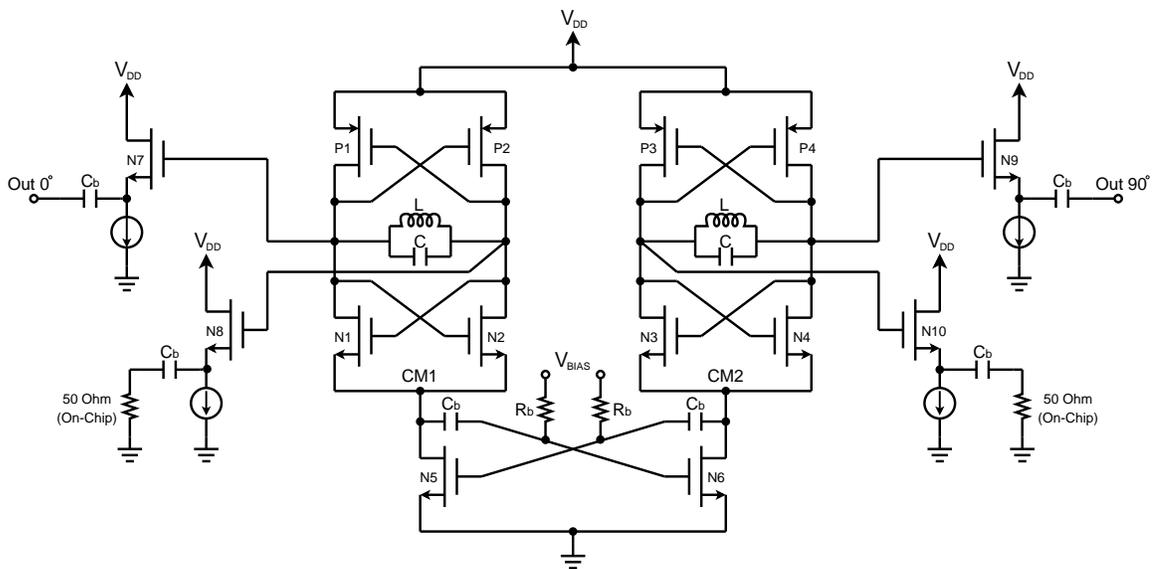


Figure 5.3: Complete quadrature oscillator circuit.

5.4 Measurement Results

To characterize the quadrature oscillator chip, coplanar waveguide probes were used and several measurements were performed. The DC supply voltage was set to 1.8 V and the bias voltage for the coupling circuit, V_{BIAS} , was set to 0.85 V. To verify that the circuit is producing outputs that have a 90° mutual phase shift, a digital sampling oscilloscope (Tektronix TDS8000) was used. The test setup for this measurement is shown in Figure 5.4. As shown in this figure, one output of the oscillator is split in order to generate the trigger signal for the oscilloscope with the other splitter output connected to *Channel 1*. An identical splitter is used in the other path with one output terminated in a 50Ω load and the other splitter output connected to the *Channel 2* input of the oscilloscope. This setup is used in order to maintain the phase and amplitude relationships between the oscillator outputs while also generating the required trigger signal. The loss and phase error introduced by the cables and splitters was measured using a vector network analyzer (Agilent 8510C). Shown in Figure 5.5 are the time-domain output waveforms compensated for the loss and phase shift due to the measurement setup for a time-span from 21.0 ns to 21.5 ns. The phase error was determined to be less than 6° .

To view the spectrum of the output signal, one of the quadrature oscillator outputs was connect to a spectrum analyzer (Agilent E4446A PSA) while the other output was terminated in a 50Ω load. The spectrum analyzer was set for a frequency range from 1.0 GHz to 14.0 GHz with 601 points, a RBW and VBW of 3 MHz, a sweep time of 28 ms, no averaging and a 10 dB internal attenuation. The resulting spectrum is shown in Figure 5.6. The strongest spectral component is at 3.007 GHz with a power of approximately -6 dBm. The second harmonic at 6 GHz is below -20 dBc from the

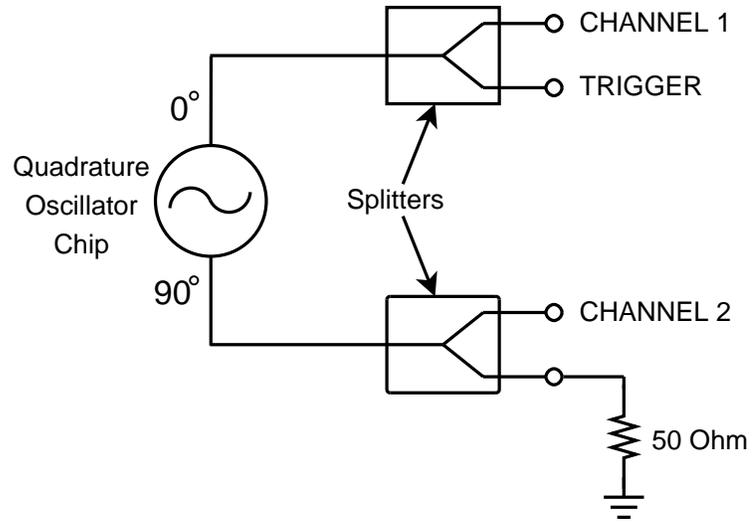


Figure 5.4: Time-domain measurement setup for the quadrature oscillator.

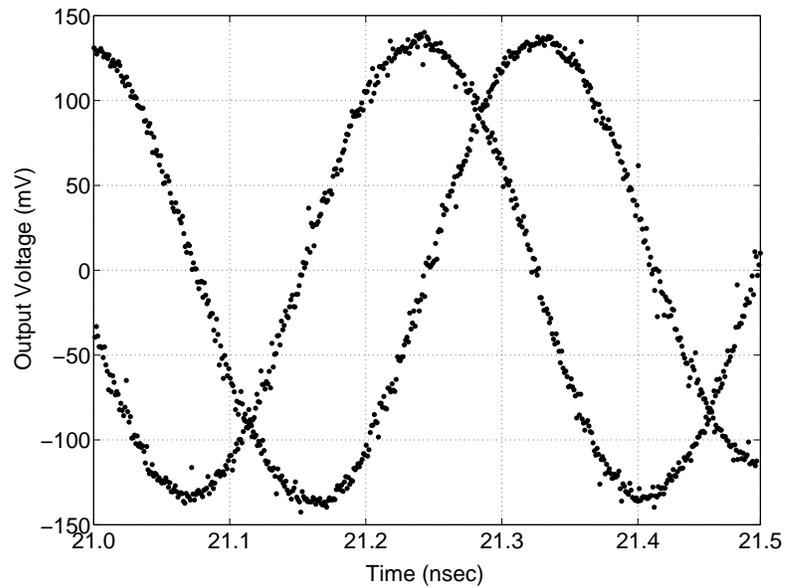


Figure 5.5: Measured time-domain quadrature oscillator output.

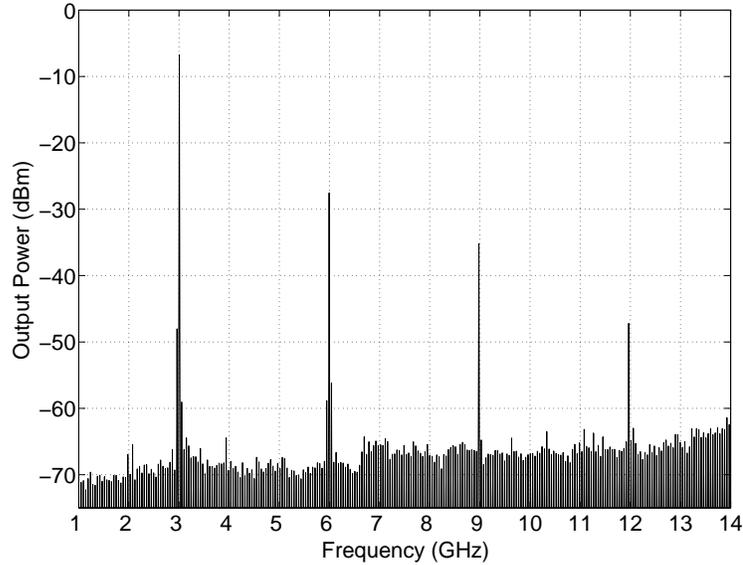


Figure 5.6: Measured quadrature oscillator output spectrum.

fundamental. The phase noise of the oscillator was also measured using the spectrum analyzer from 10 kHz to 10 MHz with 4207 points using the signal tracking option and 0 dB internal attenuation. The results are shown in Figure 5.7. The phase noise at 100 kHz, 1 MHz, and 10 MHz offsets are approximately -90 dBc/Hz, -116 dBc/Hz, and -134 dBc/Hz, respectively. A commonly used figure of merit for oscillators is defined as [95]:

$$FOM = L(\Delta f) - 20 \log \left(\frac{f_c}{\Delta f} \right) + 10 \log(P_{DC}) \quad (5.1)$$

where f_c is the frequency of oscillation, Δf is the offset frequency, $L(\Delta f)$ is the phase noise in dBc/Hz at Δf , and P_{DC} is the power consumption in mW. The power consumption of the core of the quadrature oscillator is 7.5 mW (34 mW including

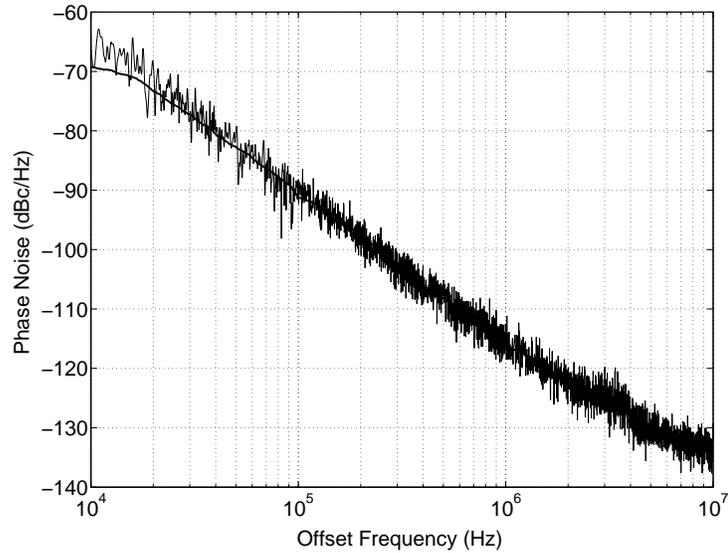


Figure 5.7: Measured phase noise of quadrature oscillator.

buffers). Therefore, the figure of merit for this oscillator is -177 dBc/Hz at a 1 MHz offset. This result compares favorably with the VCO in [59], which uses a similar superharmonic coupling circuit and has a FOM of -170 dBc/Hz. Aided by the use of a complementary cross-coupled topology, an improved phase noise and figure of merit were achieved in this work compared to the oscillator in [59] despite having a lower tank Q -factor in each oscillator. While better phase noise performance has been obtained with the use of a passive inverting transformer in [56–58], it comes at the cost of the significantly increased chip area required with that technique. The proposed CMOS quadrature oscillator in this work has an area of $650 \mu\text{m} \times 500 \mu\text{m}$ excluding pads and $800 \mu\text{m} \times 670 \mu\text{m}$ including pads. This area is only 27% of the area used in [56] ($2000 \mu\text{m} \times 1000 \mu\text{m}$) and 34% of the area used in [57] ($1250 \mu\text{m} \times 1250 \mu\text{m}$), which both use superharmonic coupling with inverting transformers. The layout area

is 83% of area used in [59], which introduced this active superharmonic coupling topology. A micro-photograph of the chip is shown in Figure 5.8.

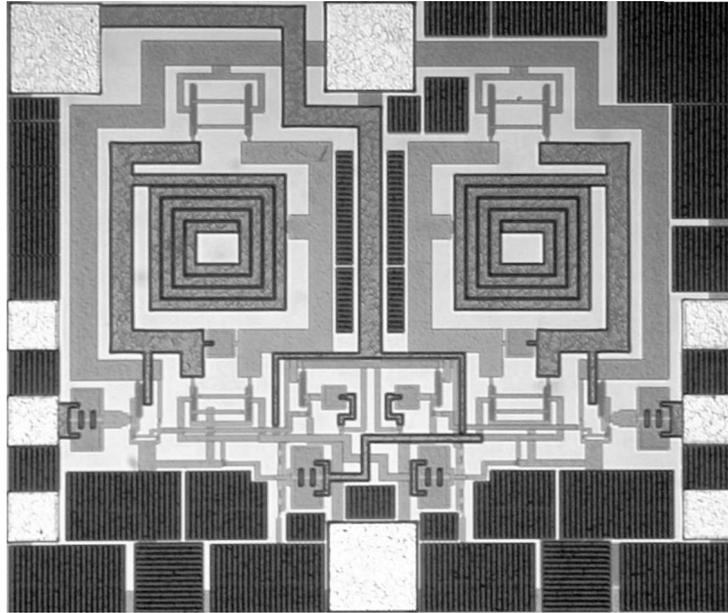


Figure 5.8: Photograph of the proposed CMOS quadrature oscillator chip.

5.5 Summary

A CMOS quadrature oscillator was designed at 3.0 GHz using superharmonic coupling. This technique couples the second-order harmonics between two oscillators and forces an anti-phase relationship, which in turn forces a quadrature relationship at the fundamental. To perform this coupling with a 180° phase shift, a cross-coupled differential NMOS pair was used at the common-mode nodes. A pair of cross-coupled PMOS transistors were used in each of the oscillator circuits in order to reduce phase noise. This circuit could easily be adapted to a VCO by simply replacing the lumped

capacitors in the tank circuits with varactors. This CMOS quadrature oscillator using active superharmonic coupling shows very good performance with an output power of -6 dBm, phase noise of -116 dBc/Hz at a 1 MHz offset, and a figure of merit of -177 dBc/Hz. Furthermore, by using a cross-coupled differential pair as opposed to an inverting transformer to create the 180° phase shift in the second-order harmonics, significant chip area and design time can be saved (since EM simulations of a passive on-chip inverting transformer are not necessary).

Chapter 6

A Dual-Band Mixer/Oscillator

6.1 Introduction

The desire to realize multi-function wireless communications devices has led to an interest in designing circuits that operate in multiple bands in an attempt to avoid a duplication of the RF circuitry. Often, in multi-band wireless communications systems there is a separate RF front-end for each frequency band of operation, consisting of multiple low-noise amplifiers, mixers, and oscillators. Clearly, there is significant potential to reduce power consumption and chip area required if some of the RF front-end circuits can be used for more than one frequency band.

There have been several demonstrations of dual-band mixer circuits. For example, in [96], a switched inductor matching network was used to match the input impedance in the two bands of interest. Similarly, in [97], an $L-C$ network was used to achieve input and output matching simultaneously in the two desired bands. In [98], a dual-band front-end was demonstrated, but used redundant circuitry as opposed to realizing a dual-band mixer with a single mixer core. A dual-band up-converter

was discussed in [99], but also used two mixer cores. In [100], a dual-band mixer was realized using composite right/left-handed transmission lines, however, this implementation would be difficult to employ monolithically. In each of these previous designs, multiple local oscillators (LOs) were used, or an external LO signal was used as the input to the mixer. In this chapter, a dual-band mixer/oscillator circuit is demonstrated that uses a single oscillator and a single mixer core.

6.2 Concept of the Dual-Band Mixer/Oscillator

A block diagram of the proposed dual-band mixer/oscillator is shown in Figure 6.1. This figure shows a down-converting mixer with differential RF input and IF output, as well as a reconfigurable LO input. If a local oscillator is available that has a

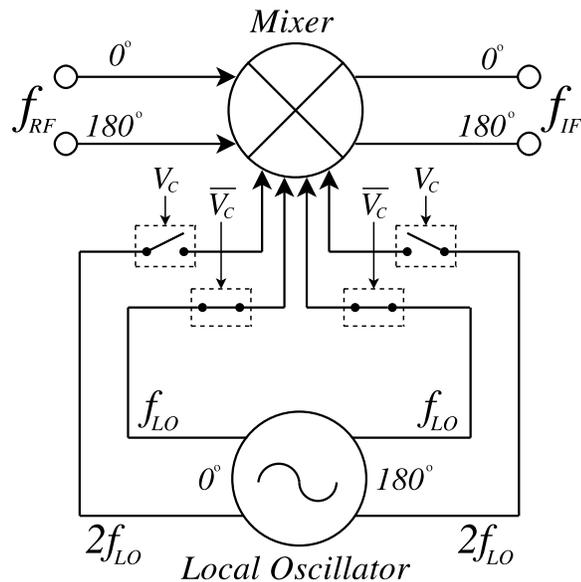


Figure 6.1: Block diagram of the proposed dual-band mixer/oscillator.

differential output at both f_{LO} and $2f_{LO}$, two pairs of complementary switches can be used to connect the desired LO signal to the mixer. Depending on the state of the switches, the mixer can have an LO input in two different frequency bands, thus permitting two different RF frequency bands at the mixer input while maintaining a constant intermediate frequency output. The result is a dual-band mixer/oscillator using a single on-chip quadrature voltage-controlled oscillator (VCO) along with a single mixer circuit. Of course, a disadvantage of this technique is that the two bands of interest can not be selected independently (due to the required second harmonic relationship of the LO). To distinguish between the two states of the dual-band mixer/oscillator, the term “fundamental-mode” will be used to describe the circuit state where the fundamental oscillator output at f_{LO} is connected to the mixer, and the term “subharmonic-mode” will be used to describe the state where the $2f_{LO}$ signal is connected to the mixer. This chapter will discuss the details of designing of a VCO that has a differential output at f_{LO} and $2f_{LO}$, as well as the mixer circuit that was used. As a demonstration of this technique, a chip was fabricated using CMOS $0.13\ \mu\text{m}$ technology with dual-band operation in C-band and X-band.

6.3 Circuit Design

The proposed circuit uses both the fundamental and the second harmonic outputs of a quadrature oscillator connected to a mixer through complementary switches, as shown in the block diagram in Figure 6.1. The design of the voltage-controlled quadrature oscillator circuit and the mixer circuit will be described in detail below.

6.3.1 Voltage-Controlled Quadrature Oscillator

The general topology chosen for the oscillator in this work is the well-known cross-coupled pair oscillator. This basic oscillator circuit uses two cross-coupled transistors to generate a negative resistance equal to $-2/g_m$ that is used to counteract the losses in the L - C tank. The output of this oscillator is differential at the drains of the two cross-coupled FETs. In order to use this technique to realize a quadrature oscillator, two identical cross-coupled oscillator circuits can be used along with a connecting circuit that enforces a quadrature relationship between the fundamental outputs, as discussed in Chapter 5. There have been several techniques proposed to enforce quadrature outputs including fundamental coupling circuits [55] and superharmonic coupling circuits [9, 56–59]. As discussed previously, superharmonic coupling exploits the existence of even-ordered harmonic signals at the common-mode nodes of an oscillator, the strongest of which is at twice the fundamental frequency. By enforcing a 180° relationship between the second harmonic signals in the two otherwise separate oscillator circuits, a quadrature relationship between the fundamental outputs is obtained. Superharmonic coupling was the natural choice for this work, since the second-harmonic signal will also be used for the mixer while in the subharmonic-mode. Superharmonic coupling can be achieved using both passive [56–58] and active [9, 59] techniques. Active superharmonic coupling was used for the quadrature oscillator in this work because of its significant advantage of requiring much less space on-chip by replacing the transformer with a cross-coupled pair of FETs.

The voltage-controlled quadrature oscillator circuit is shown in Figure 6.2. Each of the two cross-coupled oscillators will oscillate at the same frequency determined by $f_{LO} = 1/(2\pi\sqrt{LC_{tot}})$ where L is the inductance shown in Figure 6.2, and C_{tot} is

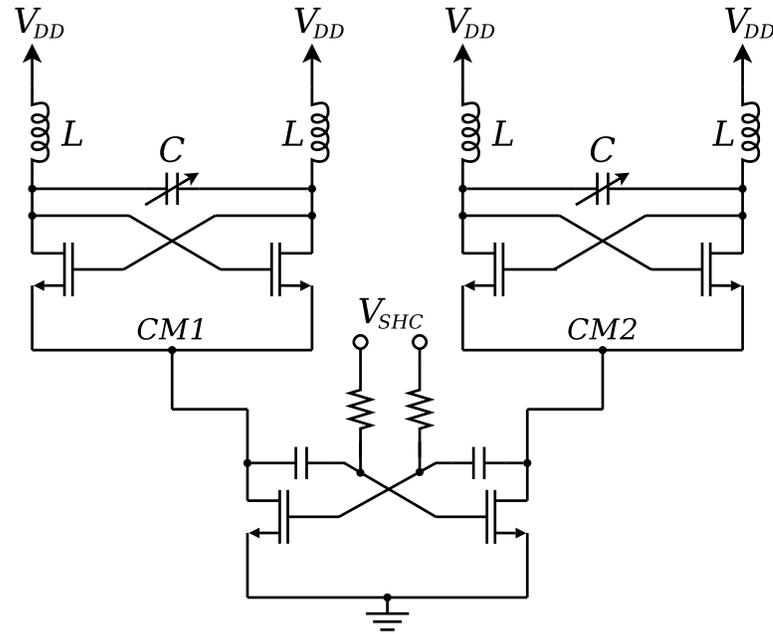


Figure 6.2: Quadrature VCO using superharmonic coupling.

the total capacitance including the varactor capacitance, C , as well as any parasitic capacitance at the output nodes. The nodes labelled $CM1$ and $CM2$ in Figure 6.2 are examples of common-mode nodes where only the even-order harmonics of the fundamental outputs exist, the most dominant of which is the second harmonic at $2f_{LO}$. An additional cross-coupled pair is used to connect the two oscillators and generate a 180° relationship between the second-order harmonic signals at $CM1$ and $CM2$, which enforces a quadrature relationship between the fundamental outputs. The frequency of the oscillator is tuned via a control voltage on the varactor shown in Figure 6.2. An advantage of using the second-harmonic signal for the mixer while in subharmonic-mode is the doubling of the tuning range of the oscillator compared to the fundamental tuning range. Compared to the quadrature oscillator demonstrated

in Chapter 5 [9], this oscillator does not use cross-coupled PMOS transistors above the cross-coupled NMOS transistors in order to maximize the $2f_{LO}$ signal at the common-mode nodes $CM1$ and $CM2$. Furthermore, whereas the oscillator in Chapter 5 was designed for a fixed frequency, varactors were used in this work to enable frequency tuning.

The bias voltage on the gates of the coupling circuit, V_{SHC} , is set to strongly couple the $2f_{LO}$ signal to ensure a differential relationship is established at $CM1$ and $CM2$ when the oscillator reaches a steady-state, thus resulting in quadrature fundamental outputs. Source-follower buffers were connected to the four fundamental outputs of the quadrature oscillator (not shown in Figure 6.2) so that the effect of connecting the oscillator output to other circuits will be minimal.

6.3.2 Mixer

The mixer circuit uses the top half of the traditional Gilbert-cell topology. Figure 6.3 shows a simplified circuit schematic of the mixer in subharmonic-mode. The common-mode nodes, where the second harmonic signal is dominant, are connected to the sources of the RF transistors. These $2f_{LO}$ signals at $CM1$ and $CM2$ are 180° out of phase with each other, which maintains the double-balanced characteristic of the Gilbert-cell. The circuit could be implemented as shown in Figure 6.3 as a single-band mixer with the doubled LO frequency output. If implemented in this way, the use of an additional frequency doubler circuit connected to the fundamental output could be avoided, thus saving chip space and reducing power consumption.

A simplified circuit diagram of the dual-band mixer/oscillator is shown in Figure 6.4. Included in this figure are the four source-follower buffers that are connected

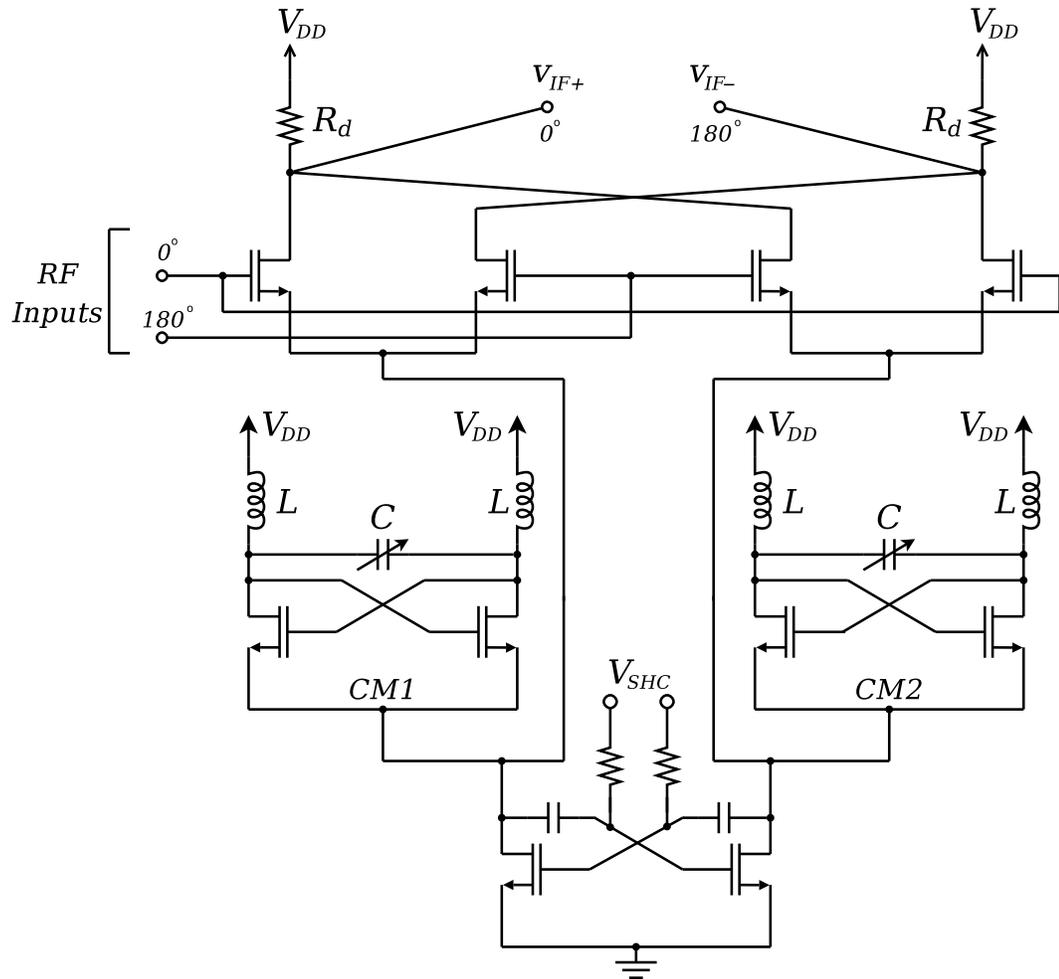


Figure 6.3: Simplified circuit schematic of the proposed dual-band mixer/oscillator in subharmonic mode.

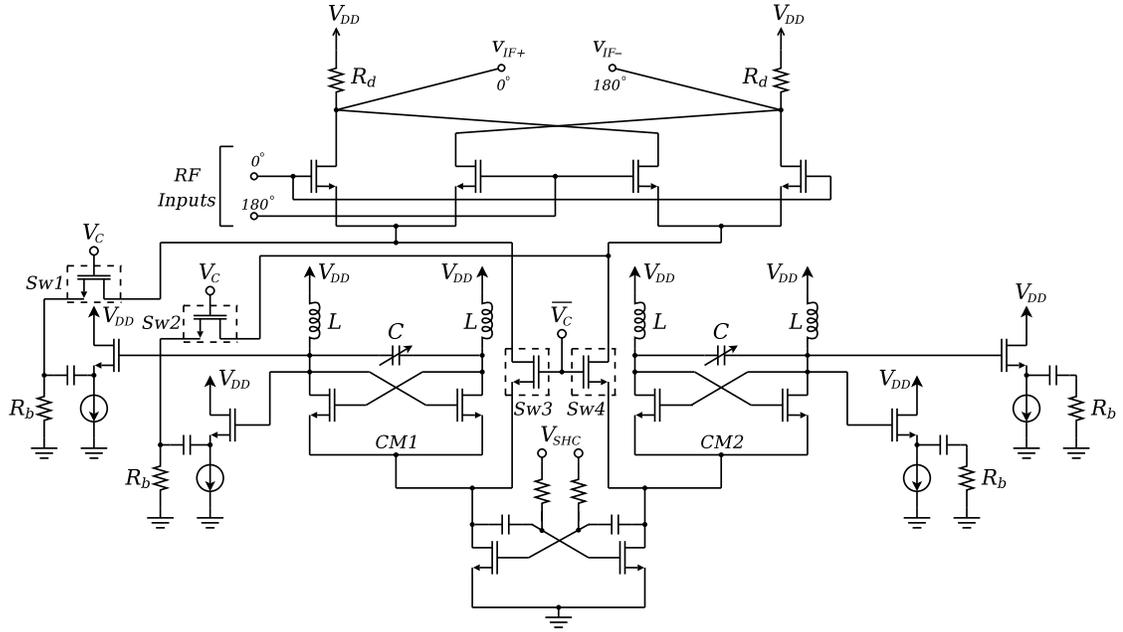


Figure 6.4: Circuit schematic of the proposed dual-band mixer/oscillator.

to the fundamental quadrature oscillator output. The value of R_b was selected to equalize the fundamental signal amplitude with the $2f_{LO}$ signal amplitude at $CM1$ and $CM2$. To select the fundamental-mode for the mixer, the control voltage, V_C , is set to V_{DD} , turning on switches $Sw1$ and $Sw2$ and turning off switches $Sw3$ and $Sw4$. This connects the 0° and 180° fundamental outputs at f_{LO} to the sources of the RF transistors. The 90° and 270° fundamental outputs are connected to identical source-follower buffers as the 0° and 180° outputs to maintain equal loads to the oscillator tank. Note that the 90° and 270° fundamental outputs of the oscillator are not used in the fundamental-mode of operation, however, they are required to generate the $2f_{LO}$ signal at $CM2$ for the subharmonic-mode, and they could be used elsewhere in the system if needed. For subharmonic-mode, the control voltage, $V_C = 0$ V, turning

off switches $Sw1$ and $Sw2$ and turning on switches $Sw3$ and $Sw4$. This connects the 0° and 180° $2f_{LO}$ signals to the sources of the RF transistors.

An alternative circuit configuration to achieve a similar dual-band mixer/oscillator would be to only use the fundamental outputs of the quadrature oscillator along with the subharmonic mixer described in Chapter 3 [8, 36]. In this subharmonic mixer, LO frequency doubling pairs of transistors are used with the 0° , 90° , 180° , and 270° oscillator outputs. In order to achieve dual-band operation, a series of switches are needed to connect the 0° , 90° , 180° , and 270° signals to the appropriate LO transistors for subharmonic-mode, and only connect the 0° and 180° to the appropriate LO transistors for fundamental-mode. It was found through simulations that greater conversion gain could be achieved by directly using the doubled frequency component already present at the common-mode as opposed to using the quadrature fundamental outputs with a LO doubling pair. Furthermore, a lower noise figure was obtained by using the $2f_{LO}$ signal directly from the oscillator due to the elimination of the switching noise that accompanies the LO doubling pairs in the subharmonic mixer topology of [8, 36].

Each of the two outputs of the mixer at V_{IF+} and V_{IF-} are connected to source-follower buffers and connected to bonding pads. These two signals are combined off-chip and connected to the $50\ \Omega$ measurement equipment. The source-follower buffers and combiner were designed such that the output voltage amplitude across the $50\ \Omega$ load of the measurement equipment is equal to $(V_{IF+} - V_{IF-})$.

6.4 Measurement Results

The dual-band mixer/oscillator was characterized using coplanar waveguide probes, signal sources and an Agilent E4446A PSA Series spectrum analyzer. The supply voltage, V_{DD} , was set to 1.5 V. The fundamental oscillation frequency was measured at various varactor control voltages, V_{cap} , and the results are shown in Figure 6.5 for the following spectrum analyzer setup: frequency range from 3.0 GHz to 8.0 GHz, 601 points, RBW = VBW = 3.0 MHz, internal attenuation of 10 dB. As shown in this figure, the oscillation frequency can be tuned from 4.8 GHz to 5.8 GHz as V_{cap} is varied from 0 V to 1.5 V. When the circuit is in subharmonic-mode, this output frequency is doubled, thus giving an LO frequency range from 9.6 GHz to 11.6 GHz.

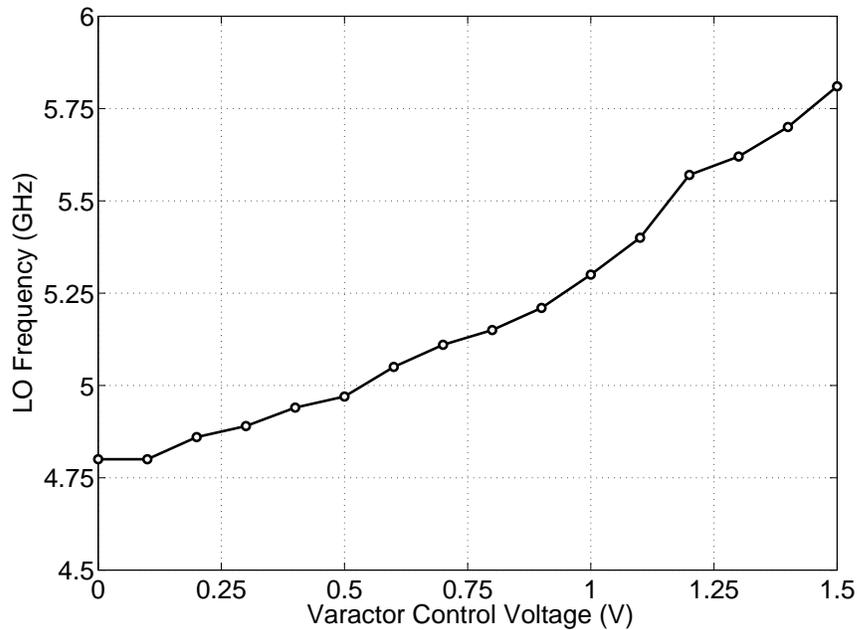


Figure 6.5: Measured fundamental LO frequency tuning range for $V_{cap} = 0 - 1.5$ V.

The setup of the spectrum analyzer was then adjusted to measure the conversion gain, 1-dB compression point, IP2 and IP3 of the mixer. For these measurements, the frequency range was set to 1.0 MHz to 500.0 MHz with 601 points, RBW = VBW = 3.0 MHz, continuous sweeping with a sweep time of 1 ms, an internal attenuation of 10 dB, and the average of 5 sweeps were used.

The conversion gain of the mixer was measured in both states at various LO frequencies and the results are shown in Figure 6.6. An IF frequency of 200 MHz was used, giving an RF input frequency range from 5.0 GHz to 6.0 GHz and 9.8 GHz to 11.8 GHz for the fundamental- and subharmonic-modes, respectively. Figure 6.6 shows a power conversion gain of between approximately 10 dB and 12 dB for the fundamental-mode of the mixer, and a range from 5 dB to 12 dB for the subharmonic-mode. The decrease in conversion gain at higher RF frequencies for the subharmonic-mode is due to parasitic capacitances reducing the $2f_{LO}$ signal amplitude as the frequency is increased. Since the input RF signal to the circuit is applied directly to the gates of MOSFETs, as shown in Figure 6.4, the input is not matched to a $50\ \Omega$ system. This situation would likely be the case when the mixer is a sub-circuit of a larger RFIC. The *voltage* conversion gain of the mixer is approximately 6 dB lower than shown in Figure 6.6.

The RF power performance of the circuit was measured using a fixed LO fundamental frequency of 4.8 GHz ($2f_{LO} = 9.6$ GHz), the input RF power was varied and the output power of the IF signal was measured. The results of the fundamental-mode measurement with an RF frequency of 5.0 GHz and the subharmonic-mode measurements with an RF frequency of 9.8 GHz are shown in Figure 6.7. The two curves are very similar, and the output 1-dB compression points both occur at -5 dBm. The

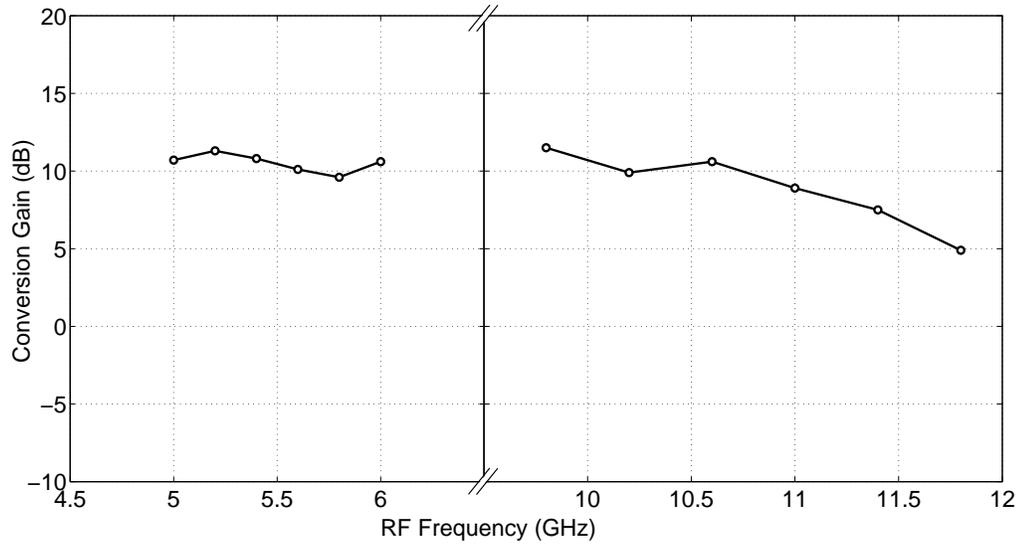


Figure 6.6: Measured conversion gain at various RF input frequencies for a fixed IF frequency of 200 MHz.

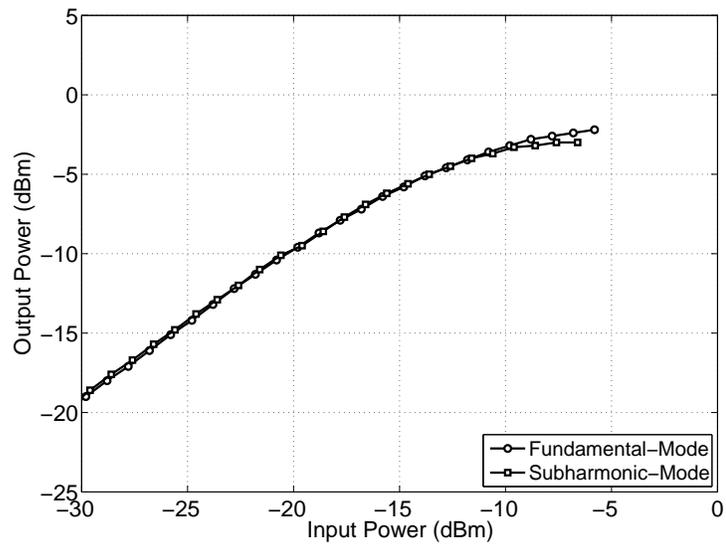


Figure 6.7: Measured IF output power at 200 MHz for various RF input power levels for both fundamental-mode (RF = 5.0 GHz) and subharmonic-mode (RF = 9.8 GHz).

third-order intermodulation products were also measured using two-tone RF inputs of 5.00 GHz and 5.02 GHz for the fundamental mode, and 9.80 GHz and 9.82 GHz for the subharmonic-mode (IM3 signals at 180 MHz and 240 MHz). The results, shown in Figure 6.8, display an OIP3 of 12 dBm for the fundamental-mode and 13 dBm for the subharmonic-mode. The second-order intermodulation products were also measured at an IM2 signal frequency of 20 MHz and the results are shown in Figure 6.9. The mixer demonstrates strong linearity with an OIP2 of 40 dBm in fundamental-mode, and an OIP2 of 50 dBm for subharmonic-mode.

The LO feedthrough was measured at the RF and IF ports and the results are shown in Table 6.1. For this measurement, the spectrum analyzer was configured as follows: frequency range from 1.0 MHz to 15.0 GHz with 601 points, RBW = VBW = 3.0 MHz, a sweep time of 50 ms, 10 averages, and an internal attenuation of 10 dB. This table shows the output power levels of the f_{LO} and $2f_{LO}$ signals at the RF and IF ports for an LO fundamental frequency of 4.8 GHz. In fundamental-mode, the LO signal at the RF port is -40.3 dBm, which is an isolation of approximately 40 dB since the oscillator output signal has a power of approximately 0 dBm from simulations. Similarly, the $2f_{LO}$ signal at the RF port for subharmonic-mode shows about 36 dB of isolation. The RF to IF isolation was measured to be 35 dB for both mixer states.

Since the switches are obviously not ideal, some of the $2f_{LO}$ signal will leak into the mixer while it is in the fundamental-state and some of the f_{LO} signal will leak to the mixer in the subharmonic-state. The conversion gain from the undesired LO signal was measured to evaluate the mixer performance in this regard. With the mixer in fundamental-mode ($f_{LO} = 4.8$ GHz) an RF signal input of 9.8 GHz was

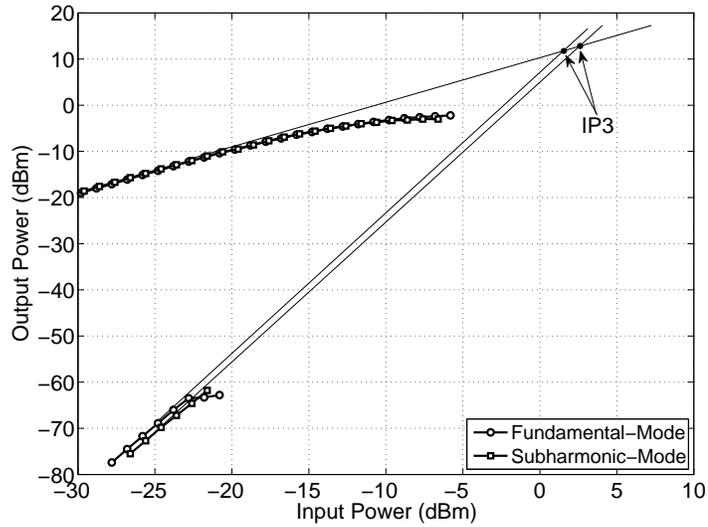


Figure 6.8: Third-order intermodulation measurement for both fundamental and subharmonic mixer modes.

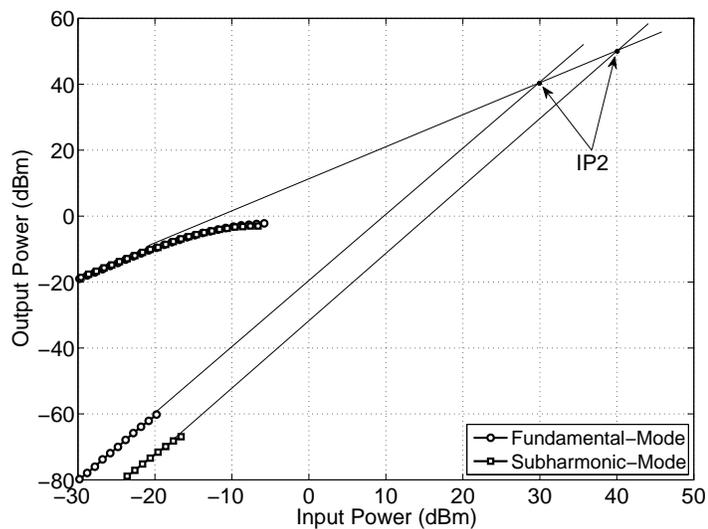


Figure 6.9: Second-order intermodulation measurement for both fundamental and subharmonic mixer modes.

	Fundamental-Mode	Subharmonic-Mode
	Feedthrough (dBm)	Feedthrough (dBm)
f_{LO} @ RF	-40.3	-36.7
$2f_{LO}$ @ RF	-25.1	-35.6
f_{LO} @ IF	-47.5	-48.4
$2f_{LO}$ @ IF	-58.9	-46.1

Table 6.1: Fundamental-mode and subharmonic-mode LO feedthrough measurements

used and the power of the output signal at 200 MHz was measured. Ideally, there should be no power at this frequency, but since some of the $2f_{LO}$ signal at 9.6 GHz leaks to the mixer, it will produce a 200 MHz IF output from the 9.8 GHz RF signal. The conversion gain for this case was -15.2 dB. Similarly, with the mixer in subharmonic-mode, an RF input of 5.0 GHz was used to measure the conversion gain due to the leakage of the fundamental LO signal at 4.8 GHz. The conversion gain for this case was -19.7 dB. In both cases the conversion gain is more than 20 dB below the conversion gain from the desired LO signal.

The noise figure was measured using the Agilent E4446A PSA Series spectrum analyzer along with an Agilent 346C noise source. A noise calibration was performed before measurements were taken on the mixer. The DSB noise figure was measured in both states and was found to be 8.7 dB for fundamental-mode and 10.9 dB for subharmonic-mode. The DC power consumption of the quadrature oscillator alone was measured to be 68 mW including the four buffers. The buffers that are connected to the fundamental outputs of the oscillator consume a total of approximately 48 mW (12 mW each). The mixer circuit adds an additional 2 mW approximately in both the

fundamental and subharmonic states. A microphotograph of the fabricated chip is shown in Figure 6.10. The dimensions of the chip were $875 \mu\text{m} \times 600 \mu\text{m}$ (0.525 mm^2) including bonding pads.

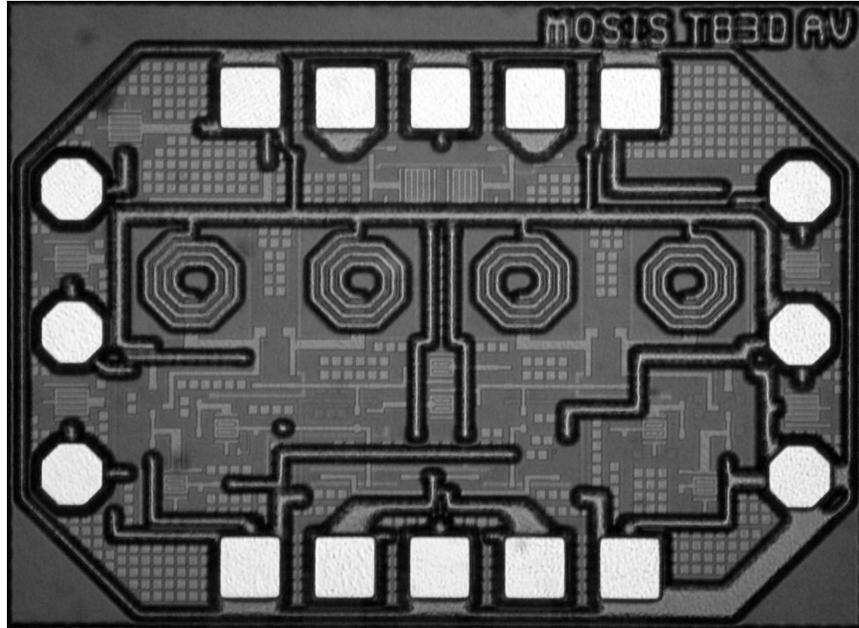


Figure 6.10: Microphotograph of the fabricated dual-band mixer/oscillator chip.

6.5 Summary

A new topology for a dual-band mixer/oscillator has been demonstrated using CMOS $0.13 \mu\text{m}$ technology. This technique uses both the fundamental and second harmonic outputs of a single on-chip quadrature voltage-controlled oscillator connected to a mixer through complementary switches. For operation in C-band, switches connect the fundamental oscillator output to the mixer, and for X-band operation, switches connect the second harmonic of the oscillator to the mixer. The mixer achieves a

conversion gain of at least 5 dB over RF frequencies of 5.0 GHz to 6.0 GHz and from 9.8 GHz to 11.8 GHz while maintaining a constant intermediate frequency output. This circuit could be used as part of a multi-standard system on a chip to reduce the number of circuit elements required, potentially resulting in lower power consumption and reduced costs. This technique could also be very attractive at millimeter-wave frequencies where the use of a frequency doubler circuit connected to the output of a local oscillator could be avoided and in cases where the use of a broadband mixer circuit is not possible.

Chapter 7

A Frequency Tripler Using a Subharmonic Mixer

7.1 Introduction

Odd-order frequency multipliers, such as frequency triplers, are generally more challenging to design than even-order multipliers (e.g. frequency doublers) because simple cubic-law devices are not readily available in standard FET or bipolar integrated circuit processes. Therefore, custom-built, strongly non-linear devices are often employed to realize frequency triplers such as heterostructure and quantum barrier varactor diodes [63–65]. In this chapter, an innovative, fully integrated CMOS frequency tripler is presented based on the $2\times$ subharmonic mixer described in Chapter 3. This technique can provide significant suppression of the fundamental signal at the output without the use of a filter and can achieve conversion gain.

7.2 Concept of the Frequency Tripler

As shown in Figure 7.1, the incident signal, f_{in} , is fed to both inputs of a $2\times$ subharmonic mixer to generate the output frequencies $3f_{in}$ and f_{in} . The circuit includes a feedforward mechanism to cancel the f_{in} signal at the output, leaving only the $3f_{in}$ signal. A demonstration circuit operating at 3.0 GHz output frequency was fabricated and it exhibits a conversion gain of up to 3 dB and a high fundamental signal rejection of up to 30 dB without using any filtering structures either on or off-chip. The use of the subharmonic mixer has the additional advantage that it naturally suppresses the second, fourth, and other harmonics. The integrated circuit was fabricated using a standard CMOS 0.18 μm process and it measures $800 \mu\text{m} \times 1000 \mu\text{m}$.

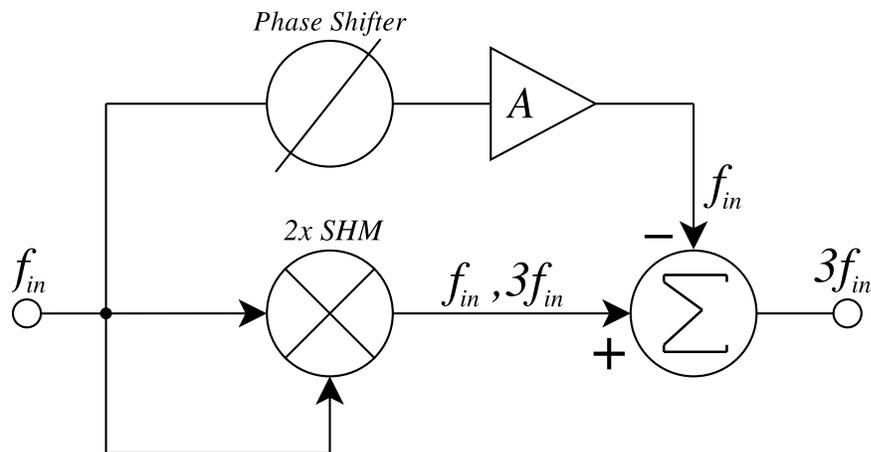


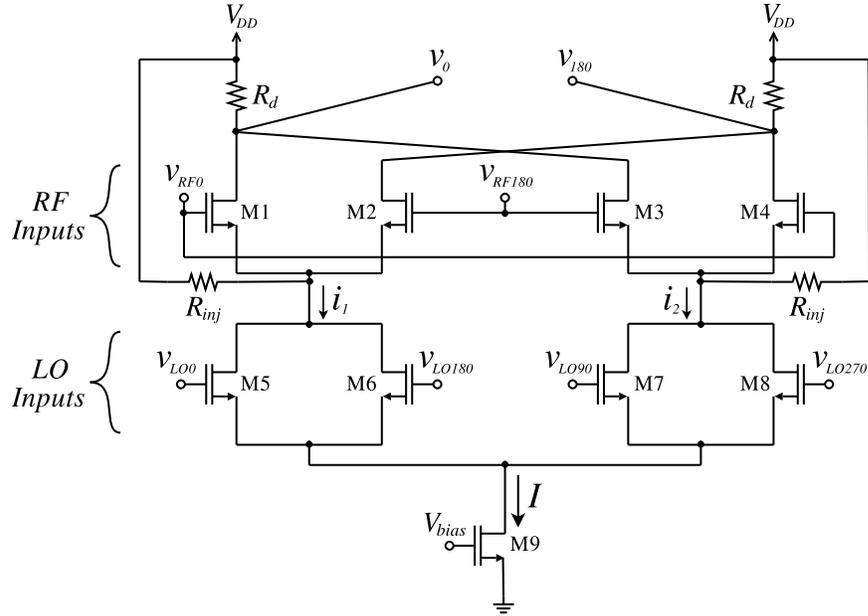
Figure 7.1: Block diagram of the proposed frequency tripler.

7.3 Circuit Design

As shown in Figure 7.1, there are four sub-circuits in the proposed frequency tripler: a $2\times$ SHM, a subtractor circuit, and a feedforward circuit consisting of a phase shifter and an amplifier. At the output of the SHM are the up- and down-converted frequency components ($2f_{in} \pm f_{in}$) at $3f_{in}$ and f_{in} . The fundamental feedforward phase shifter and amplifier are designed to match the phase and amplitude of the fundamental component at the SHM output so that significant fundamental cancellation can occur in the subtractor circuit. Each sub-circuit of the tripler will be discussed in detail below.

7.3.1 Subharmonic Mixer

The schematic of the subharmonic mixer is shown in Figure 7.2. This SHM uses a topology similar to the one discussed in Chapter 3 with the RF and LO ports exchanged from the traditional Gilbert-cell. There are two pairs of LO switching transistors with 0° and 180° inputs and 90° and 270° inputs. These pairs of switching transistors generate the second harmonic of the LO that enables subharmonic mixing. The mixer also uses injection resistors, R_{inj} , connected between V_{DD} and the sources of the RF transistors (drains of the LO transistors). As discussed in [101], this injection method can increase the conversion gain of the mixer. Most of the DC bias current in the mixer flows through the injection resistors, which permits a larger bias current for the LO transistors and generates a larger second harmonic signal current. Without the injection resistors, the bias current flowing through each drain resistor would be $I/2$, and R_d would be limited to values which maintain the saturation region for all FETs. However, since most of the DC current flows through the injection

Figure 7.2: Core of the $2\times$ SHM used in the frequency tripler.

resistors, the bias current can be increased to improve the conversion gain while simultaneously having a large R_d .

The generation of the quadrature LO signals was accomplished with RC - CR phase shifters, as shown in Figure 7.3 (R_1 and C_1). Of course, if the fundamental signal is generated by a quadrature oscillator, then the RC - CR phase shifters would not be required and the outputs of oscillator could be connected directly to the LO transistors, $M5$ to $M8$. In order to increase the LO drive of the SHM, and counteract the loss in the RC - CR phase shifters, two inverter-amplifiers were used before the phase shifters, as shown in Figure 7.3.

Due to parasitics, the amplitude of the output signals at f_{in} and $3f_{in}$ will not be equal, with the $3f_{in}$ component obviously being slightly lower. In this work, the SHM was designed to provide a conversion gain of approximately 3 dB for the SHM output

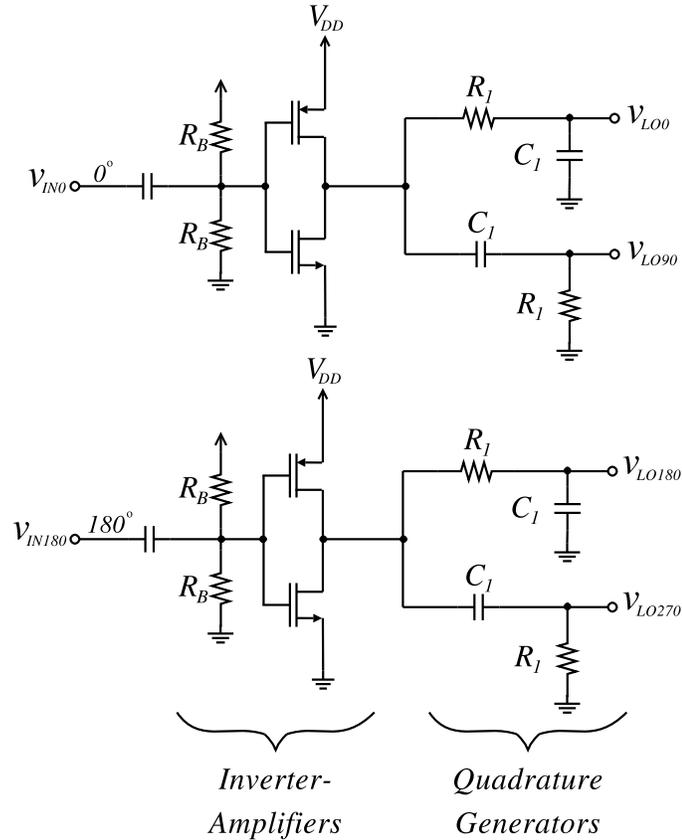


Figure 7.3: Generation of the frequency tripler quadrature LO signals.

signal at $3f_{in}$. For the signal component at f_{in} , the conversion gain was about 4 dB.

7.3.2 Fundamental Feedforward Circuit

As shown in the block diagram in Figure 7.1, a feedforward technique is used along with a subtraction circuit to suppress the fundamental tone that is present at the output of the subharmonic mixer. In order to have significant cancellation of the fundamental tone at the output of the tripler, the input signals into the subtraction circuit must have very similar amplitudes and phases. Therefore, the fundamental

feedforward circuit has to match the amplitude and phase of the fundamental tone at the output of the subharmonic mixer. To this end, a phase shifter circuit is used, followed by an amplifier as shown in Figure 7.4.

Only one of the two input differential signals was used for the feedforward circuit (v_{IN180}), while the other input (v_{IN0}) was terminated in an impedance closely matching the input impedance of the feedforward circuit to maintain equal amplitude input voltage signals to the rest of the circuit.

To implement the phase shifter, an R - C network was used (R_2 and C_2 in Figure 7.4). A varactor was used for C_2 so that the phase shifter could be tuned for optimal fundamental cancellation. An inverter amplifier was used after the phase shifter and its gain was designed to be slightly larger than the conversion gain of the subharmonic mixer to account for the losses in the phase shifter. The output of the feedforward

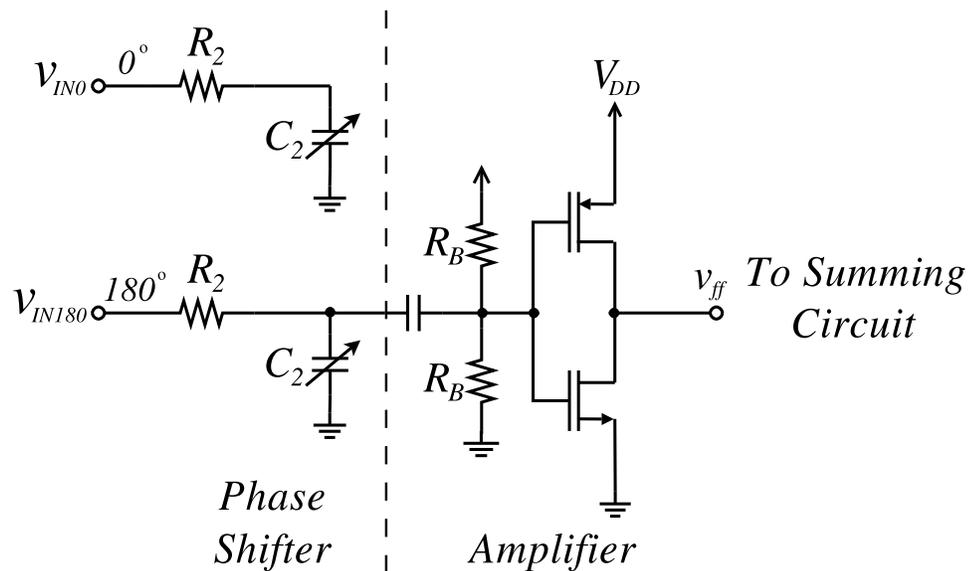


Figure 7.4: Fundamental feedforward circuit used in the frequency tripler.

circuit is given by:

$$v_{ff} = \frac{-A_{ff}v_{IN180}}{1 + j\omega_{in}C_2R_2}, \quad (7.1)$$

where A_{ff} is the gain of the feedforward amplifier. This output signal, v_{ff} , is then used as one of the inputs to the subtractor circuit that cancels the fundamental frequency signal present in the subharmonic mixer output.

7.3.3 Fundamental Cancellation Circuit

The schematic of the circuit used at the output of the subharmonic mixer to suppress the fundamental is shown in Figure 7.5. An active balun, simply implemented as a differential pair with a single-ended output, is used to convert the differential output of the SHM to single ended. Any signals that are in common-mode at the output of the SHM will be suppressed due to the inherent signal subtraction that occurs in this differential pair active balun. Next, the single-ended active balun output, v_{SHM} , is used as the second input to another differential pair that is used for the subtraction circuit. The other input to the subtraction circuit is the output of the feedforward circuit, v_{ff} , shown in Figure 7.4 and as discussed in the previous section. The down- and up-converted components of the subharmonic mixer output are given by:

$$v_{SHM} = A_1\cos(\omega_{in}t + \phi_1) + A_2\cos(3\omega_{in}t + \phi_2), \quad (7.2)$$

and the feedforward input to the subtraction circuit is given by:

$$v_{ff} = A_3(\cos(\omega_{in}t + \phi_3)), \quad (7.3)$$

Whereas the phase of the feedforward signal is controlled by the phase shifter in the feedforward circuit, the amplitude of the feedforward signal is controlled by the

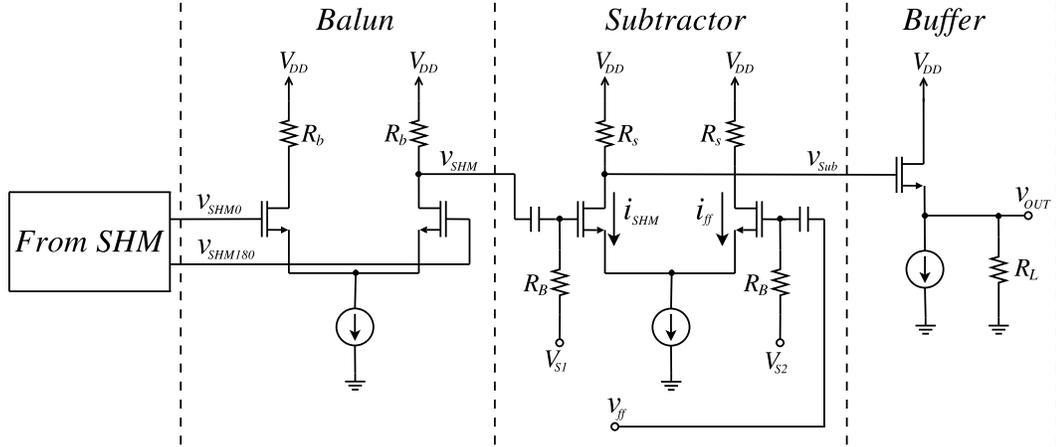


Figure 7.5: Simplified schematic of the active balun, subtractor, and output buffer circuits.

gate bias of the subtractor differential pair (V_{S1} and V_{S2}). By adjusting these gate bias voltages, the amplitudes of the fundamental frequency components in the signal currents, i_{SHM} and i_{ff} , can be made equal for maximum cancellation.

Shown in Figure 7.6 is a calculation of the amount of fundamental tone cancellation at the output that occurs for various amplitude and phase mismatches assuming an ideal differential pair subtractor circuit. The phase difference on the figure is given by $\Delta\phi = \phi_1 - \phi_3$, and the amplitude match is quantified as $\alpha = i_{ff}/i_{SHM}$ (the currents generated by v_{ff} and v_{SHM} , as labeled in Figure 7.5). The ideal case where $\Delta\phi = 0^\circ$ and $\alpha = 1$ provides a complete elimination of the fundamental, as shown in the figure. In order to obtain fundamental suppressions of 30 dB or more, $0.97 \leq \alpha \leq 1.03$ and $|\Delta\phi| < 2^\circ$.

The output of the subtractor circuit, V_{Sub} , is connected to a source follower buffer to drive the external 50Ω load. The output voltage, v_{OUT} of the tripler at $3\omega_{in}$ is

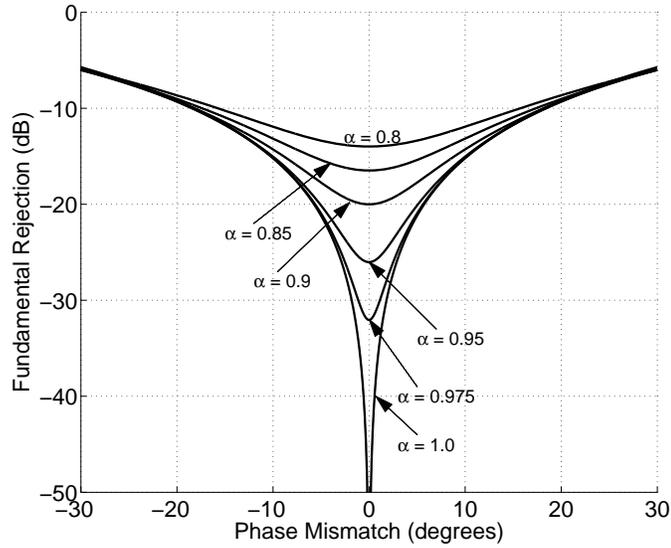


Figure 7.6: Fundamental suppression at various subtractor phase and amplitude matches.

given by:

$$v_{OUT} = A_{Buf} A_{Sub} (v_{SHM} - v_{ff}), \quad (7.4)$$

where A_{Sub} is the gain of the subtractor and A_{Buf} is the gain of the buffer. The overall gain of the cascaded balun, subtractor, and buffer circuits was designed to be approximately one and therefore the gain of the subharmonic mixer determines the conversion gain of the frequency tripler. In other words, the third harmonic signal amplitude at the subharmonic mixer output, $v_{SHM0} - v_{SHM180}$, is equal to the third harmonic voltage amplitude at the output, v_{OUT} .

7.4 Measurement Results

To demonstrate the validity of this tripler concept, a 1.0 GHz to 3.0 GHz multiplier was designed and fabricated. Coplanar waveguide probes were used to contact the on-chip pads. The input signal was differential and the output spectrum was measured using an Agilent E4446A PSA Series spectrum analyzer. The spectrum analyzer was set to a frequency range from 200.0 MHz to 4.2 GHz with 601 points, an internal attenuation of 10 dB, a resolution bandwidth and video bandwidth equal to 3.0 MHz, a sweep time of 6.68 ms, and no averaging. The bias points were set and not changed for any of the following measurements (with the exception of the tuned performance plot, Figure 7.9). A typical plot of the output power spectrum is shown in Figure 7.7 for an input power of -10 dBm. From this figure, the output power of the third harmonic is approximately -7 dBm, which is a 3 dB gain, and the fundamental is suppressed by more than 30 dB. The second harmonic in Figure 7.7 is approximately 26 dB below the third harmonic, and the fourth (and all higher-order harmonics) are more than 30 dB below the desired tripled frequency output. Note that these high levels of suppression are achieved without any filtering (on- or off-chip), and without the use of any inductors.

To measure the output power of the various harmonics at different input powers, the spectrum analyzer was set to: a frequency range from 500.0 MHz to 4.0 GHz with 601 points, $RBW = VBW = 3.0$ MHz, a sweep time of 5.84 ms, an internal attenuation of 10 dB, and the average of 20 sweeps.

Figure 7.8 shows the output powers of the fundamental, second harmonic, and third harmonic at various input power levels. At low input power levels the LO signals are not large enough for the switching pairs in the SHM to generate a strong doubled

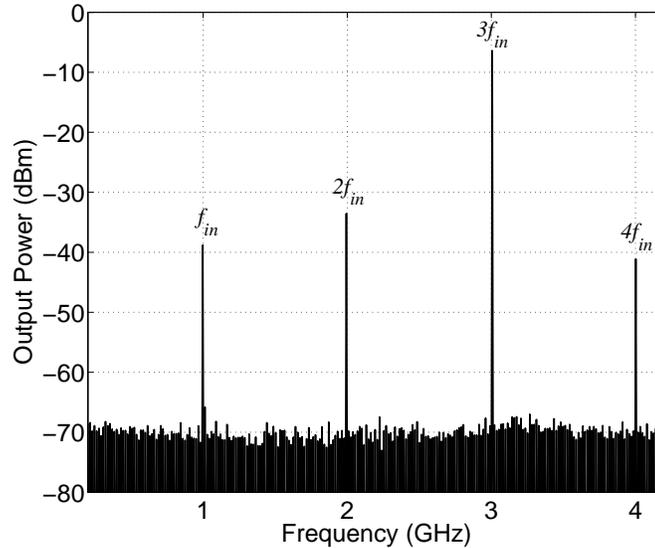


Figure 7.7: Measured frequency tripler output spectrum with -10 dBm input power at 1 GHz.

frequency signal, and therefore there is a low third-order output power. However, at about -16 dBm input power, the SHM is in full operational mode. From -16 dBm to -10 dBm input power the tripler is in its linear range. The slope of this line is slightly greater than one, since the LO power is increasing simultaneously with the RF signal. A peak conversion gain of approximately 3 dB is obtained at an input power level of -10 dBm. The power of the fundamental at the output is below the third harmonic at input powers above -17 dBm with significant rejection (greater than 10 dB) between -15 dBm and -8 dBm input power. At an input power of -10 dBm there is a very large fundamental suppression of 30 dB. At this point the input signals to the summer circuit are very closely matched (see Figure 7.6). The reason why there is an optimal match at a certain input power level is due to the various leakage fundamental signals that degrade the amplitude and phase match at other power

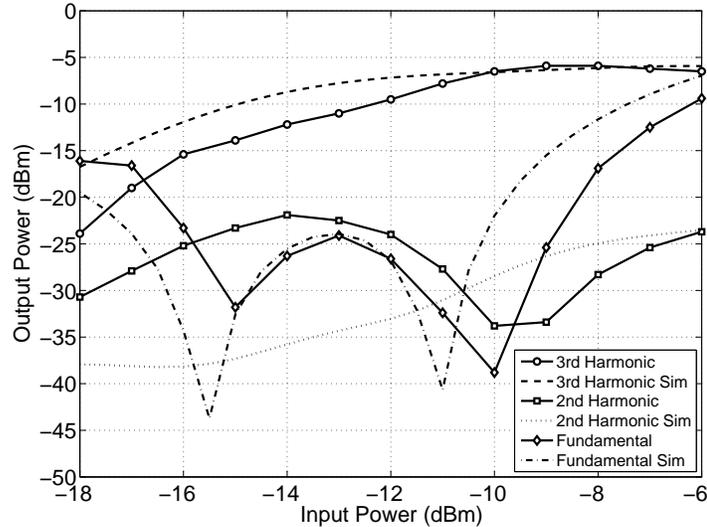


Figure 7.8: Measured and simulated output power levels at various input power levels.

levels. The fundamental signal at the output shows two points at which there is high suppression (at approximately -15 dBm and -10 dBm input power levels). These two minima correspond to the point at which there is an optimal amplitude match and the point at which there is an optimal phase match. The second harmonic in Figure 7.8 is below the third-order signal by -10 dB or more for input powers above -16 dBm. The second harmonic signal at the output is due predominately to the non-linear distortion in the active balun at the output of the SHM since the fundamental signal components at the gates of the differential pair are strong. The simulation results shown in this figure are similar to the experimental results for the fundamental and third-order harmonic output power levels, but noticeably differ in the second harmonic response at low power levels. The difference in the measured and simulated results for the second harmonic could be due to leakage of this signal through the

substrate to other circuits (e.g. the second-harmonic distortion generated from the strong fundamental signal at the balun could leak to the input of the feedforward amplifier) and/or possibly limitations of the non-linear BSIM3 FET model that was used for simulations.

By adjusting the phase shifter, a greater cancellation of the fundamental signal can be achieved over a wider input power range. Shown in Figure 7.9 is the output power spectrum with the fundamental feedforward circuit tuned for optimal fundamental cancellation. The fundamental suppression is greater than 15 dB between -16 dBm and -6 dBm input powers, and greater than 20 dB between input power levels of -12 dBm to -6 dBm. The second harmonic is at least 10 dB below the third harmonic over the entire input power range shown in Figure 7.9 and at least 15 dB below the third harmonic from -12 dBm to -6 dBm.

Given this tripler circuit's inherent reliance on balancing the fundamental signal amplitude and phase at the output of the subharmonic mixer and in the feedforward path, a built-in self-test and calibration circuit may be required if this topology was used in mass production applications. For example, digital processing circuitry could be used to automatically adjust the bias of the fundamental feedforward circuit in correspondence with the input power level (see Figure 7.9). Due to process variations, it may also be required that a self-test circuit be used to determine the current power of the fundamental signal at the output and automatically adjust the feedforward circuit to obtain maximum level of fundamental suppression.

Measurements were made at only one input frequency, 1.0 GHz, due to the quadrature generator $RC-CR$ phase shifter for the subharmonic mixer that works optimally

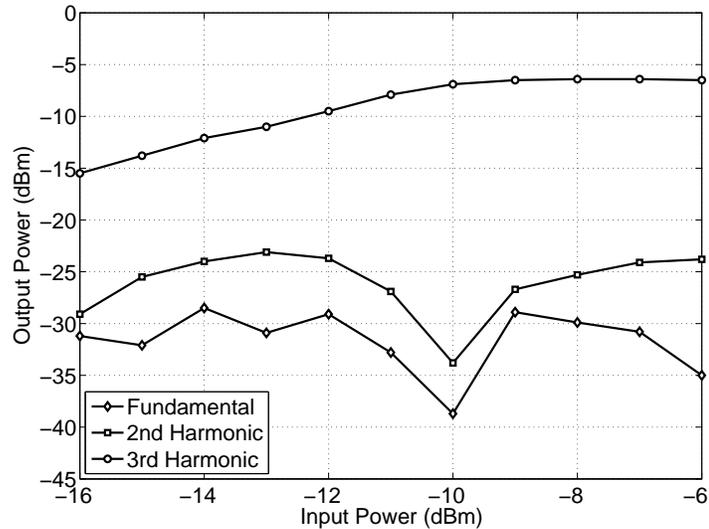


Figure 7.9: Measured output power levels while the feedforward circuit is tuned for optimal performance.

at only this frequency. However, there is not an inherent narrowband frequency limitation with the proposed frequency multiplier topology. In fact, if a quadrature VCO was used for the input signal then the multiplier circuit would work over a wide bandwidth, with the only potential bandwidth restriction being from the tuning range of the feedforward phase shifter (and obviously the frequency limits of the chosen process technology). To evaluate the performance of the proposed tripler circuit over a range of input frequencies without the limitation of the $RC-CR$ phase shift network, a simulation was performed using an ideal broadband quadrature input signal with -11 dBm input power. The results, shown in Figure 7.10, indicate that without the limitation of the phase shifter the circuit achieves a conversion gain and a fundamental suppression of over 10 dB for input signals between 400 MHz and 1.4 GHz without tuning the feedforward circuit.

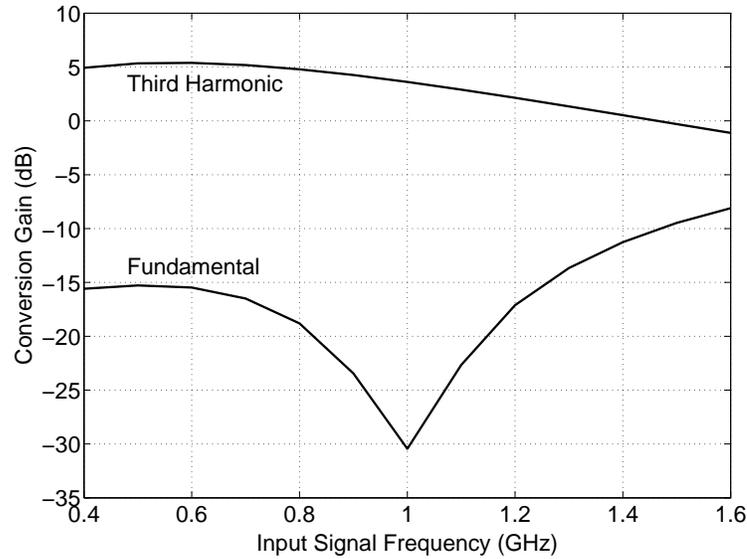


Figure 7.10: Simulated broadband performance of the tripler using an ideal quadrature input signal with a power of -11 dBm.

The phase noise degradation of the tripler was measured using the spectrum analyzer for offset frequencies between 10 kHz and 1 MHz with 4207 points with 0 dB internal attenuation and the signal-tracking option. The raw data and averaged input and output phase noise results are shown in Figure 7.11. From theory, the minimum phase noise degradation (PND) in a frequency multiplier is given by,

$$PND = 20\log(n), \quad (7.5)$$

where n is the order of multiplication. For the case of a frequency tripler, the minimum phase noise degradation is 9.54 dB relative to the input signal phase noise. For this circuit, the difference between the input and output phase noise from an offset of 10 kHz to 1 MHz is 9.69 dB on average, which is quite close to the theoretical minimum.

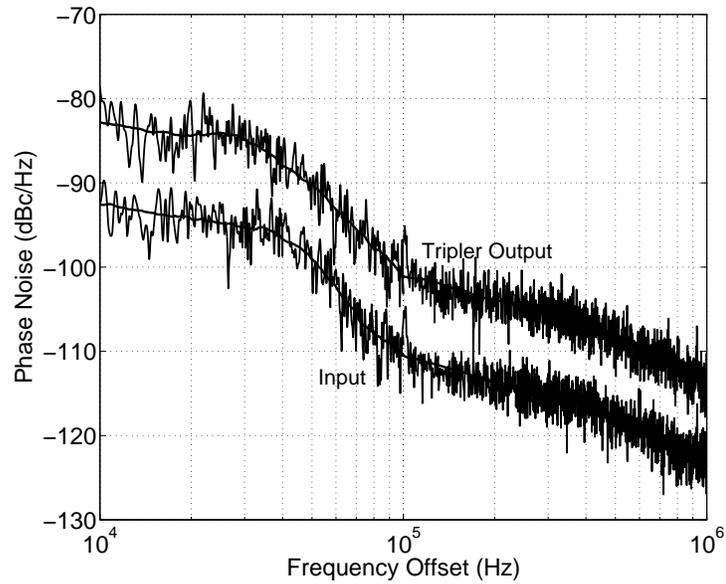


Figure 7.11: Measured input and output phase noise for the frequency tripler.

The supply voltage of the circuit was set to 2.0 V and the DC current consumed was 34 mA, resulting in a power consumption of 68 mW. A microphotograph of the chip is shown in Figure 7.12. The dimensions of the chip including bonding pads was $1.0 \text{ mm} \times 0.8 \text{ mm}$ (0.8 mm^2). A performance comparison of several recent MMIC frequency triplers with this work is presented in Table 7.1, which shows that the proposed tripler method has advantages in terms of conversion gain and fundamental suppression.

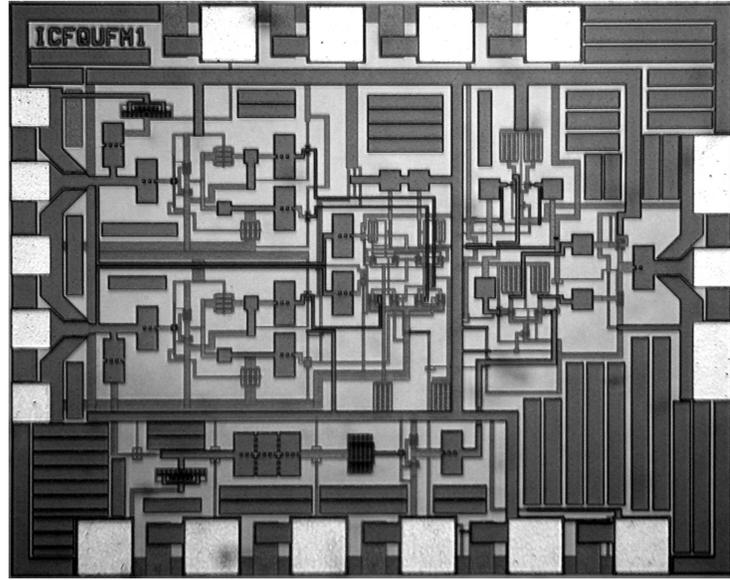


Figure 7.12: Microphotograph of the frequency tripler with fundamental suppression chip.

Ref.	Technology	f_{in} (GHz)	Conversion Gain (dB)	Fundamental Supp. (dB)	Area (mm^2)
[70]	GaAs (Hybrid)	1	-5.7	62.7	~ 7000
[71]	InGaAs PHEMT	12	-9.4	22.3	5.0
[72]	GaAs PHEMT	15	-5.6	40	2.32
[73]	CMOS 0.18 μm	8.8	-10.9	22.7	0.46
[74]	CMOS 90 nm	20	-	-	0.81
[75]	CMOS 0.18 μm	2	-5.6	13	0.18
This Work	CMOS 0.18 μm	1	3	30	0.8

Table 7.1: Comparison of several recent frequency triplers with this work

7.5 Summary

A new topology for a frequency tripler circuit has been demonstrated. This technique uses a $2\times$ subharmonic mixer along with a feedforward circuit and a subtraction circuit to realize fundamental cancellation. An input signal with frequency, f_{in} , is converted to f_{in} and $3f_{in}$ at the output of the subharmonic mixer ($2f_{in} \pm f_{in}$). A feedforward circuit is used for the input signal at f_{in} and is connected to a summing junction along with the output of the subharmonic mixer. In the summing junction, the fundamental frequency signals, f_{in} , in both the subharmonic mixer output and the feedforward circuit output are cancelled, ideally leaving only the third harmonic, $3f_{in}$. Advantages of this technique include the ability to realize very high levels of fundamental suppression without the use of a filter (up to 30 dB was obtained in this work), as well the ability to obtain conversion gain (up to 3 dB was shown in this work). Since no filters or inductors are required, this circuit can be implemented entirely on chip in a relatively small area. Furthermore, phase noise measurements show that the degradation is very close to the theoretical minimum. While the demonstration circuit was at S-band, this technique could be used at much higher frequencies (e.g. millimeter-wave) where the use of frequency multiplication circuits may be required. If the proposed frequency tripler topology was implemented at a higher frequency it may be possible to use a passive feedforward phase shifter and/or a passive subtractor circuit on-chip, which would reduce the power consumption of the circuit.

Chapter 8

A Frequency Divider Using a Subharmonic Mixer

8.1 Introduction

Similar to the odd-order frequency multiplier discussed in Chapter 7, odd-order high-frequency analog frequency dividers are also much less common than even-order dividers (most commonly divide-by-2 or divide-by-4). Odd-order dividers can potentially increase the flexibility and number of design options in a transceiver as well as possibly reduce circuit complexity. In this chapter, a divide-by-3 frequency divider is proposed that uses a subharmonic mixer to divide a 5.4 GHz input signal to 1.8 GHz in CMOS 0.13 μm technology [11].

8.2 Concept of the Frequency Divider

The concept of the proposed divide-by-three frequency divider is based on the regenerative divider first introduced by Miller [79]. That circuit is commonly used to implement a divide-by-two circuit using a mixer, a low-pass filter and possibly an amplifier. The block diagram of the traditional regenerative divider is shown in Figure 8.1.

As discussed in Chapter 2, in its steady-state this circuit has two potential mixer outputs, $\frac{1}{2}f_{in}$ and $\frac{3}{2}f_{in}$. A low-pass filter is then used to suppress the $\frac{3}{2}f_{in}$ signal, which leaves the $\frac{1}{2}f_{in}$ for the feedback to the fundamental mixer as well as the output. By using a $2\times$ subharmonic mixer instead of a fundamental mixer it is possible to obtain a frequency division by three. Shown in Figure 8.2 is the block diagram of the divide-by-three circuit proposed in this thesis. The most significant change of this circuit compared to the traditional regenerative divider shown in Figure 8.1 is the use of a $2\times$ subharmonic mixer in place of the fundamental mixer. If the two inputs to the subharmonic mixer are f_{in} and f_{out} , as shown in Figure 8.2 then at the output of the

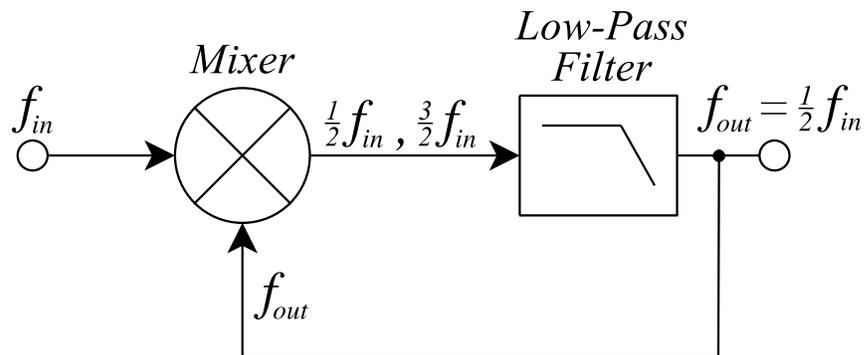


Figure 8.1: Traditional Miller regenerative frequency divider.

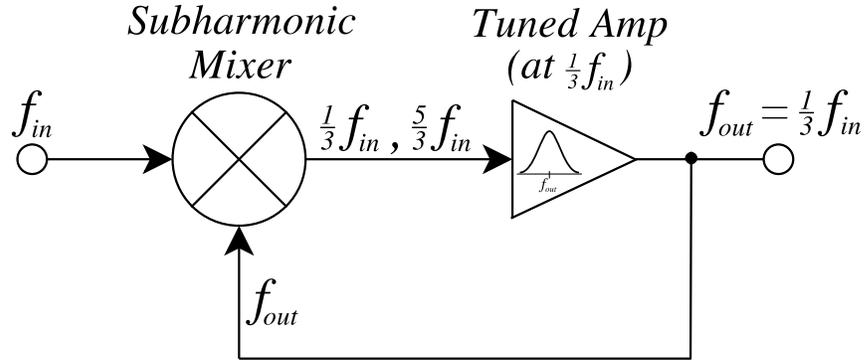


Figure 8.2: Block diagram of the proposed divide-by-three frequency divider.

mixer are two frequencies,

$$f_{in} + 2f_{out} \quad (8.1)$$

and

$$f_{in} - 2f_{out}. \quad (8.2)$$

The down-converted term in 8.2 is amplified by the tuned amplifier while the upconverted term is attenuated, leaving (ideally) only the down-converted component at the output. Therefore,

$$f_{in} - 2f_{out} = f_{out} \quad (8.3)$$

which shows the desired output,

$$f_{out} = \frac{1}{3}f_{in}. \quad (8.4)$$

As mentioned above, the low-pass filter in Figure 8.1 has been changed to an amplifier that is tuned to the $\frac{1}{3}f_{in}$ frequency to ensure that the $\frac{5}{3}f_{in}$ frequency has significantly lower power at the output (and in the feedback path to the subharmonic mixer). The use of this amplifier can improve the output power at $\frac{1}{3}f_{in}$, but also

ensures that there is sufficient gain around the loop to ensure start-up of the circuit. This tuned amplifier, however, will limit the tuning range of the frequency divider.

8.3 Circuit Design

The divide-by-three circuit is based on a single-balanced version of the $2\times$ subharmonic mixer demonstrated in Chapter 3, as shown in Figure 8.3. This circuit, which is essentially half of the $2\times$ subharmonic mixer discussed in previous chapters, requires only a differential LO input as opposed to the quadrature LO input required for the double-balanced subharmonic mixer. Transistors $M1$ and $M2$ produce the doubled

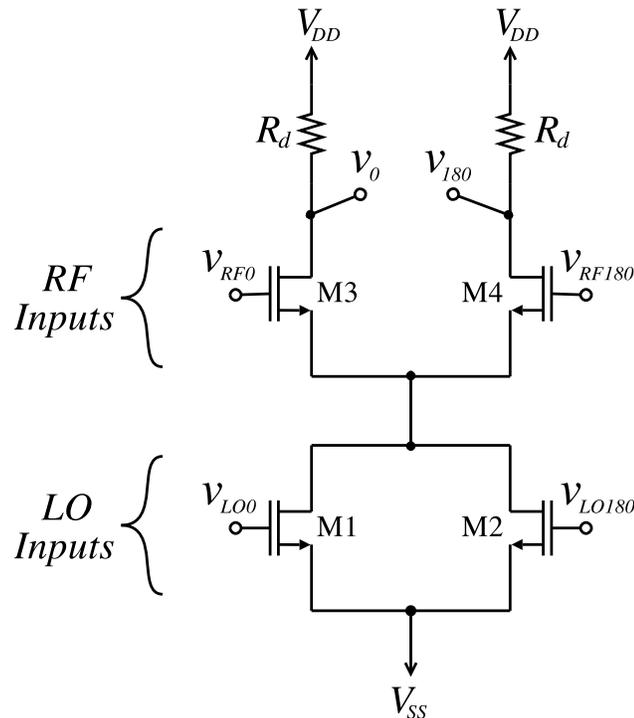


Figure 8.3: Single-balanced $2\times$ subharmonic mixer circuit.

frequency, which is then mixed with the RF input to produce an output at the drains of the RF transistors with frequency $f_{RF} \pm 2f_{LO}$.

In addition to the subharmonic mixer, Figure 8.2 also shows a tuned amplifier. To implement this amplifier, a differential pair was used with L - C loads, as shown in Figure 8.4. The output of the subharmonic mixer will be used as input to the differential amplifier and the output of the tuned amplifier will be fed to the gates of the LO transistors shown in Figure 8.3.

The simplified schematic for the entire circuit is shown in Figure 8.5 (biasing not shown). It consists of the single-balanced subharmonic mixer shown in Figure 8.3 along with the tuned amplifier in Figure 8.4 and output buffers to drive the $50\ \Omega$ load from either the measurement equipment or the input impedance of the next stage in the circuit.

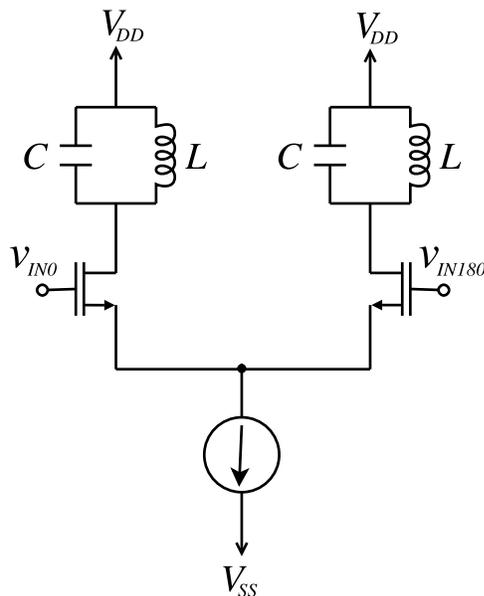


Figure 8.4: Tuned differential amplifier circuit.

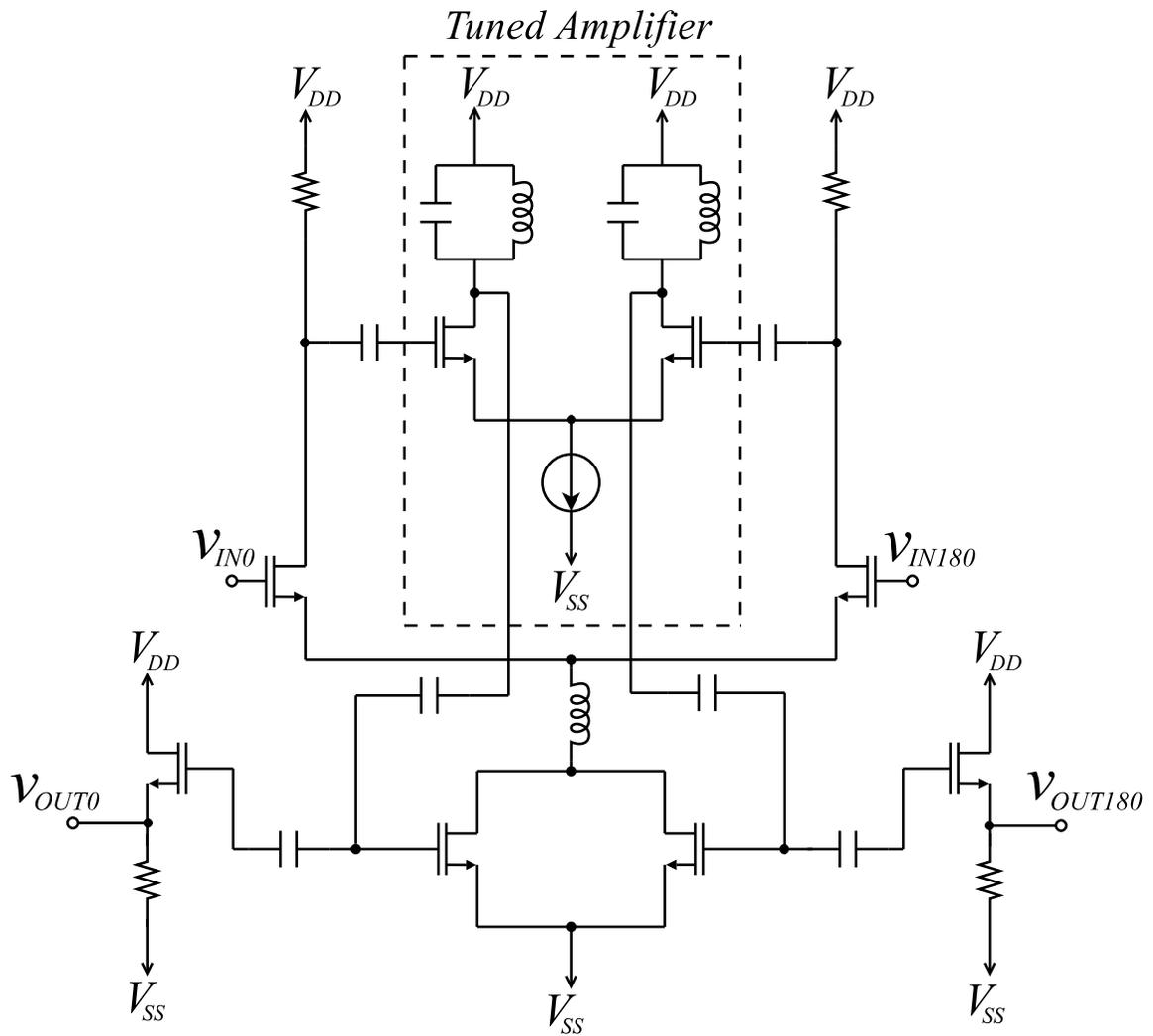


Figure 8.5: Simplified schematic of the proposed frequency divider (biasing not shown).

An inductor is used above the LO transistors as described in Chapter 4 in order to increase the conversion gain of the subharmonic mixer. DC blocking capacitors are used between the mixer output and the amplifier input and also between the output of the amplifier and the LO transistors in order for optimal bias points to be used. The bias point for the LO frequency doubling transistors is somewhat sensitive and simulations showed that the optimal point is at $V_{SS} + V_t$ where V_{SS} is the negative supply voltage and V_t is the FET threshold voltage. Assuming ideal FETs that do not conduct any current when the gate-source voltage is less than threshold voltage the selection of this bias voltage will produce an absolute value signal (see Chapters 3 and 4 for detailed subharmonic mixer analysis). The current source shown for the tuned differential amplifier is implemented using a standard current mirror.

8.4 Measurement Results

To evaluate the performance of the proposed divide-by-3 frequency divider, measurements were performed using a probe station with differential coplanar waveguide probes. The supply voltages were set to 1.5 V and -0.8 V for V_{DD} and V_{SS} , respectively, and differential input and output signals were used, as shown in Figure 8.5. An Agilent E4446A PSA Series spectrum analyzer was used with the following settings: start frequency: 1.0 GHz, stop frequency: 6.0 GHz, RBW: 3 MHz, VBW: 3 MHz, sweep time: 8.36 ms, 601 points, internal attenuation: 10 dB. With an input power of -7 dBm at 5.4 GHz, the output spectrum is shown in Figure 8.6. The output spectral component at 1.8 GHz ($\frac{1}{3}f_{in}$) is clearly the strongest at approximately -7 dBm, which is a conversion gain of 0 dB. The fundamental signal power at the output is -37 dBm and therefore the fundamental suppression is 30 dB. All other harmonics

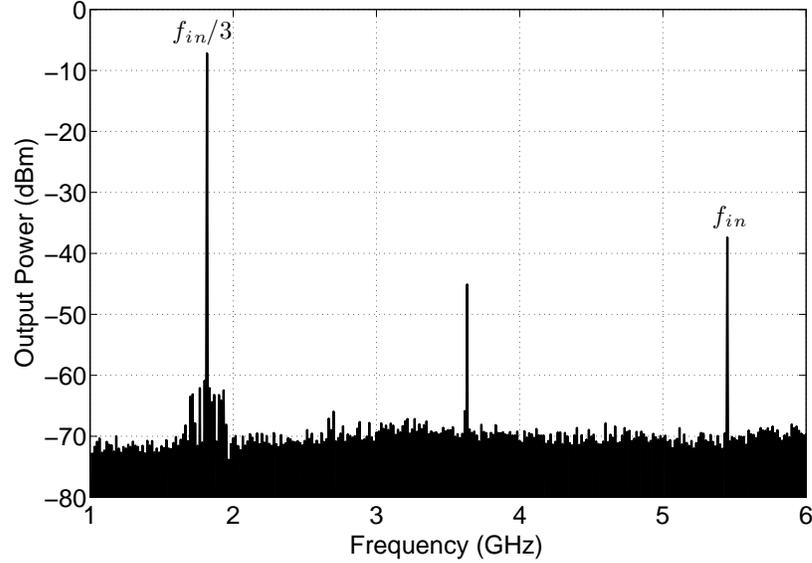


Figure 8.6: Measured frequency divider output spectrum with a -7 dBm input at 5.4 GHz.

at the output are suppressed by at least 35 dB.

To evaluate the performance of the circuit with various input frequencies, a constant input power of -7 dBm was used and the output spectrum was observed. As discussed previously, the bandwidth of the circuit is limited by the LC tank shown in Figure 8.5 and outside this input frequency range no output at the divide-by-three frequency will be obtained. The measured bandwidth for a -7 dBm input power is shown in Figure 8.7. With an input power of -7 dBm the circuit operates from 5.2 GHz to 5.5 GHz with varying levels of output power at the desired divide-by-3 spectral component. The conversion gain of the divide-by-three frequency divider has a minimum of -1.1 dB at 5.5 GHz and a maximum of 0 dB at a 5.35 GHz input frequency. This increased output power can be attributed to the peak tank Q -factor

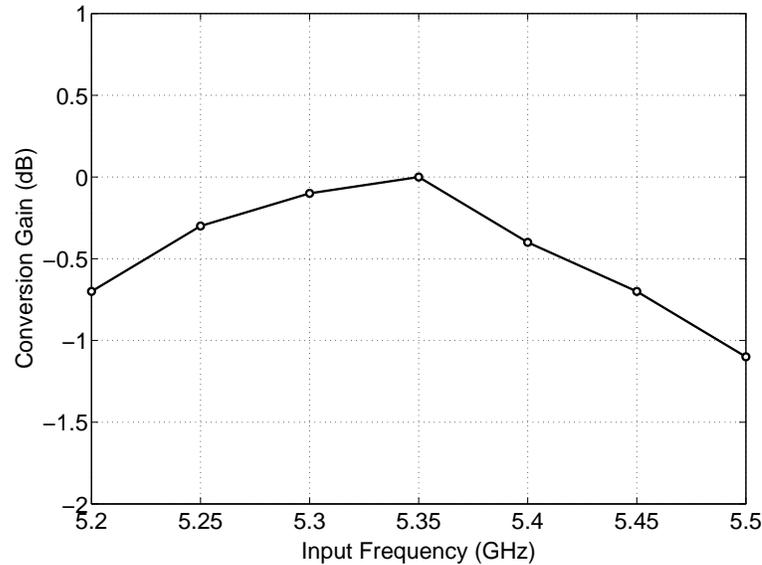


Figure 8.7: Measured frequency divider conversion gain for various input frequencies (-7 dBm input power).

at 5.35 GHz. Since this is a regenerative topology, the output power at the divide-by-3 frequency is relatively constant and does not increase proportionally to the input signal power.

The initial power of the $\frac{1}{3}f_{in}$ signal at the output of the subharmonic mixer is a function of both the power of the input signal as well as the power of the feedback signal at the other subharmonic mixer input port. Since regenerative dividers require that the gain around the loop be greater than unity, it follows that the circuit will cease operation at some point as the input power is decreased. Similarly, the bandwidth of the divider will increase as the input power increases since the $\frac{1}{3}f_{in}$ signal at the subharmonic mixer output will be stronger and will compensate for the lower amplifier gain away from the centre frequency of the amplifier. Figure 8.8 shows

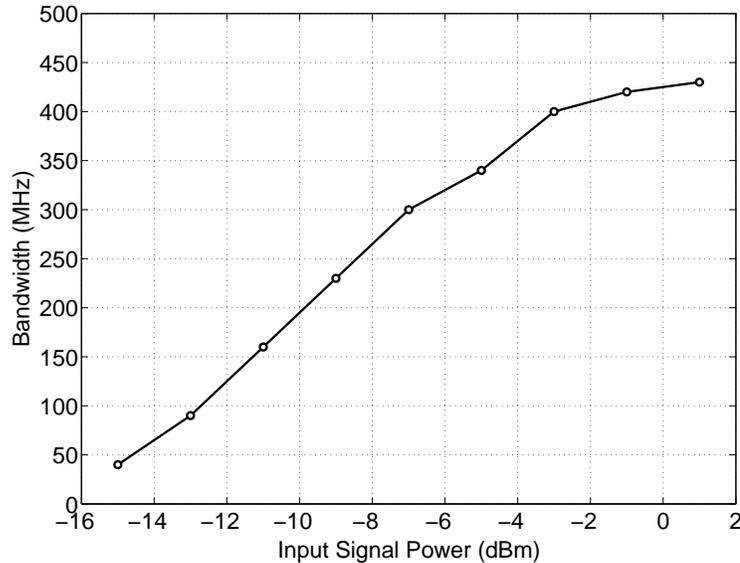


Figure 8.8: Measured frequency divider bandwidth for various input power levels.

the bandwidth attainable for various input power levels. In order for this circuit to operate, the minimum input power level is -15 dBm and a maximum bandwidth of 430 MHz can be obtained for an input power of 1 dBm.

The phase noise of the input signal at 5.4 GHz was measured as well as the output signal at 1.8 GHz. From theory, it would be expected that the divide-by-3 output signal would have a $20\log(n)$ phase noise improvement, where $n = 3$ (a phase noise improvement of approximately 9.54 dB). At a 100 kHz offset, the input signal phase noise at 5.4 GHz is -112.6 dBc/Hz and at the 1.8 GHz frequency divider output the phase noise is -122.1 dBc/Hz. The difference between input and output phase noise is 9.5 dB, which is very close to the theoretical value.

The dimensions of this integrated circuit measures $1000 \mu\text{m} \times 1000 \mu\text{m}$ (1.0 mm^2) and a photograph of the chip is shown in Figure 8.9. The power consumption for the

divider core circuit is 44 mW and for the entire circuit including the output buffers it is 55 mW (similar to, for example, the divide-by-3 circuit in [84], which had a power consumption of 45 mW).

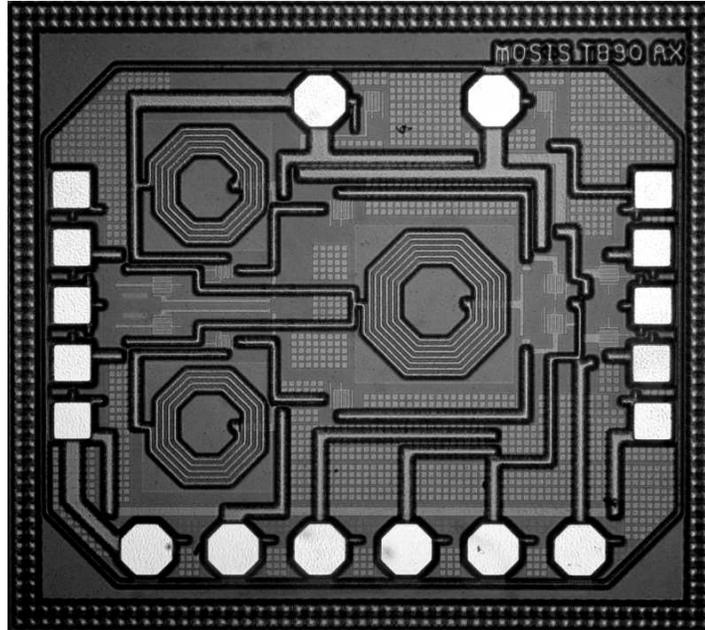


Figure 8.9: Frequency divider chip photograph.

8.5 Summary

An analog frequency divider was presented in this chapter that can divide the frequency of an input signal by a factor of three as opposed to the much more common even-order division ratios. The proposed circuit uses a subharmonic mixer instead of a fundamental mixer in the Miller regenerative divider as well as a tuned amplifier. The circuit achieved a maximum conversion gain of 0 dB and a bandwidth of up to 430 MHz. All harmonic components at the output were more than 30 dB below the

desired output signal. The layout for the circuit was compact at 1.0 mm^2 and the power consumption for the core of the divider was 44 mW.

Chapter 9

Summary and Conclusions

9.1 Summary

Subharmonic mixers have applications in superheterodyne systems as a method of reducing the local oscillator frequency, as well as in direct-conversion architectures where the use of a subharmonic mixer can reduce the significant problem of LO self-mixing. Furthermore, subharmonic mixers can be used to realize new circuits that would not be possible using only fundamental mixers.

This thesis' investigation of subharmonic mixers began with a $2\times$ subharmonic mixer demonstrated in CMOS technology. This down-converting subharmonic mixer used a modified Gilbert-cell topology with quadrature LO signals that were generated on-chip from a single-ended LO input. The RF, LO, and IF ports all used active baluns, which simplifies the use of this circuit in a system that uses single-ended signals. A formula for the conversion gain of this mixer was derived and compared to simulation results. The circuit was designed for an RF input signal at 2.1 GHz and an LO frequency of 1.0 GHz, which produces a 100 MHz IF output. Measurement

results show a conversion gain of approximately 8 dB, an input 1-dB compression point of -14 dBm, and an IIP3 of -8.5 dBm. Since the on-chip baluns have active input matching, the measured input reflection coefficients for both the RF and LO ports are better than -10 dB at the frequencies of interest.

Building upon the $2\times$ subharmonic mixer results described above, a Ku-band $4\times$ down-converting subharmonic mixer was proposed. This is the first $4\times$ subharmonic mixer demonstrated in CMOS technology and achieves the highest conversion gain for any $4\times$ subharmonic mixer regardless of circuit topology or process technology used. A differential LO input signal is converted to an octet-phase signal on-chip and is used to internally multiply the LO frequency by a factor of four. The input RF signal is single-ended and is converted to differential on-chip using an active balun, and the mixer's differential output signal is converted back to single-ended also with an active balun. An RF signal at 12.1 GHz was used for measurement along with a 3.0 GHz LO frequency, generating a 100 MHz IF output. Measurement results show a conversion gain of approximately 6 dB, an input 1-dB compression point of -12 dBm, IIP3 of -2 dBm, and very high isolations between the ports (e.g. $4LO-RF$ isolation of 59 dB).

While the required LO signals for the $2\times$ and $4\times$ subharmonic mixers described above were generated off-chip using a signal generator, in most cases there will be an on-chip quadrature oscillator that eliminates the need for the $RC-CR$ 90° phase shifters. A suitable quadrature oscillator was designed for use with either of the proposed subharmonic mixers using active superharmonic coupling. Two identical differential oscillators were used with a 180° coupling circuit connected to common-mode nodes where the second-order harmonics are predominant, which results in a

quadrature relationship is established between the fundamental outputs. A frequency of 3.0 GHz was used since it is the LO frequency required by the $4\times$ subharmonic mixer. The frequency could be adjusted for use with the $2\times$ subharmonic mixer by simply changing the inductors and capacitors in the resonators appropriately. This circuit is the most compact in terms of layout area compared to other oscillators using the superharmonic coupling technique. The oscillator output power was -6 dBm, the phase noise was -116 dBc/Hz at a 1 MHz offset, and the phase error was less than 6° .

A dual-band mixer/oscillator was presented that operates in either C-band or X-band. Whereas many dual-band systems require a complete set of RF front-end circuits for each band of operation, this circuit uses only a single mixer core and oscillator core to realize operation in both bands. Since both a fundamental and second harmonic LO signal are available in the quadrature oscillator circuit described above, either of these signals can be connected to a mixer. By using a set of complementary switches that control whether the fundamental or second harmonic LO signal is connected to the mixer, operation in two frequency bands is possible. Measured results show an RF frequency range from 5.0 GHz to 6.0 GHz for the fundamental state of the mixer where the fundamental LO signal is connected to the mixer for a constant IF output of 200 MHz. When the second-harmonic LO signal is connected to the mixer the circuit is in its subharmonic state and operates with RF frequencies between 9.8 GHz and 11.8 GHz for a constant 200 MHz IF output. Conversion gain was attained over the entire operational frequency range for both states of the circuit.

A new frequency tripler circuit was demonstrated that uses the $2\times$ subharmonic mixer described previously. This circuit uses a single input for both the RF and

LO ports of the subharmonic mixer, thus producing output signal components at the fundamental input frequency and at *three times* the fundamental. A feedforward circuit is used to cancel the fundamental at the output, ideally leaving only the third-harmonic. A 1.0 GHz input signal was used and the circuit achieved a conversion gain of up to 3 dB at the 3.0 GHz output and a fundamental suppression of over 30 dB without using a filter at the output.

Lastly, a frequency divider was presented that is unique in that it divides the frequency of an input signal by a factor of three, whereas the vast majority of frequency dividers divide the input signal by an even-ordered factor (usually two or four). This circuit uses a single-balanced $2\times$ subharmonic mixer in a Miller regenerative divider topology. Measurement results show a maximum conversion gain of 0 dB and suppression of the input signal frequency at the output of up to 30 dB. With an input power of -7 dBm this circuit operates with an input signal frequency between 5.2 GHz and 5.5 GHz, producing an output from 1.73 GHz to 1.83 GHz.

9.2 Review of Contributions

This thesis has contributed to the field of microwave engineering in several ways regarding the design and applications of CMOS subharmonic mixers. In this thesis one of the first subharmonic mixers with measured results in CMOS technology was presented; this was the first to use the proposed mixer topology. Furthermore, this $2\times$ subharmonic mixer had a conversion gain and other performance metrics similar to fundamental mixers. Since single-ended signals are often used, this subharmonic mixer used input and output active baluns to make the conversion from single-ended

inputs to differential for internal operation, and then back to single-ended for measurements.

The concept of the $2\times$ subharmonic mixer was used as a basis for a more advanced $4\times$ subharmonic mixer that operates at Ku-band. This circuit was the first $4\times$ subharmonic mixer using CMOS technology and it achieves the highest conversion gain for any $4\times$ subharmonic mixer regardless of circuit topology or fabrication technology used.

Since both the $2\times$ and $4\times$ subharmonic mixers require a quadrature oscillator, a new design was shown that could be used with either of the aforementioned mixers. This oscillator was designed to require minimal chip area, and in fact was the most compact quadrature oscillator that could be found in the literature that uses the superharmonic coupling technique. Furthermore, this oscillator had the lowest phase noise for an oscillator using active superharmonic coupling.

A dual-band mixer/oscillator was presented that can operate in either the C-band or the X-band using single mixer and oscillator core circuits. Since these two circuits can operate in two bands, the use of duplicate circuitry for each band, as has often been used in the past, is avoided.

Next, a frequency tripler circuit was presented that is based on the $2\times$ subharmonic mixer previously discussed. This circuit is unique in several aspects. First, there are very few frequency triplers in the literature – most frequency multipliers are *times two* or *times four*. The addition of a tripler circuit allows for more flexibility in the transceiver design and can potentially eliminate the need for additional oscillators. Also, this circuit can achieve high levels of fundamental suppression without filtering the output signal since a feedforward circuit is used to cancel the fundamental signal

component at the output. The elimination of a filter at the output of the frequency multiplier can save significant space on-chip or avoid taking the signal off-chip to be filtered by an off-chip SAW or FBAR filter, for example.

Finally, a divide-by-three frequency divider was demonstrated that is based on a $2\times$ subharmonic mixer. Measurement results show that this topology can achieve very low conversion loss or even conversion gain and high-levels of suppression of the undesired signals at the output. There have been very few odd-order frequency divider circuits previously demonstrated, and this work can add flexibility to circuits and systems by removing the limitation imposed by even-ordered dividers that have been dominant in the past.

9.3 Future Work

There are several potential directions for future work on subharmonic mixers. The $4\times$ subharmonic mixer topology described in this thesis becomes even more attractive as the operational frequency is increased since it becomes more difficult to design a local oscillator. Therefore, the $4\times$ subharmonic mixer circuit could be implemented at a much higher frequency, for example, 40 GHz or above. Similarly, the frequency tripler topology could be applied at millimeter-wave frequencies where frequency multipliers are often required.

A direct-conversion receiver could be designed around either the $2\times$ or $4\times$ subharmonic mixers in order to determine the maximum performance that is attainable with the use of these subharmonic mixers.

An increase in the order of subharmonic mixing could be investigated. For example, an $8\times$ subharmonic mixer. However, this may be challenging using the proposed

topologies since it would require splitting the LO into 16 phases. Furthermore, a study into increasing the performance of the proposed subharmonic mixers could be undertaken. For example, a low-noise or high-linearity version of the $2\times$ or $4\times$ subharmonic mixers could be designed to further increase the attractiveness of using subharmonic mixers in a variety of applications.

Lastly, a modification to the dual-band mixer/oscillator could be performed to realize a tri-band circuit that could operate as either a fundamental mixer, a $2\times$ subharmonic mixer, or a $4\times$ subharmonic mixer.

References

- [1] T. Lee, *The Design of CMOS Radio-Frequency Integrated Circuits*. Cambridge University Press, 2002.
- [2] B. Razavi, “A 60-GHz CMOS Receiver Front-End,” *IEEE Journal of Solid-State Circuits*, vol. 41, pp. 17–22, January 2006.
- [3] C. Cao, E. Seok, and K. O, “192 GHz Push-Push VCO in 0.13 μm CMOS,” *Electronics Letters*, vol. 42, pp. 208–210, Feb. 2006.
- [4] S. Lee, B. Jagannathan, S. Narasimha, A. Chou, N. Zamdmer, J. Johnson, R. Williams, L. Wagner, J. Kim, J.-O. Plouchart, J. Pekarik, S. Springer, and G. Freeman, “Record RF Performance of 45-nm SOI CMOS Technology,” *IEEE International Electron Devices Meeting*, pp. 255–258, Dec. 2007.
- [5] Y.-J. E. Chen, K.-H. Wang, T.-N. Luo, S.-Y. Bai, and D. Heo, “Investigation of CMOS Technology for 60-GHz Applications,” *IEEE SoutheastCon*, pp. 92–95, April 2005.
- [6] B. Jackson and C. E. Saavedra, “A CMOS Ku-Band 4x Subharmonic Mixer,” *IEEE Journal of Solid-State Circuits*, vol. 43, pp. 1351–1359, June 2008.

-
- [7] B. Jackson and C. E. Saavedra, "A Frequency Tripler using a Subharmonic Mixer and Fundamental Cancellation," *IEEE Transactions on Microwave Theory and Techniques*. to appear May 2009.
- [8] B. R. Jackson and C. E. Saavedra, "A CMOS Subharmonic Mixer with Input and Output Active Baluns," *Microwave and Optical Technology Letters (Wiley InterScience)*, vol. 48, pp. 2472–2478, December 2006.
- [9] B. Jackson and C. Saavedra, "A 3 GHz CMOS Quadrature Oscillator using Active Superharmonic Coupling," *European Microwave Conference*, pp. 1109–1112, Oct. 2007.
- [10] B. Jackson and C. E. Saavedra, "A Dual-Band Mixer/Oscillator for C-Band and X-Band Applications," *IEEE Transactions on Microwave Theory and Techniques*. Submitted for review January 2009.
- [11] B. Jackson and C. E. Saavedra, "A Divide-By-3 Frequency Divider using a Subharmonic Mixer," *2010 IEEE Radio Frequency Integrated Circuits Symposium (RFIC 2010)*. To be submitted.
- [12] C. E. Saavedra, "ELEC 457 Course Notes," 2008.
- [13] E. Armstrong, "Method of Receiving High Frequency Oscillation," *U.S. Patent 1,342,885*, June 8, 1920.
- [14] D. Manstretta, M. Brandolini, and F. Svelto, "Second-order Intermodulation Mechanisms in CMOS Downconverters," *IEEE Journal of Solid-State Circuits*, vol. 38, pp. 394–406, March 2003.

-
- [15] R. Svitek and S. Raman, "DC Offsets in Direct-Conversion Receivers: Characterization and Implications," *IEEE Microwave Magazine*, vol. 6, pp. 76–86, September 2005.
- [16] R. G. Meyer, W. D. Mack, and J. J. E. M. Hageraats, "A 2.5-GHz BiCMOS Transceiver for Wireless LAN's," *IEEE Journal of Solid-State Circuits*, vol. 32, pp. 2097–2104, December 1997.
- [17] B. Gilbert, "A Precise Four-Quadrant Multiplier with Subnanosecond Response," *IEEE Journal of Solid-State Circuits*, vol. 3, pp. 365–373, December 1968.
- [18] C.-S. Lin, P.-S. Wu, H.-Y. Chang, and H. Wang, "A 9-50 GHz Gilbert-Cell Down-Conversion Mixer in 0.13- μm CMOS Technology," *Microwave and Wireless Components Letters, IEEE*, vol. 16, pp. 293–295, May 2006.
- [19] M.-D. Tsai and H. Wang, "A 0.3-25 GHz Ultra-Wideband Mixer Using Commercial 0.18 μm CMOS Technology," *IEEE Microwave and Wireless Component Letters*, vol. 14, pp. 522–524, November 2004.
- [20] F. Ellinger, "26.5–30-GHz Resistive Mixer in 90-nm VLSI SOI CMOS Technology With High Linearity for WLAN," *Microwave Theory and Techniques, IEEE Transactions on*, vol. 53, pp. 2559–2565, Aug. 2005.
- [21] M. Bao, H. Jacobsson, L. Aspemyr, G. Carchon, and X. Sun, "A 9–31-GHz Subharmonic Passive Mixer in 90-nm CMOS Technology," *IEEE Journal of Solid-State Circuits*, vol. 41, pp. 2257–2264, October 2006.

-
- [22] H.-C. Chen, T. Wang, S.-S. Lu, and G.-W. Huang, "A Monolithic 5.9-GHz CMOS I/Q Direct-Down Converter Utilizing a Quadrature Coupler and Transformer-Coupled Subharmonic Mixers," *IEEE Microwave and Wireless Components Letters*, vol. 16, pp. 197–199, April 2006.
- [23] J.-H. Tsai, H.-Y. Yang, T.-W. Huang, and H. Wang, "A 30–100 GHz Wideband Sub-Harmonic Active Mixer in 90 nm CMOS Technology," *Microwave and Wireless Components Letters, IEEE*, vol. 18, pp. 554–556, Aug. 2008.
- [24] H. Feng, Q. W. X. Guan, R. Zhan, A. Wang, and L. W. Yang, "A 5 GHz Sub-Harmonic Direct Down-Conversion Mixer for Dual-Band System in 0.35 μm SiGe BiCMOS," in *IEEE International Symposium on Circuits and Systems*, vol. 5, (Kobe Japan), pp. 4807–4810, May 2005.
- [25] H.-M. Hsu and T.-H. Lee, "A Zero-IF Sub-Harmonic Mixer with High LO-RF Isolation using 0.18 μm CMOS Technology," in *IEEE European Microwave Integrated Circuits Conference*, (Manchester, UK), pp. 336–339, September 2006.
- [26] M.-F. Huang, S.-Y. Lee, and C. J. Kuo, "A 5.25 GHz CMOS Even Harmonic Mixer with an Enhancing Inductance," in *IEEE International Symposium on Circuits and Systems*, vol. 3, (Kobe Japan), pp. 2116–2119, May 2005.
- [27] J.-J. Hung, T. M. Hancock, and G. M. Rebeiz, "A 77 GHz SiGe Sub-Harmonic Balanced Mixer," *IEEE Journal of Solid-State Circuits*, vol. 40, pp. 2167–2173, November 2005.

- [28] R. M. Kodkani, L. E. Larson, and E. Lawrence, "A 24-GHz CMOS Direct-Conversion Sub-Harmonic Downconverter," in *IEEE Radio Frequency Integrated Circuits (RFIC) Symposium*, (Honolulu, Hawaii, USA), pp. 485–488, June 2007.
- [29] K.-J. Koh, M.-Y. Park, C.-S. Kim, and H.-K. Yu, "Subharmonically Pumped CMOS Frequency Conversion (Up and Down) Circuits for 2-GHz WCDMA Direct-Conversion Transceiver," *IEEE Journal of Solid-State Circuits*, vol. 39, pp. 871–884, June 2004.
- [30] M.-Y. Lee, C.-Y. Jeong, C. Yoo, Y.-H. Kim, J.-H. Hwang, and J.-S. Park, "Fully-Integrated CMOS Direct-Conversion Receiver for 5GHz Wireless LAN," in *IEEE Topical Meeting on Silicon Monolithic Integrated Circuits in RF Systems*, (Long Beach, CA, USA), pp. 201–204, January 2007.
- [31] R. Svitek and S. Raman, "5–6 GHz SiGe Active I/Q Subharmonic Mixers with Power Supply Noise Effect Characterization," *IEEE Microwave and Wireless Components Letters*, vol. 14, pp. 319–321, July 2004.
- [32] P. Upadhyaya, M. Rajashekharaiyah, Y. Zhang, D. Heo, and Y.-J. Chen, "A High IIP2 Doubly Balanced Sub-Harmonic Mixer in 0.25- μm CMOS for 5-GHz ISM Band Direct Conversion Receiver," in *IEEE Radio Frequency Integrated Circuits Symposium*, (Long Beach, California, USA), pp. 175–178, June 2005.
- [33] T.-H. Wu, S.-C. Tseng, C.-C. Meng, and G.-W. Huang, "GaInP/GaAs HBT Sub-Harmonic Gilbert Mixers Using Stacked-LO and Leveled-LO Topologies," *IEEE Transactions on Microwave Theory and Techniques*, vol. 55, pp. 880–889, May 2007.

-
- [34] T.-Y. Yang and H.-K. Chiou, "A 28 GHz Sub-Harmonic Mixer using LO Doubler in 0.18- μm CMOS Technology," in *IEEE Radio Frequency Integrated Circuits (RFIC) Symposium*, (San Francisco, California, USA), June 2006.
- [35] L. Sheng, J. C. Jensen, and L. E. Larson, "A Wide-Bandwidth Si/SiGe HBT Direct Conversion Sub-Harmonic Mixer/Downconverter," *IEEE Journal of Solid-State Circuits*, vol. 35, pp. 1329–1337, September 2000.
- [36] K. Nimmagadda and G. Rebeiz, "A 1.9 GHz Double-Balanced Subharmonic Mixer for Direct Conversion Receivers," *IEEE Radio Frequency Integrated Circuits (RFIC) Symposium*, pp. 253–256, 2001.
- [37] B. G. Perumana, C.-H. Lee, J. Laskar, and S. Chakraborty, "A Subharmonic CMOS Mixer Based on Threshold Voltage Modulation," *IEEE MTT-S International Microwave Symposium Digest*, pp. 33–36, June 2005.
- [38] M. W. Chapman and S. Raman, "A 60-GHz Uniplanar MMIC 4x Subharmonic Mixer," *IEEE Transactions on Microwave Theory and Techniques*, vol. 50, pp. 2580–2588, November 2002.
- [39] K. Kanaya, K. Kawakami, T. Hisaka, T. Ishikawa, and S. Sakamoto, "A 94 GHz High Performance Quadruple Subharmonic Mixer MMIC," *IEEE MTT-S International Microwave Symposium Digest*, vol. 2, pp. 1249–1252, June 2002.
- [40] A. Madjar and M. Musia, "Design and Performance of a x4 Millimeter Wave Subharmonic Mixer," in *IEEE European Microwave Conference*, (Madrid, Spain), pp. 246–247, October 1993.

-
- [41] S. Sarkar, D. Yeh, S. Pintel, and J. Laskar, "Wideband Direct Conversion Hybrid LCP Millimeter-Wave $4\times$ Subharmonic Mixer for Gigabit Wireless Module," in *IEEE European Microwave Conference*, (Paris, France), October 2005.
- [42] W.-Y. Uhm, W.-S. Sul, H.-J. Han, S.-C. Kim, H.-S. Lee, D. An, S.-D. Kim, D.-H. Shin, H.-M. Park, and J.-K. Rhee, "A High Performance V-band Monolithic Quadruple Sub-Harmonic Mixer," *IEEE MTT-S International Microwave Symposium Digest*, vol. 2, pp. 1319–1322, June 2003.
- [43] D. An, S. C. Kim, W. S. Sul, H. J. Han, H. S. Lee, W. Y. Uhm, H. M. Park, S. D. Kim, D. H. Shin, and J. K. Rhee, "High Conversion Gain V-band Quadruple Subharmonic Mixer using Cascode Structure," *IEEE MTT-S International Microwave Symposium Digest*, vol. 2, pp. 911–914, June 2003.
- [44] A. A. Abidi, "Direct-Conversion Radio Transceivers for Digital Communications," *IEEE Journal of Solid-State Circuits*, vol. 30, pp. 1399–1410, December 1995.
- [45] A. Niknejad and R. Meyer, "Analysis, Design, and Optimization of Spiral Inductors and Transformers for Si RF ICs," *IEEE Journal of Solid-State Circuits*, vol. 33, pp. 1470–1481, Oct 1998.
- [46] C. Yue and S. Wong, "On-Chip Spiral Inductors with Patterned Ground Shields for Si-Based RF ICs," *IEEE Journal of Solid-State Circuits*, vol. 33, pp. 743–752, May 1998.
- [47] A. Sedra and K. Smith, *Microelectronic Circuits*. Oxford University Press, 1998.

- [48] M.-D. Tsai, Y.-H. Cho, and H. Wang, "A 5-GHz Low Phase Noise Differential Colpitts CMOS VCO," *Microwave and Wireless Components Letters, IEEE*, vol. 15, pp. 327–329, May 2005.
- [49] Z. Liu, E. Skafidas, and R. Evans, "A 60 GHz VCO with 6 GHz Tuning Range in 130 nm Bulk CMOS," *U.S.*, vol. 1, pp. 209–211, April 2008.
- [50] A. Hajimiri and T. Lee, "Design Issues in CMOS Differential LC Oscillators," *IEEE Journal of Solid-State Circuits*, vol. 34, pp. 717–724, May 1999.
- [51] N. Pletcher, *Micro Power Radio Frequency Oscillator Design*. M.Sc. Thesis, University of California, Berkeley, 2004.
- [52] L. Jia, J.-G. Ma, K. Yeo, and M. Do, "9.3–10.4-GHz-Band Cross-Coupled Complementary Oscillator With Low Phase-Noise Performance," *IEEE Transactions on Microwave Theory and Techniques*, vol. 52, pp. 1273–1278, April 2004.
- [53] J. Craninckx and M. S. J. Steyaert, "A Fully Integrated CMOS DCS-1800 Frequency Synthesizer," *IEEE Journal of Solid-State Circuits*, vol. 33, pp. 2054–2065, December 1998.
- [54] J. P. Maligeorgos and J. R. Long, "A Low-Voltage 5.1-5.8 GHz Image-Reject Receiver with Wide Dynamic Range," *IEEE Journal of Solid-State Circuits*, vol. 35, pp. 1917–1926, December 2000.
- [55] A. Rofougaran, G. Chang, J. Rael, J.-C. Chang, M. Rofougaran, P. Chang, M. Djafari, M.-K. Ku, E. Roth, A. Abidi, and H. Samueli, "A Single-Chip 900-MHz Spread-Spectrum Wireless Transceiver in 1- μm CMOS. I. Architecture and

- Transmitter Design,” *IEEE Journal of Solid-State Circuits*, vol. 33, pp. 515–534, Apr 1998.
- [56] C. Meng, Y. Chang, and S. Tseng, “4.9-GHz Low-Phase-Noise Transformer-Based Superharmonic-Coupled GaInP/GaAs HBT QVCO,” *IEEE Microwave and Wireless Components Letters*, vol. 16, pp. 339–341, June 2006.
- [57] J. Cabanillas, L. Dussopt, J. Lopez-Villegas, and G. Rebeiz, “A 900 MHz Low Phase Noise CMOS Quadrature Oscillator,” *IEEE Radio Frequency Integrated Circuits (RFIC) Symposium*, pp. 63–66, 2002.
- [58] S. Gierkink, S. Levantino, R. Frye, C. Samori, and V. Bocuzzi, “A Low-Phase-Noise 5-GHz CMOS Quadrature VCO using Superharmonic Coupling,” *IEEE Journal of Solid-State Circuits*, vol. 38, pp. 1148–1154, July 2003.
- [59] T. Hancock and G. Rebeiz, “A Novel Superharmonic Coupling Topology for Quadrature Oscillator Design at 6 GHz,” *IEEE Radio Frequency Integrated Circuits (RFIC) Symposium*, pp. 285–288, June 2004.
- [60] F. Ellinger and H. Jackel, “Ultracompact SOI CMOS Frequency Doubler for Low Power Applications at 26.5–28.5 GHz,” *IEEE Microwave Wireless Component Letters*, vol. 14, pp. 53–55, February 2004.
- [61] J. Wong and H. Luong, “A 1.5-V 4-GHz Dynamic-Loading Regenerative Frequency Doubler in a 0.35 μm CMOS Process,” *IEEE Trans. on Circuits and Systems II: Analog and Digital Signal Processing*, vol. 50, pp. 450–455, August 2003.

- [62] M. Yang, S. Oh, and S. Lee, “Low Power Fully Differential Frequency Doubler,” *IEE Electronics Letters*, vol. 39, pp. 1388–1389, September 2003.
- [63] Q. Xiao, J. Hesler, T. Crowe, R. Weikle, Y. Duan, and B. Deaver, “High-Efficiency Heterostructure-Barrier-Varactor Frequency Triplers using AlN Substrates,” in *IEEE MTT-S Int. Microwave Symp. Digest*, (Long Beach, USA), pp. 443–446, June 2005.
- [64] R. Meola, J. Freyer, and M. Claassen, “Improved Frequency Tripler with Integrated Single-Barrier Varactor,” *IEE Electronics Lett.*, vol. 36, pp. 803–804, April 2000.
- [65] J. R. Jones, W. L. Bishop, S. H. Jones, and G. B. Tait, “Planar Multibarrier 80/240-GHz Heterostructure Barrier Varactor Triplers,” *IEEE Trans. Microwave Theory and Tech.*, vol. 45, pp. 512–518, April 1997.
- [66] S.-S. Liao, H.-K. Chen, P.-T. Sun, C.-Y. Lai, H.-Y. Liao, and Y.-C. Chang, “Novel Design for Small-Size Coplanar Waveguide Frequency Tripler,” *IEEE Microwave Wireless Component Lett.*, vol. 13, pp. 529–531, December 2003.
- [67] Y. Campos-Roca, L. Verweyen, M. Fernandez-Barciela, E. Sanchez, M. C. Curras-Francos, W. Bronner, A. Hulsmann, and M. Schlechtweg, “An Optimized 25.5–76.5 GHz PHEMT-Based Coplanar Frequency Tripler,” *IEEE Microwave Guided Wave Lett.*, vol. 10, pp. 242–244, June 2000.
- [68] A. Boudiaf, D. Bachelet, and C. Rumelhard, “38 GHz MMIC PHEMT-Based Tripler with Low Phase-Noise Properties,” in *IEEE MTT-S Int. Microwave Symp. Digest*, vol. 1, (Boston, USA), pp. 509–512, June 2000.

- [69] B. Bunz and G. Kompa, "Broadband HEMT-Based Frequency Tripler for use in Active Multi-Harmonic Load-Pull System," in *34th European Microwave Conference*, (Amsterdam, The Netherlands), pp. 193–196, October 2004.
- [70] S. Seo, Y. Jeong, J. Lim, B. Gray, and J. Kenney, "A Novel Design of Frequency Tripler Using Composite Right/Left Handed Transmission Line," *Microwave Symposium, 2007. IEEE/MTT-S International*, pp. 2185–2188, June 2007.
- [71] J.-C. Chiu, C.-P. Chang, M.-P. Houng, and Y.-H. Wang, "A 12–36GHz PHEMT MMIC Balanced Frequency Tripler," *Microwave and Wireless Components Letters, IEEE*, vol. 16, pp. 19–21, Jan. 2006.
- [72] H. Fudem and E. Niehenke, "Novel Millimeter Wave Active MMIC Triplers," *Microwave Symposium Digest, 1998 IEEE MTT-S International*, vol. 2, pp. 387–390, Jun 1998.
- [73] M.-C. Chen and C.-Y. Wu, "Design and Analysis of CMOS Subharmonic Injection-Locked Frequency Triplers," *Microwave Theory and Techniques, IEEE Transactions on*, vol. 56, pp. 1869–1878, Aug. 2008.
- [74] W. Chan, J. Long, and J. Pekarik, "A 56-to-65GHz Injection-Locked Frequency Tripler with Quadrature Outputs in 90nm CMOS," *Solid-State Circuits Conference, 2008. ISSCC 2008. Digest of Technical Papers. IEEE International*, pp. 480–629, Feb. 2008.
- [75] Y. Zheng and C. E. Saavedra, "A Broadband CMOS Frequency Tripler using a Third-Harmonic Enhanced Technique," *IEEE Journal of Solid-State Circuits*, vol. 42, pp. 2197–2203, October 2007.

- [76] F. Cheng, C. Chen, and O. Choy, "A 1.0 μm CMOS All Digital Clock Multiplier," in *IEEE 40th Midwest Symposium on Circuits and Systems*, pp. 460–462, August 1997.
- [77] S. Henzler and S. Koeppe, "Design and Application of Power Optimized High-Speed CMOS Frequency Dividers," *Very Large Scale Integration (VLSI) Systems, IEEE Transactions on*, vol. 16, pp. 1513–1520, November 2008.
- [78] T. S. Aytur and B. Razavi, "A 2 GHz, 6 mW BiCMOS Frequency Synthesizer," *IEEE Journal of Solid-State Circuits*, vol. 30, pp. 1457–1462, December 1995.
- [79] R. L. Miller, "Fractional-Frequency Generators Utilizing Regenerative Modulation," *Proc. IRE*, vol. 27, pp. 446–456, July 1939.
- [80] J. Lee and B. Razavi, "A 40-GHz Frequency Divider in 0.18- μm CMOS Technology," *IEEE Journal of Solid-State Circuits*, vol. 39, pp. 594–601, April 2004.
- [81] L. Landen, C. Fager, and H. Zirath, "Regenerative GaAs MMIC Frequency Dividers for 28 and 14 GHz," *European Microwave Conference, 2000. 30th*, pp. 1–3, Oct. 2000.
- [82] H. Rategh and T. Lee, "Superharmonic Injection-Locked Frequency Dividers," *IEEE Journal of Solid-State Circuits*, vol. 34, pp. 813–821, Jun 1999.
- [83] J.-C. Chien, C.-S. Lin, L.-H. Lu, H. Wang, J. Yeh, C.-Y. Lee, and J. Chern, "A Harmonic Injection-Locked Frequency Divider in 0.18- μm SiGe BiCMOS," *Microwave and Wireless Components Letters, IEEE*, vol. 16, pp. 561–563, Oct. 2006.

- [84] H. Wu and L. Zhang, "A 16-to-18 GHz 0.18- μm Epi-CMOS Divide-by-3 Injection-Locked Frequency Divider," *Solid-State Circuits Conference, 2006. ISSCC 2006. Digest of Technical Papers. IEEE International*, pp. 2482–2491, 6-9, 2006.
- [85] M. Acar, D. Leenaerts, and B. Nauta, "A Wide-Band CMOS Injection-Locked Frequency Divider," *IEEE Radio Frequency Integrated Circuits (RFIC) Symposium*, pp. 211–214, June 2004.
- [86] Z. Zhaofeng, L. Tsui, C. Zhiheng, and J. Lau, "A CMOS Self-Mixing-Free Front-End for Direct Conversion Applications," in *IEEE International Symposium on Circuits and Systems*, (Sydney, Australia), pp. 386–389, May 2001.
- [87] P. Upadhyaya, M. Rajashekharaiyah, Y. Zhang, D. Heo, and Y.-J. Chen, "A 5 GHz Novel 0.18 μm Inductor-less CMOS Sub-harmonic Mixer," in *IEEE Fourth International Symposium on Information Processing in Sensor Networks*, (Los Angeles, California, USA), pp. 71–74, April 2005.
- [88] V. Krizhanovskii and S.-G. Lee, "0.18 μm CMOS Sub-harmonic Mixer for 2.4 GHz IEEE 802.15.4 Transceiver," in *IEEE 14th International Crimean Conference on Microwave and Telecommunication Technology*, (Sevastopol, Crimea, Ukraine), pp. 141–142, September 2004.
- [89] P. Upadhyaya, M. Rajashekharaiyah, and D. Heo, "A 5.6 GHz CMOS Doubly Balanced Sub-Harmonic Mixer for Direct Conversion Zero IF Receiver," in *IEEE Workshop on Microelectronics and Electron Devices*, (Boise, Idaho, USA), pp. 129–130, April 2004.

- [90] M. Goldfarb, J. B. Cole, and A. Platzker, "A Novel MMIC Biphase Modulator with Variable Gain using Enhancement-Mode FETs Suitable for 3 V Wireless Applications," in *IEEE Microwave and Millimeter-Wave Monolithic Circuits Symposium*, pp. 99–102, 1994.
- [91] L. M. Devlin, B. J. Buck, J. C. Clifton, A. W. Dearn, , and A. P. Long, "A 2.4 GHz Single Chip Transceiver," in *IEEE Microwave and Millimeter-Wave Monolithic Circuits Symposium*, pp. 23–26, 1993.
- [92] M. Kawashima, T. Nakagawa, and K. Araki, "A Novel Broadband Active Balun," in *IEEE 33rd European Microwave Conference*, (Munich, Germany), pp. 495–498, October 2003.
- [93] M. Rajashekharaiyah and E. Chen, "A New 0.25 μm CMOS On-Chip Active Balun with Gain Controllability for 5 GHz DCR," in *IEEE 7th International Conference on Solid-State and Integrated Circuits Technology*, (Beijing, China), pp. 1295–1298, October 2004.
- [94] H. Darabi and A. A. Abidi, "Noise in RF-CMOS Mixers: A Simple Physical Model," *IEEE Journal of Solid-State Circuits*, vol. 35, pp. 15–25, January 2000.
- [95] P. Andreani and X. Wang, "On the Phase-Noise and Phase-Error Performances of Multiphase LC CMOS VCOs," *IEEE Journal of Solid-State Circuits*, vol. 39, pp. 1883–1893, November 2004.
- [96] Y.-S. Hwang, S. sun Yoo, and H.-J. Yoo, "A 2 GHz and 5 GHz Dual-Band Direct Conversion RF Frontend for Multi-Standard Applications," *IEEE International SOC Conference*, pp. 189–192, Sept. 2005.

-
- [97] T. Abdelrheem, H. Elhak, and K. Sharaf, "A Concurrent Dual-Band Mixer for 900 MHz/1.8 GHz RF Front-Ends," *Proceedings of the 46th IEEE International Midwest Symposium on Circuits and Systems, 2003*, vol. 3, pp. 1291–1294 Vol. 3, Dec. 2003.
- [98] W. Kim, J. Yu, H. Shin, S.-G. Yang, W. Choo, and B.-H. Park, "A Dual-Band RF Front-End of Direct Conversion Receiver for Wireless CDMA Cellular Phones with GPS Capability," *IEEE Transactions on Microwave Theory and Techniques*, vol. 54, pp. 2098–2105, May 2006.
- [99] M. Arasu, Y. Zheng, and W. G. Yeoh, "A 3 to 9-GHz Dual-band Up-Converter for a DS-UWB Transmitter in 0.18- μm CMOS," *IEEE Radio Frequency Integrated Circuits (RFIC) Symposium*, pp. 497–500, June 2007.
- [100] P. de Paco, R. Villarino, G. Junkin, O. Menendez, E. Corrales, and J. Parron, "Dual-Band Mixer Using Composite Right/Left-Handed Transmission Lines," *IEEE Microwave and Wireless Components Letters*, vol. 17, pp. 607–609, Aug. 2007.
- [101] M. Schmatz, C. Biber, and W. Baumberger, "Conversion Gain Enhancement Technique for Ultra Low Power Gilbert-Cell Down Mixers," in *IEEE Gallium Arsenide Integrated Circuit (GaAs IC) Symposium*, (San Diego, CA, USA), pp. 245–248, October 1995.